



RIGA TECHNICAL
UNIVERSITY

Deniss Mironovs

**DEVELOPMENT OF STRUCTURAL HEALTH
MONITORING SYSTEM FOR STRUCTURES
IN OPERATIONAL CONDITIONS**

Doctoral Thesis



RTU Press
Riga 2023

RIGA TECHNICAL UNIVERSITY

Faculty of Civil Engineering
Institute of Materials and Structures

Deniss Mironovs

Doctoral Student of the Study Programme “Civil Engineering”

**DEVELOPMENT OF STRUCTURAL HEALTH
MONITORING SYSTEM FOR STRUCTURES IN
OPERATIONAL CONDITIONS**

Doctoral Thesis

Scientific supervisors

Dr. sc. ing.

ALEKSEJS MIRONOVS

Professor *Dr. sc. ing.*

ANDRIS ČĀTE

RTU Press

Riga 2023

Mironovs, D. Development of structural health monitoring system for structures in operational conditions. Doctoral Thesis. Riga: RTU Press, 2023. 113 p.

Published in accordance with the decision of the Promotion Council “P-06” of 16 June 2023, Minutes No. 04030-9.6.2/4.

Cover photo by Deniss Mironovs

DOCTORAL THESIS PROPOSED TO RIGA TECHNICAL UNIVERSITY FOR THE PROMOTION TO THE SCIENTIFIC DEGREE OF DOCTOR OF SCIENCE

To be granted the scientific degree of Doctor of Science (Ph. D.), the present Doctoral Thesis has been submitted for the defence at the open meeting of RTU Promotion Council on 3 November, 2023 at 14:15 at the Faculty of Civil Engineering of Riga Technical University, 6A Kļipsalas Street, Room 342.

OFFICIAL REVIEWERS

Associate Professor Dr. sc. ing. Līga Gaile
Riga Technical University, Latvia

Associate Professor Dr. sc. ing. Andrzej Katunin
Silesian University of Technology, Poland

Associate Professor Dr. sc. ing. Mirosław Wesołowski
Koszalin University of Technology, Poland

DECLARATION OF ACADEMIC INTEGRITY

I hereby declare that the Doctoral Thesis submitted for the review to Riga Technical University for the promotion to the scientific degree of Doctor of Science (Ph. D.) is my own. I confirm that this Doctoral Thesis had not been submitted to any other university for the promotion to a scientific degree.

Deniss Mironovs (signature)

Date:

The Doctoral Thesis has been written in English. It consists of an Introduction; 4 Chapters; Conclusions; 54 figures; 7 tables; the total number of pages is 113. The Bibliography contains 123 titles.

ABSTRACT

The present thesis is devoted to application of state-of-the-art structural health monitoring techniques, aiming to development of functional structural health monitoring system for objects in operation, as well as development of methodologies, aiding in damage recognition, data processing and analysis.

The first part of the presented thesis covers literature review of topic connected to structural health monitoring and operational modal analysis in particular as an established vibration-based technique for SHM. Apart from methodological aspects, technological ones are discussed. Thesis offers to substitute commonly used accelerometers with PVDF piezo film deformation sensors. Theoretical background and experimental validation shows, that the use of deformation instead of acceleration signals allows to perform modal analysis of a structure with the same quality.

Harmonics extraction algorithm from vibrational responses of a structure with periodical excitation component was proposed. In practical implementations the algorithm utilizes tachometer signal from a rotating shaft, which keeps the phase variance for each rotation. This is later used to enhance the signal of structural response and obtain a significantly emphasized periodical component. This component is subtracted from the response in frequency domain and inverse Fourier transform gives a filtered structural response, with significantly reduced presence of harmonics.

A road map for developing an SHM system is formulated in this thesis. This road map serves as a step-by-step instruction for assembling and using SHM system for fixed and rotating structures like helicopter or wind turbine blades. As part of the road map a concept of modal passport is introduced, which serves as a framework for storing and analysis modal data. Two damage detection algorithms are introduced – Modal Field Comparison method and Modal Parameter Variation. These methods are useful tools for detecting damage in measured structures.

The last Section of the thesis shows case studies, where the introduced concepts are tested and validated during experiments on several structures. These structures are – aluminium beam, wind turbine laboratory model, airport radar tower and small helicopter composite blades.

ANOTĀCIJA

Šis promocijas darbs ir veltīts mūsdienīgu konstrukciju stāvokļa monitoringa (SHM) metožu pielietošanai, ar mērķi izstrādāt funkcionējošu konstrukciju stāvokļa monitoringa sistēmu ekspluatācijā esošajiem objektiem, kā arī metodoloģiju izstrādei bojājumu atpazīšanā, datu apstrādē un analīzē.

Iesniegtā promocijas darba pirmā daļa aptver literatūras pārskatu par tematiem, kas ir saistīti ar konstrukciju stāvokļa monitoringu un operacionālo modālo analīzi, kā vispāratzītu uz vibrācijas balstītu SHM pieeju. Papildus metodoloģiskajiem aspektiem tiek apspriesti tehnoloģiskie aspekti. Disertācija piedāvā aizstāt parasti izmantotos akselerometrus ar PVDF pjezo plēves deformācijas sensoriem. Teorētiskais pamatojums un eksperimentālā validācija parāda, ka deformācijas izmantošana paātrinājuma signālu vietā ļauj veikt konstrukciju modālo analīzi ar vienādu kvalitāti.

Ir piedāvāts harmoniku izņemšanas algoritms no konstrukcijas vibrācijas atbalsim ar periodisku ierosmes komponentu. Praksē algoritms izmanto tahometra signālu no rotējošas vārpstas, kas saglabā fāzes novirzi katrai rotācijai. Vēlāk to izmanto, lai uzlabotu konstrukcijas atbalss signālu un iegūtu uzsvētu periodisko komponentu. Šī komponente tiek atņemta no atbalss frekvences domēnā, un apgrieztā Furjē transformācija nodrošina filtrētu konstrukcijas atbalsi ar ievērojami samazinātu harmonikas klātbūtni.

Šajā disertācijā ir formulēts ceļvedis SHM sistēmas izstrādei. Šis ceļvedis kalpo kā pakāpeniska instrukcija SHM sistēmas izstrādei un izmantošanai fiksētām un rotējošām konstrukcijām, piemēram, helikopteru un vēja ģeneratoru lāpstiņām. Ceļveža ietvaros tiek ieviests modālās pases jēdziens, kas kalpo kā satvars modālo datu glabāšanai un analīzei. Tiek ieviesti divi bojājumu noteikšanas algoritmi – modālo lauku salīdzināšanas metode un modālo parametru variāciju intensitāte. Šīs metodes ir noderīgi instrumenti bojājumu noteikšanai izmērītajās konstrukcijās.

Pēdējā disertācijas sadaļā ir parādīti pētījumi, kuros ieviestās koncepcijas tiek pārbaudītas un apstiprinātas eksperimentos ar vairākām konstrukcijām. Šīs konstrukcijas ir – alumīnija sija, vēja turbīnas laboratorijas modelis, lidostas radara tornis un mazi helikopteru kompozītmateriāla lāpstiņas.

ACKNOWLEDGEMENTS

The author expresses sincere gratitude to both supervisor of this thesis – Dr. sc. ing. Aleksey Mironov and professor Dr. sc. ing. Andris Čate.

Aleksey Mironov has been the true inspiration for this work and works associated with the topic of structural health monitoring and operational modal analysis. Many Dr. Mironov's ideas have led to meaningful work and resulted in fascinating experiments and measurements. He provided information, knowledge, and substantial support.

Big appreciation goes to the Aviation Research Centre (ARC) and all its' staff. ARC, being RTU subsidiary, has been providing all the necessary scientific, technological and practical assistance for this thesis to be developed. ARC made it possible to perform tests on all presented structures. Engineers from ARC – Ivars Unte, Aleksejs Safonovs, Pavel Doronkin and Vitalijs Kuzmickis as well as other colleagues – have all been more than helpful and supportive during time spent there. Special thanks go to the late Dr. sc. ing. Aleksander Priklonskiy, former specialist from ARC, whose guidance and massive theoretical knowledge have left a very positive impact on this work.

The honourable mention and gratitude go out to the Institute of Materials and Structures of Riga Technical University, especially to professor Andris Čate, who was very supportive and helpful in all organisational questions regarding this thesis. Dr. Čate's help allowed to avoid many mistakes and hardships, he has inspired to apply for the doctoral program and was always there to help in times of need.

Special thanks to Dr. Sandris Ručevskis for providing guidance, support and for very useful tips. Warm acknowledgements to the colleagues and academic staff from IMS – Rimas Janeliukštis, Andrejs Kovaļovs, Pavels Akišins, Jana Galilejeva and Jevgenijs Barkanovs. Their contribution and sharing with experience have allowed a smoother workflow. True acknowledgement also goes to RTU staff for professional support, University's Doctoral Grant Program and the European Regional Development Fund project No. 1.1.1.1/20/A/016 "A prototype of typical structural health monitoring system of operating objects for condition based maintenance" for financial support, without which this thesis might not be possible.

Of course, last but not least, author expresses sincere gratitude to his family, supportive father and mother, brothers, friends and dear colleagues from acoustical consultancy company Akukon for support and understanding during work on this thesis.

NACIONĀLAIS
ATTĪSTĪBAS
PLĀNS 2020



EIROPAS SAVIENĪBA
Eiropas Reģionālās
attīstības fonds

IEGULDĪJUMS TAVĀ NĀKOTNĒ

AVIATION RESEARCH CENTER

TABLE OF CONTENTS

ABSTRACT	4
ANOTÁCIJA	5
ACKNOWLEDGEMENTS	6
TABLE OF CONTENTS	7
NOMENCLATURE AND ABBREVIATIONS	9
INTRODUCTION.....	10
Motivation and scope	10
Aims of the thesis.....	12
Tasks of the thesis	12
Scientific novelty.....	12
Practical significance.....	13
Methodology of the research.....	13
Applicability limitations.....	13
Arguments for defence of the thesis.....	14
Structure	14
Publications	15
Conferences	16
1. LITERATURE REVIEW	18
1.1. Structural health monitoring.....	18
1.2. Operational modal analysis	20
1.3. Vibration sensors	26
1.4. Harmonics extraction.....	33
1.5. Structural damage identification.....	34
2. STRUCTURAL HEALTH MONITORING SYSTEM.....	38
2.1. SHM related problems.....	38
2.2. SHM problems solutions	39
2.3. SHM system development steps.....	40
2.4. Application of deformation sensors for OMA.....	42
2.5. Measurement system	47
2.6. Periodic component suppression	49
2.7. Data processing and analysis	51
3. DAMAGE DETECTION AND EVALUATION.....	53
3.1. Modal Passport	53
3.2. Modal Parameter Variation	60
3.3. Modal Field Comparison Method.....	61
4. CASE STUDIES	67
4.1. Application of deformation sensors.....	67
4.2. Harmonics extraction.....	71
4.3. Modal Passport application	77
4.4. Wind turbine laboratory model.....	84

4.5. Aluminium beam	93
4.6. Radar tower.....	97
5. CONCLUSIONS.....	102
REFERENCES.....	106

NOMENCLATURE AND ABBREVIATIONS

DAQ	Data acquisition
EFDD	Enhanced frequency domain decomposition
FDD	Frequency domain decomposition
FE	Finite element
FFT	Fast Fourier transform
FRF	Frequency response function
GFRP	Glass fibre reinforced plastics
NDT	Non-destructive testing
MAC	Modal assurance criterion
MCF	Mode complexity factor
MDOF	Multi degree of freedom system
MFCM	Modal field comparison method
MP	Modal passport
MPV	Modal parameter variation
MPVI	Modal parameter variation integrated
OMA	Operational modal analysis
PCA	Principal component analysis
PP	Peak picking
PSD	Power spectral density
SDOF	Single degree of freedom system
SHM	Structural health monitoring
SSI	Stochastic subspace identification
SSI-cov	Covariance driven stochastic subspace identification
SSI-data	Data driven stochastic subspace identification
SVCA	Singular value change assessment
SVD	Singular value decomposition
TSA	Time synchronous averaging

INTRODUCTION

Motivation and scope

Structures are integral part of civil engineering, aviation, energy and transportation. These fields of economy demand structures to be reliable, safe, functional and at the same time cost-efficient. It is one of the hardest tasks in engineering to meet these demands. Cost efficiency of production and maintenance drives structures to be less reliable, which in turn creates the necessity to observe structural health during its lifetime, i.e., to perform structural health monitoring. United States Department of Defence spends 60-85% of a military systems life cycle costs on operational and supporting expenses [1]. A significant amount of these costs are attributed to aircraft structures, due to the necessity to perform scheduled condition checks. These checks can sometimes be unnecessary due to healthy state of a structure. The International Air Transport Association (IATA) indicates that civil aircraft Maintenance, Repair and Overhaul (MRO) costs represent 10-13% of airline costs. IATA estimates that a 1% reduction in maintenance costs could mean \$800 million in savings for the industry [2].

Planned structural checks can still be insufficient to prevent failures. From 2009 to 2012, only in China there were 3 major wind turbine component failures, either blades or tower [3]. A recent accident has happened in Estonia in 2022 [4], when a 60-meter-tall wind turbines tower collapsed under heavy wind conditions. Another example of a serious accident is Boeing 737 fuselage part crack and opening during flight. This has caused a rapid depressurization, but fortunately the plane was landed safely in Yuma, Arizona [5].

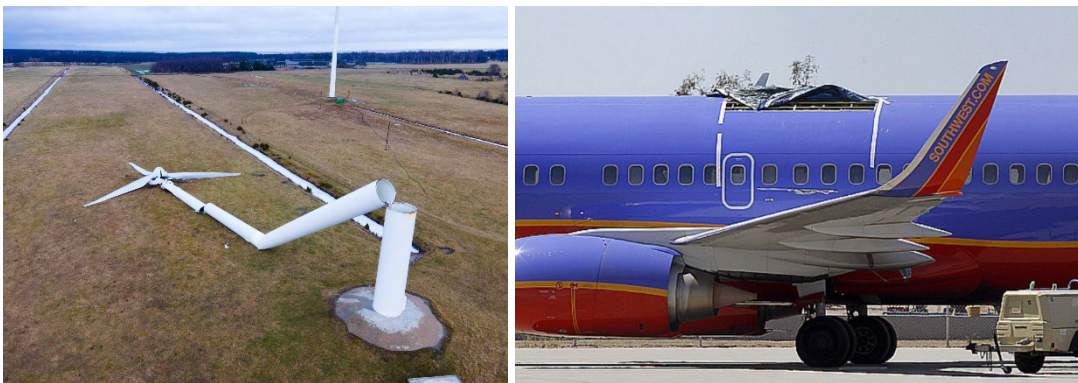


Fig. 1. Major structural failures. Left: Saaremaa, Estonia 2022; right: Yuma, Arizona 2011.

Larger wind turbine blades are exposed to larger mechanical stresses, more pronounced aerodynamic effects, structural instability and more complicated failure mechanisms [6] as compliance increases with blade length. This, in turn, renders the blades more prone to damage. For example, wind turbine blade failures account for 30% of total failures related to wind turbine [7], while the cost of blade manufacturing accounts for 15-20% of the cost of a whole wind turbine [8].

The necessity to reduce unnecessary structural checks while improving the overall reliability of structures suggests that a constant or at least frequent structural health monitoring

is needed. The goal of structural health monitoring is to timely detect damage, which allows to plan repairs in optimal fashion and enables safety of the structure.

The topic of structural health monitoring is very popular among scholars and practitioners and has been developing rapidly during several last decades. Many works have been published on the topic, for example book by Balageas et al [9] or numerous scientific papers. Quite a few commercial SHM systems exist on the market, e.g., several systems introduced by HBM [10] and SGS [11]. In these systems structural health is evaluated by the means of non-destructive testing. Existing NDT techniques are based on measuring different physical phenomena, like strain, electrical resistance of materials, acoustic emission of structures inhomogeneity, vibration. Vibration-based structural evaluation methods [12] rely mostly on modal analysis [13] and particularly on operational modal analysis (OMA) [14]. As it is shown in this thesis, OMA methods are very promising due to its applicability potential. Some works show OMA based SHM being used on large static civil structures, like buildings [15] and bridges [16], [17].

Few studies show OMA based SHM applied on smaller sized structures (blades, wings), which are part of a moving entity (aircraft). These studies are mostly done in laboratory environment using high-cost instrumentation [18], [19], which provides high quality scientific results, but can be difficult (not affordable) to implement in real life structures. In a health monitoring systems survey [20] it was concluded that SHM systems for foundation, tower and blades of a wind turbine are mostly limited to experimental and research installations.

As mentioned, continuous SHM for static civil structures exists, but for moving structures like wind turbine blades or aircraft there are some significant challenges. The costs of downtime for a wind turbine or especially an aircraft are quite high, thus taking a structure out of operation for SHM testing is not desirable. Back in 2011 the National Renewable Energy Laboratory in USA estimated that operational and maintenance expenses per MW were around 17000 USD for onshore and 46000 USD for offshore wind turbine [20].

What is more, planned maintenance has a risk of missing a potential damage that can occur between maintenance sessions. So continuous SHM during operation is needed for some structures. This type of SHM can only be realised by having damage sensing system installed on the structure (or in some cases integrated into the structure). This system should be affordable and the health assessment process must not be sophisticated.

The affordability of such a system is supposed to be achieved by choosing alternative sensors for OMA. Instead of traditional accelerometers, which can be the most significant part of an SHM system in terms of cost if tens or even hundreds of sensors are implemented, a more affordable piezo film sensors are proposed. Conventional accelerometers are also not feasible for application in real operational conditions for wind turbine and helicopter blades due to their size and mass. Piezo film sensors on the other hand, having negligible weight, small size and very small thickness, are advantageous for application for aerodynamic parts in this regard.

As mentioned above, the main structures to be considered in this thesis are wind turbine blades and helicopter blades, which are one of the most noticeable examples of moving (rotating) structures and require SHM without interruption of their operation. However, the design of a proposed SHM system is not limited to blades and wings and can be implemented for other structures.

Aims of the thesis

This thesis aims to develop a vibration based structural health diagnostics system technology, which would create prerequisites for full structural monitoring system development during normal operation of the surveyed object in their operating conditions. The technology includes important stages of SHM system development – sensors network, data acquisition, data storage and processing, as well as analysis and damage detection. In the presented thesis SHM system prototypes are demonstrated, which are affordable, reliable and user friendly.

Tasks of the thesis

To achieve the aims of the thesis following tasks were formulated:

1. Perform scientific literature review in the field of SHM, OMA, vibration sensors, damage detection algorithms. Implement existing solutions that do not require modification.
2. Formulate SHM system development and usage process.
3. Develop an intermediary damage detection algorithm on the basis of evaluation of vibration responses without modal parameter estimation. Validate such an algorithm on actual structure.
4. Formulate an approach for taking into account natural conditions, that could influence the precision of damage detection.
5. Validate application of piezo film sensors as an alternative to accelerometers for OMA and test SHM systems' prototype data processing methods for condition monitoring.

Scientific novelty

The scientific novelty of the thesis comes from:

1. Experimental application of piezo film sensors for OMA purposes. Previous studies did not show examples of using piezo film sensors for operational modal analysis. Piezo film sensors application has its differences compared to application of accelerometers – different installation techniques and different vibrational data interpretation. Compared to accelerometer response, piezo films provide deformation (strain) velocity signal. Deformation mode shapes differ from displacement mode shapes.
2. Development of two new algorithms for damage detection. These algorithms evaluate change of modal characteristics in different manner compared to existing algorithms. The first algorithm is able to compare structural states without performing modal analysis, which saves time on data analysis. Another algorithm is a comprehensive modal parameters (frequency and mode shape) change analysis tool. It gives estimates of how modal parameters changes compared to a previously set reference.

3. Introduction of *modal passport* concept. Modal passport is a database of modal parameters expressed as functions of different influence factors, like temperature and loads.

Practical significance

This thesis can be used as a guidance for development of SHM systems for various structures. Alternatively, the proposed SHM system prototype can be applied directly on structures, although one must make sure to perform all necessary certifications of the SHM system, especially in aviation field. The system would require an engineer to operate it, record data, read influence factors values, and check if the damage detection parameter shows any sign of damage. In case it does show a sign of damage, then more in-depth analysis is performed primarily using mode shapes for the potentially damaged structure.

Methodology of the research

The presented work relies on existing SHM technologies, mainly modal analysis and operational modal analysis testing techniques, commercial hardware and software. Operational modal analysis techniques used in this thesis include enhanced frequency domain decomposition and stochastic subspace identification.

Novel approach of signal sensing is applied, i.e., using piezo film sensors instead of conventional accelerometers or strain gauges.

Applicability limitations

A widely acknowledged set of features that a fully developed SHM system possesses include the ability to operate without interruptions, mostly automatically and autonomously, as well as such systems robustness against various mechanical and environmental impacts and longevity. The proposed SHM system prototype, however, is not fully automatic, and has not yet been tested for robustness. Still, for the purpose of brevity, the proposed SHM system prototype shall be called SHM system in the scope of this thesis.

This SHM system prototype is limited to small and medium scale structures (0.5 m – 20 m) in dimensions, as other structures haven't been tested with this prototype. Smaller structures (<0.5 m) will not be enough to accommodate necessary number of sensors. For larger structures it is yet unknown, whether deformation sensors would be able to correctly register large-scale deformations for mode shapes of lower order to be successfully identified. Also, it is unknown how electrical signals in wires would translate between sensors and data acquisition systems inputs on large distances (>20 m). This might be an issue due to electro-magnetic interference and absence of preamplification in sensors. However, this limitation might be lifted in future studies.

Another limitation is rather technical – in order to install the system, the structure has to be equipped with sensing system. Installation process can take hours or even days for complex structures. If this process is performed during post-production in a factory, then this is not a serious issue. However, for existing and operating structures, especially for wind turbine blades and helicopter blades, it would be necessary to detach those from the machine, apply sensors indoors (to guard against wind and rain), then attach blades back.

The proposed SHM system is not a commercial product, and it lacks intuitive all-in-one user interface in application form.

Arguments for defence of the thesis

This thesis shows how even with limited financial resources it is possible to develop an SHM system and monitor a large number of typical structures condition. One would need a set of cheap piezo film sensors, wiring, data acquisition module, a PC and software. For in-depth structural condition analysis, one would also need modal parameter estimation software, like *ARTEMIS*.

Newly developed damage detection algorithms have different purposes and different implementations. Modal field comparison method, for example, does not require use of commercial software, and can be realised using code in *Matlab*, *Octave* or *Python*. Modal parameters variation parameter does require modal parameter estimation, but, as an advantage, provides damage localization.

All of the above give operators of structures helpful information about structural condition, so that repairs can be planned in optimal manner. This also increases safety and reliability of structures, which helps to bring costs down. SHM system is an investment, that pays off after some time.

Structure

The thesis consists of several parts.

First, a scientific and commercial literature review is presented, covering topics such as operational modal analysis, including modal parameters identification, vibration sensors, integrated sensors, harmonics extraction and structural damage identification.

Next, the thesis will go through steps of SHM system development, with emphasis on the technological novelty like the application of piezo film sensors. A formulation for harmonics extraction algorithm is introduced.

A concept of modal passport is introduced – a framework for modal parameters assessment between multiple measurements with different operating conditions.

Then newly developed modal parameters evaluation methods are shown, describing the mathematical background and application. Two methods were developed for this thesis:

- Modal parameter variation – a method to evaluate mode shape and modal frequency changes due to damage with possibility to compare the results with healthy states.

This method allows to evaluate the intensity of the damage, as well as perform damage localization.

- Modal field comparison method, also called singular value change assessment – a method to approach structural state damage detection, without prior modal parameters estimation, which saves time and computing power.

Lastly, SHM technology application cases will be discussed, concluding both challenges and limitations, which surfaced during real life experiments, and successful examples of damage detection in a beam and helicopter blades. The overall structure of the thesis is shown in Fig. 2.

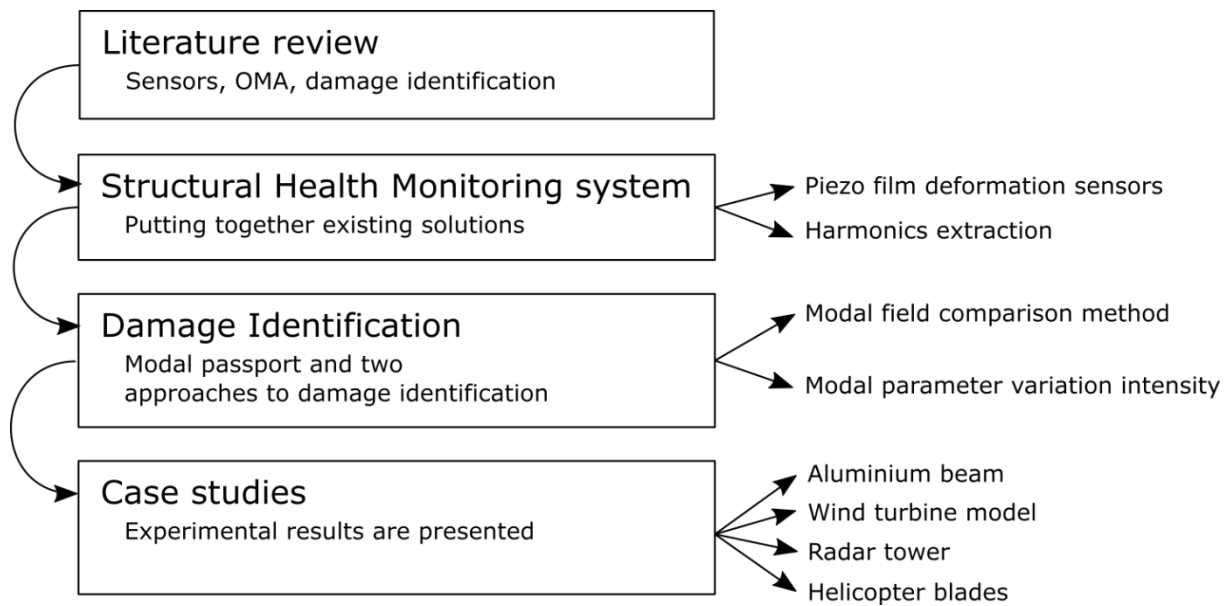


Fig. 2. Thesis structure.

Publications

1. Janeliukstis, R., Mironovs, D., Safonovs, A. Statistical Structural Integrity Control of Composite Structures Based on an Automatic Operational Modal Analysis — a Review, (2022), *Mechanics of Composite Materials*, Volume 58, Issue 2, Pages 181 – 208. DOI: 10.1007/s11029-022-10026-1 (indexed in Scopus)
2. Mironovs, D., Ručevskis, S., Dzelzītis, K. Prospects of Structural Damage Identification Using Modal Analysis and Anomaly Detection, (2022) *Procedia Structural Integrity*, Volume 37, pages 410-416. DOI: 10.1016/j.prostr.2022.01.103 (indexed in Scopus)
3. Janeliukstis, R., Mironovs, D. Smart Composite Structures with Embedded Sensors for Load and Damage Monitoring – A Review, (2021) *Mechanics of Composite Materials*, Volume 57, Issue 2, Pages 131 – 152. DOI: 10.1007/s11029-021-09941-6 (indexed in Scopus)
4. Solovyev, D., Dadunashvili, S., Mironov A., Doronkin, P., Mironov, D. Mathematical Modeling and Experimental Investigations of a Main Rotor Made from Layered Composite Materials, (2020) *Mechanics of Composite Materials*, 56 (1), pp. 103-110. DOI: 10.1007/s11029-020-09864-8 (indexed in Scopus)

5. Mironov, A., Prikloński, A., Mironovs, D., Doronkin, P. Application of Deformation Sensors for Structural Health Monitoring of Transport Vehicles (2020) *Lecture Notes in Networks and Systems*, 117, pp. 162-175. DOI: 10.1007/978-3-030-44610-9_17 (indexed in Scopus)
6. Mironovs, A., Mironovs, D. Modal Passport of Dynamically Loaded Structures on the Example of Composite Blades. In: Proceedings of 13th International Conference "Modern Building Materials, Structures and Techniques", Lithuania, Vilnius, 16-17 May, 2019. Vilnius: VGTU Press, 2019, pp.1-8. DOI: 10.3846/mbmst.2019.091
7. Mironovs, D., Mironovs, A., Čate, A. Harmonic Components Extraction Influence on Resulting Modal Parameters of Vibrating Structures. In: Proceedings of 13th International Conference "Modern Building Materials, Structures and Techniques", Lithuania, Vilnius, 16-17 May, 2019. Vilnius: VGTU Press, 2019, pp.1-8. DOI: 10.3846/mbmst.2019.012
8. Mironovs, D., Mironov, A. Vibration Based Signal Processing Algorithm for Modal Characteristics Change Assessment, (2018) *AIP Conference Proceedings*, 2029, art. no. 020043, DOI: 10.1063/1.5066505 (indexed in Scopus)
9. Mironov, A., Mironovs, D., Kabashkin, I. Advanced Structural Health Monitoring and Diagnostics of Transport, Industrial and Energy Facilities (2018) *Lecture Notes in Networks and Systems*, 36, pp. 159-171. DOI: 10.1007/978-3-319-74454-4_15 (indexed in Scopus)
10. Mironovs D., Mironov, A., Chate, A. Application Case: Prototype of Radar Tower Structural Health Monitoring System, (2018) *Engineering for Rural Development*, 17, pp. 1301-1307. DOI: 10.22616/ERDev2018.17.N106 (indexed in Scopus)
11. Mironov, A., Mironovs, D. Experimental Application of OMA Solutions on the Model of Industrial Structure (2017) *IOP Conference Series: Materials Science and Engineering*, 251 (1). DOI: 10.1088/1757-899X/251/1/012092 (indexed in Scopus)

Conferences

1. 4th International Conference on Structural Integrity, ICSI 2021, Spain, Funchal, Madeira, 30 August – 2 September 2021, online. “Prospects of Structural Damage Identification Using Modal Analysis and Anomaly Detection” paper presentation and publication in conference proceedings.
2. The 19th International Multi-Conference “Reliability and Statistics in Transportation and Communication” (RelStat-2019), Latvia, Riga, 16-19 October 2019. “Application of Deformation Sensors for Structural Health Monitoring of Transport Vehicles” paper presentation and publication as a book chapter.
3. 13th International Conference "Modern Building Materials, Structures and Techniques", Lithuania, Vilnius, 16-17 May 2019. “Harmonic Components Extraction Influence on Resulting Modal Parameters of Vibrating Structures” paper presentation and publication in conference proceedings.
4. 14th International Conference “Mechatronic Systems and Materials”, MSM 2018, Poland, Zakopane, 4-6 June 2018. “Vibration Based Signal Processing Algorithm for Modal Characteristics Change Assessment” paper presentation and publication in conference proceedings.
5. The 18th International Multi-Conference “Reliability and Statistics in Transportation and Communication” (RelStat-2018), Latvia, Riga, 17-20 October 2018. “Condition Monitoring of Helicopter Main Gearbox Planetary Stage” paper presentation and publication in conference proceedings.
6. 17th International Scientific Conference Engineering for Rural Development, Latvia, Jelgava, May 23-25, 2018. “Application Case: Prototype of Radar Tower Structural Health Monitoring System” paper presentation and publication in conference proceedings.

7. The 17th International Multi-Conference “Reliability and Statistics in Transportation and Communication” (RelStat-2017), Latvia, Riga, 18-21 October 2018. “Advanced Structural Health Monitoring and Diagnostics of Transport, Industrial and Energy Facilities” paper presentation and publication in conference proceedings.
8. 3rd International Conference “Innovative Materials, Structures and Technologies” (IMST 2017), Latvia, Riga, 27-29 September 2017. “Experimental Application of OMA Solutions on the Model of Industrial Structure” paper presentation and publication in conference proceedings.
9. Riga Technical University 61st International Scientific Conference, 22 October 2020, Riga, Latvia, Online. Presentation of the ongoing research.
10. Riga Technical University 62nd International Scientific Conference, 28 October 2021, Riga, Latvia, Online.

1. LITERATURE REVIEW

1.1. Structural health monitoring

Any structure is designed to perform some function, whether it is being a foundation (e.g., towers), an encapsulation and protection (car body, aircraft fuselage) or energy transformation (blades and wings). To successfully perform said functions a structure must be in a healthy state, determined by design. Normal aging, wear and tear, environmental impacts or accidents alter the nominal structural state. Structural Health Monitoring gives information about the current structural state at any given time during structures operation [9].

As the name implies, SHM is different from conventional non-destructive testing, as the later often requires halting structures operation and perform test in controlled environment. SHM system involves integration of sensors, like smart layers inside the structures, with or without data transmission, computing and acquired data processing [9], [21]. It allows to re-evaluate structures design in later production, improving on acquired damage data. Data processing algorithm's function is to compare freshly acquired data with a healthy state data, often utilizing some forms of damage indices. Comparison should involve corrections for environmental factors [21].

Fig. 1.1 shows an overview of a typical SHM system. One of the most important aspects is the definition of monitored physical phenomenon, which depends on damage. These can be strain, electrical resistance of materials, acoustic emission of structures inhomogeneity, and the phenomenon used in this thesis – vibration. Another aspect is the type of signal produced by the sensor, usually being electric or optical. Complementary to the damage sensing, there is

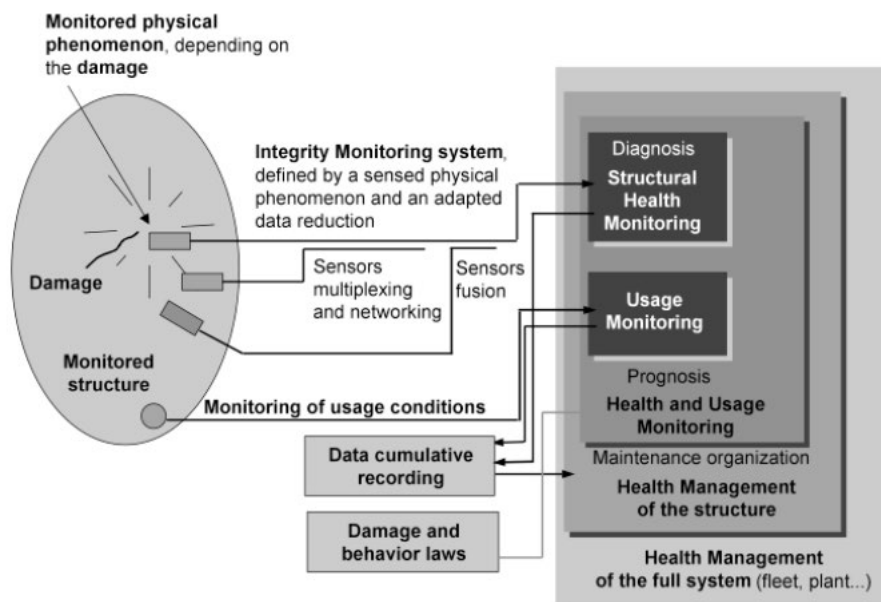


Fig. 1.1. Principle and organization of a Structural Health Monitoring system. [9]

also usage conditions sensing, i.e., environmental effects, temperature, loads, operational modes.

The field of structural health monitoring has been rapidly developing during the last three decades, with the advances in measurement techniques and data processing abilities of modern computers.

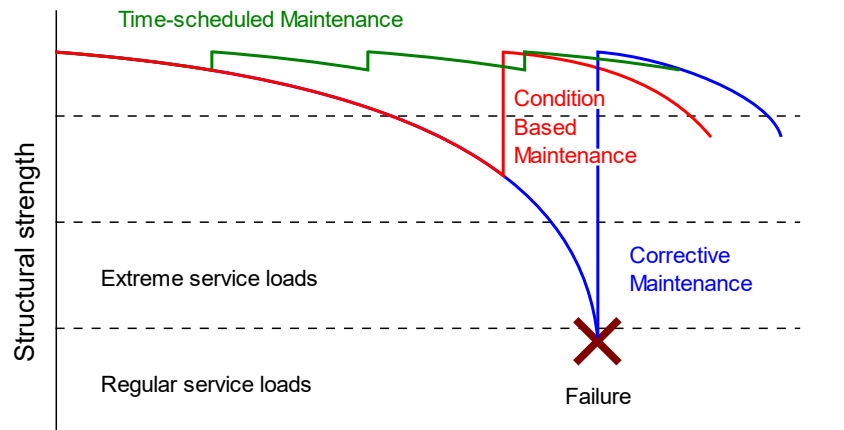


Fig. 1.2. Maintenance strategies with/without structural health monitoring [21].

Fig. 1.2 shows the degradation process experienced in service for every mechanical system or structure. The task is to decrease the slope of the curve by improving structure’s properties, which provides structural durability. Three maintenance strategies are:

- Corrective maintenance is performed when the damage is obvious or when failure occurs. This has advantage of low costs, but due to high failure risk, this strategy cannot be implemented in fields, where human lives or large financial sums are at stake. It is only acceptable for low responsibility, very lightly loaded structures.
- Time-scheduled maintenance means regular inspection after some period of time. This may require access to the structure or its disassembly. This is a very safe strategy, but results in high life cycle costs.
- Condition-based maintenance is possible if provided by an early damage detection system. This requires integration of sensors and constant or regular monitoring. Condition-based maintenance allows to plan repair works, which bring costs down, without jeopardizing safety.

Condition-based maintenance has been widely used for rotating machinery for decades. Its’ vibration based version requires a very small number of sensors (accelerometers), even a single sensor is often enough, installed on bearing supports. Acceleration or velocity signals are processed using e.g., Fast Fourier transform (FFT), sometimes together with extra data processing, and conclusions can be made on the condition of mechanical system [22].

For fixed structures, however, condition-based maintenance that involves structural health monitoring, has not reached the same level of technology readiness, as reported in 2011 by Sandia National Labs [23]. Some progress has been made since then and some applications are operational in the industry, as will be shown in the next paragraph.

Vibration-based methods [12] are widely used as a primary tool for SHM, thanks to well developed and affordable instrumentation – sensors, data acquisition systems, like *Bruel & Kjaer LAN-XI* or *National Instruments CompactDAQ* [24], [25] and software solutions, like *Structural Vibration Solutions ARTEMIS Modal* [26]. A report by Fraunhofer [27] mentions 25

different vibration-based SHM systems, which mostly utilize amplitude spectra analysis, order analysis and other forms of dynamic signal analysis. However, none of the SHM systems feature modal analysis as a tool for damage detection. So, there is a possibility to introduce an alternative SHM system, with a more advanced signal processing approach, allowing for a more reliable condition-based maintenance.

1.2. Operational modal analysis

The main concept behind vibration-based SHM methods is that damage induced structural changes are reflected in modifications of mass, stiffness and damping of the structure [13]. Any structure is a dynamic multi degree of freedom system, which can be described with an equation of motion:

$$M\ddot{x}(t) + C\dot{x}(t) + Kx(t) = f(t), \quad (1.1)$$

where M – mass matrix, kg,

C – damping matrix,

K – stiffness matrix,

$x(t)$ – response vector, $\dot{x}(t)$ and $\ddot{x}(t)$ are the first and the second time derivatives of the response,

$f(t)$ – applied force vector, N.

The response vector is typically displacement of a structural point, thus the first time derivative is velocity, and the second time derivative is acceleration. In frequency ω domain the equation of motion can be shown as

$$(-M\omega^2 + j\omega C + K)x(\omega) = f(\omega). \quad (1.2)$$

The matrix of Frequency Response Functions of a system is defined as

$$H(\omega) = \frac{x(\omega)}{f(\omega)} = \frac{1}{(-M\omega^2 + j\omega C + K)}. \quad (1.3)$$

Equation (1.3) shows how FRF of a structure depends on mass, damping and stiffness, and how one can obtain FRF by measuring applied force f and registering the vibrational response x . Using FRF from multiple points on the structure it is possible to estimate modal parameters of a structure by applying the following equation:

$$H_{pq}(\omega) = \sum_{m=1}^M \frac{A_{pqm}}{j\omega - \lambda_m} + \frac{A_{pqm}^*}{j\omega - \lambda_m^*} \quad (1.4)$$

where p – index for input location where force is applied,

q – index for output location where response is measured,

m – index for mode number,

M – total number of natural modes,

λ_m – systems pole for mode m ,

A_{pqm} – residue.

In a unique case when $M = 1$, this is a single degree of freedom system.

Systems poles contain natural frequencies f and damping ratios ζ :

$$f_m = \frac{\text{Im}(\lambda_r)}{2\pi}, \quad \zeta_m = -\frac{\text{Re}(\lambda_r)}{|\lambda_r|} \quad (1.5)$$

Systems residue contains information about the mode shape ψ of the structures vibration, as well as scaling factor Q – the amount of particular mode shapes participation in the total response, related to the excitation force, and is shown as

$$A_{pqm} = Q_{pqm} \psi_{pqm} \psi_{pqm}^T \quad (1.6)$$

The above formulation is universal for all types of Modal Analysis. The common type is the so-called Experimental Modal Analysis (EMA). For EMA an engineer provides a controlled excitation force $f(t)$ to a structure. This force is measured, along with the responses $x(t)$, so the FRF can be estimated using Eq. (1.3). The actual setup needs a controlled excitation force source – a shaker or an impact hammer with force transducer. Sufficient energy should be applied on the structure, to excite the necessary modes. This is problematic when one needs to perform modal analysis for a remote structure, especially one which is in constant operation, for example wind turbine blades. EMA application for such structures would require full stop of the structure, possible disassembly and transportation to a laboratory for controlled testing, or testing on site, which is a very tedious and not safe endeavour. So another type of modal analysis is used – Operational Modal Analysis, which is an output-only method. OMA is a sequence of both measurement procedures and mathematical processing of measured data.

As forces are not measured in OMA and thus are unknown, it is assumed, that forces are evenly distributed in space across the structure and in frequency domain [28]. This means that in order to use OMA in practice, natural excitation forces should be random in time and have sufficient energy to excite necessary modes. Examples of such excitation are wind, rain, earthquake, significant number of moving vehicles, etc. Mentioned natural types of excitation meet the OMA requirements only in part, as these are not theoretically “ideal”, however, longer observation/recording times provide better agreement with the OMA requirements.

From Eq. (1.3) it follows that

$$x(\omega) = H(\omega)f(\omega), \quad (1.7)$$

which allows to write the same relation in power spectra matrix form

$$G_{xx}(\omega) = H(\omega)G_{ff}(\omega)H(\omega)^H, \quad (1.8)$$

where G_{xx} – power spectra matrix of the output response,

G_{ff} – input force power spectra matrix,

$H(\omega)^H$ – Hermitian of the FRF.

If one applies above mentioned OMA assumptions, then mathematically $G_{ff} = I$, i.e., the unity matrix, so Eq. (1.8) becomes

$$G_{xx}(\omega) = H(\omega)H(\omega)^H. \quad (1.9)$$

From this point it is possible to perform modal parameter estimation from power spectra matrix $G_{xx}(\omega)$.

The mentioned assumption is crucial for OMA, as its violation can result in erroneous estimated modal parameters. In practice this becomes a serious challenge, as excitation can include periodic sources, like rotational machinery. This obstacle can be avoided using post-processing techniques for harmonic components suppression in vibrational response. For instance, Time Synchronous Averaging [29] is the technique that allows accumulation and extraction of most of the periodic excitation energy from vibrational signal. Influence of rotational forces is also dependent on the distance from observation point to the source of said excitation. Other irregularities of excitation are dealt with by taking enough power spectra averages. Also, the excitation energy should be sufficient, as mentioned above. For example, OMA based SHM of a wind turbine during periods of no still weather, without wind, would not give any meaningful results. Depending on the structure and excitation quality from OMA assumptions perspective, a single measurement recording can last from 1 minute up to several hours and even more.

In the context of this thesis the word *mode* is referred to the self-oscillation representation, which is not to be confused with the term *operational mode*, which refers to the working condition of the structure, e.g., rotor blade rotation speed of 100 RPM is an operational mode of this rotor blade.

OMA advantages and disadvantages

The tested structure can remain in operation, without disrupting objects normal exploitation. No excitation mechanisms are needed, which saves costs and time.

On the other hand, OMA results depend on the excitation and environmental conditions. Another disadvantage is the unscaled nature of estimated mode shapes. The scaling of individual mode shape can vary between measurements, which might give erroneous results. However, this can be overcome by post processing the measurement results.

Modal parameters estimation

OMA modal parameter estimation techniques are divided in two categories – time domain and frequency domain techniques [30]. Techniques differ in their mathematical complexity, computational efficiency and identification accuracy. Frequency domain techniques are Peak Picking (PP), Frequency Domain Decomposition (FDD), Enhanced Frequency Domain Decomposition (EFDD) among others. Examples of time domain techniques are two Stochastic subspace identification (SSI) sub techniques – data driven SSI and covariance driven SSI.

Peak Picking is the oldest and least demanding techniques of all, as it allows to manually pick easily distinguishable peaks of the output response power spectra. However, PP cannot distinguish between closely spaced modes, which is a very common case in practice. Moreover, peak picking does not involve calculation of natural mode shapes, it simply shows operational deflection shapes, which makes PP technique unprecise [16].

Frequency Domain Decomposition (FDD) on the other hand, uses a more complex approach. FDD employs Singular Value Decomposition (SVD), a matrix factorization into singular vectors and singular values, which are proportional to systems eigenvectors and eigenvalues. SVD of a power spectra matrix from Eq. (1.9) is given as

$$G_{xx}(\omega) = U(\omega)S(\omega)U(\omega)^H, \quad (1.10)$$

where U is a singular vector matrix,

S – singular values diagonal matrix

U^H – conjugate transpose (Hermitian transpose)

Matrix $S(\omega)$ stores frequency dependent energy distribution, i.e., power spectral density (PSD) function. Peaks of the spectra indicate systems natural frequencies ω_r . Singular vector corresponding to a natural frequency $u(\omega_r)$ is an estimate of mode shape $\hat{\psi}_r$ at the natural frequency ω_r [31]. This decomposition procedure is also known as Principal Component Analysis (PCA) [32]. As principal components are derived from structural response, they are dependent on material properties, thus can be used for damage identification.

FDD treats singular vector $u(\omega_r)$ for singular value at a peak frequency ω_r as an estimate of mode shape.

Enhanced FDD considers each mode as a representative of a SDOF system (Fig. 1.3(a)). The singular values $s(\omega)$ corresponding to the singular vector $u(\omega_r)$ is the auto power spectral density function of the corresponding single degree of freedom system. This PSD function is identified around the peak by comparing the mode shape estimate $\hat{\psi}_r$ with singular vectors for the frequency lines around the peak. Singular values form the auto PSD function, as long as corresponding singular vectors have high modal assurance criterion (MAC, see Section 1.5) value with $\hat{\psi}_r$.

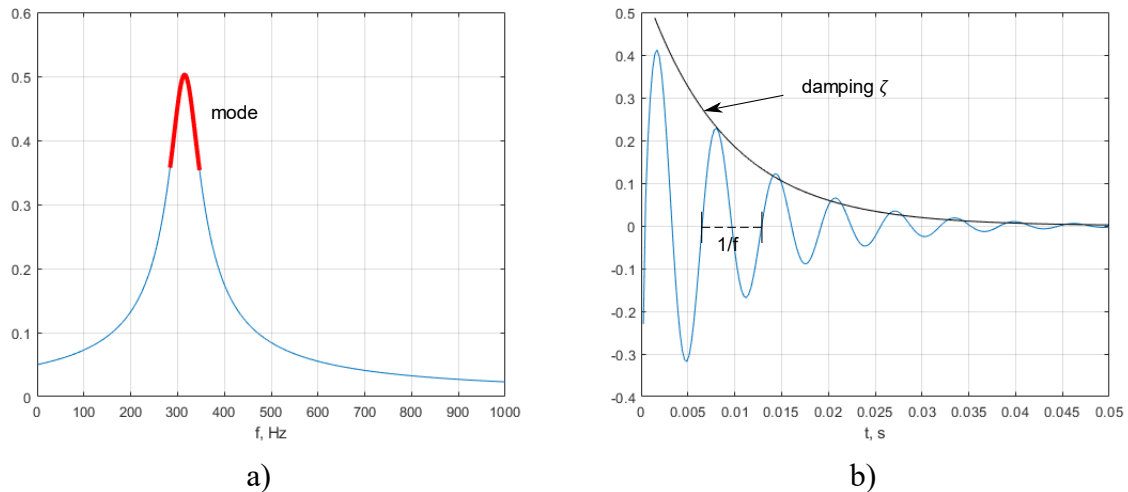


Fig. 1.3. a) SVD plot of a SDOF system; b) Inverse FFT of the SVD plot.

When auto PSD is formed, it is being processed using inverse FFT, and a time impulse decay function is obtained (Fig. 1.3(b)), from which frequency f_r is estimated from crossing times and damping ζ_r is estimated from the decay.

Somewhat different approach is applied when using time domain SSI algorithms. SSI covariance-based method, for example, is based on processing covariance, which are essentially correlations. Correlation matrix R_{xx} is obtained from power spectra matrix by making inverse FFT. Individual correlations are time domain functions, which are then modelled as mathematical polynomials. Polynomial model for Impulse Response function of a SDOF dynamic system can be written as

$$\alpha_m h(t_m) + \alpha_{m-1} h(t_{m-1}) + \dots + \alpha_0 h(t_0) = 0, \quad (1.11)$$

where h is Impulse Response function,

m – the polynomial order for coefficient α

t – time.

The goal is to fit the polynomial to the actual physical response of the structure. Polynomial models for each response are formed into Hankel matrix. From the Hankel matrix a companion matrix is formed, which is a product of the latter Hankel matrix and block shifted version of this Hankel matrix. The companion matrix is then a subject of eigenvalue problem. The solution to this eigenvalue problem are eigenvectors which are estimates of mode shapes, and eigenvalues – estimates of modal frequencies. Modal parameter estimation is performed for polynomial models with different orders. Low order polynomials might not be sufficient to estimate all modes in a given frequency range. On the contrary, too high model order gives modal overestimation, which results in spurious mathematical modes. Stabilization diagram is used to visually determine modes, which are stable across many different model orders [33].

SSI covariance-based method is summarized in [34] and can be found in [35]. Other SSI methods (Extended Unweighted Principal Component – SSI-UPCX, Unweighted Principal Component – SSI-UPC, Principal Component – SSI-PC, Canonical Variate Analysis – SSI-CVA, Unweighted Principal Component Merged Test Setups) use similar theoretical basis [36].

Multi-patch OMA

Operational Modal Analysis requires multiple sensors installed on the structure, thus the same amount of input channels on the data acquisition unit (DAU) is required. The cost of DAU and the input channel number influences the price of the SHM system in whole. It is possible to significantly reduce the cost of an SHM system if one uses multi-patch OMA. In this OMA approach vibration is measured consequently by dividing sensors in small groups called patches at a time. Each group includes two types of channels: reference channels, which are not moved, and moving or roving channels. After all patches are separately measured, signal processing algorithms combine those patches together for further modal parameter estimation. Reference channels are used here to equalize the excitation energy that varies in time for different patches. With multi-patch OMA one can measure, say, 40 signals, with only 8 input channels. Of course, the time for data recording becomes longer, but the cost of the system is reduced significantly.

Fig. 1.4 shows a multi-patch scenario. The structure is measured in two stages by means of two patches, patch one comprising locations 1, 2, 3, 5, 6, 7, 9 and 10 and another comprising locations 2, 3, 4, 6, 7, 8, 11 and 12. The four sensors common to each patch (locations 2, 3, 6 and 7) are reference sensors. It should be noted that set up depicted in Fig. 1 corresponds to measurement for first patch.

To summarize, the steps for performing multi-patch OMA are as follows:

1. choose reference locations and attach sensors to these locations,
2. attach roving sensors to the patch 1 location,
3. record vibration data,
4. move roving sensors to the next patch location,
5. repeat steps 2-4 until data from all DOFs is recorded.

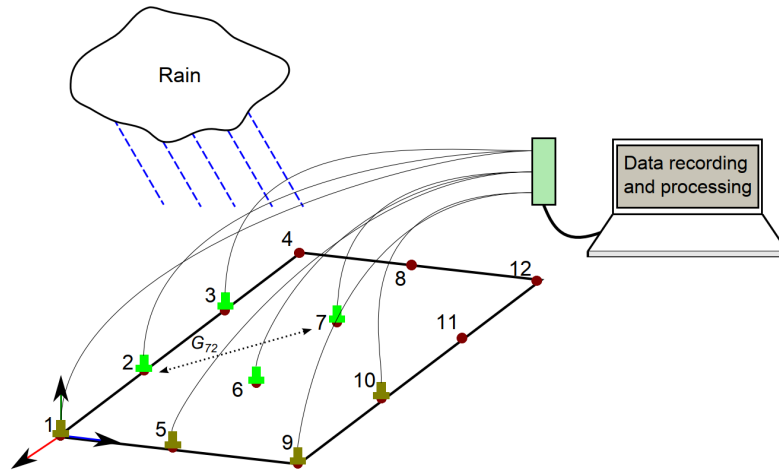


Fig. 1.4. Schematic of a multi-patch OMA measurement with 2 patches [37].

There is a problem of combining the data from different patches in order to estimate global modal parameters of a structure. Mainly two strategies are used as a solution:

1) estimating modal parameters for patches separately and then combining the parameters together – Post Global Estimation Rescaling (PoGER);

2) combining data from patches and then obtaining global modal parameters in one step by performing parameter estimation on patched, or combined, data – Pre Global Estimation Rescaling (PreGER).

The following equation constitutes PreGER [37]:

$$G_{XX^r|j \rightarrow k} = G_{XX^r|j} (G_{X^r X^r|j})^{-1} G_{X^r X^r|k} \quad (1.12)$$

where $G_{XX^r|j \rightarrow k}$ – scaled version of matrix of power spectra of vibrational responses for patch j with respect to forcing conditions in patch k ,

$G_{XX^r|j}$ – matrix of power spectra of vibrational responses of patch j taken with respect to reference sensors only,

$(G_{X^r X^r|j})^{-1}$ – inverted reference autospectra matrix of patch j ,

$G_{X^r X^r|k}$ – reference autospectra matrix of patch k .

The autospectra $G_{X^rX^r}|_k$ and $G_{X^rX^r}|_j$ are of the same sensors, but during different time frames, which gives energy relation between different patches. This allows to match energetical component of j patch $G_{X^rX^r}|_j$ to k patch $G_{X^rX^r}|_k$. A complete derivation of PreGER multi-patching approach is given in author's earlier work [37].

1.3. Vibration sensors

Piezoelectric sensors

Common type of vibration sensors utilized in OMA applications are based on piezoelectricity. These sensors are accelerometers, Lead Zirconate Titanate (PZT) among others. Piezoelectric sensors are the most popular choice in SHM communities due to their direct and inverse piezoelectric properties allowing using them both as sensors and actuators [38]. Cheap piezoelectric sensors can be embedded into composite laminates thanks to advances in flexible printed circuit board (FPCB) technologies [39]. The smallest cracks accurately detected by embedded PZT (lead-zinc-titanate) sensors were of 0.1 mm order [40]. An advantage of using an active piezoresistive sensor approach with respect to passive one is the ability to monitor both, static and dynamic loading. Passive systems, on the other hand, can only measure signals produced by dynamic loading [41].

There are two approaches to the active sensing mode [38]. The first is *electromechanical impedance* technique, where the application of alternating voltage to the transducer induces mechanical deformations of the structure sensed by the sensor. The relation of electric impedance of a PZT element to a mechanical impedance of a structure allows for direct monitoring of mechanical properties of a host structure [42]. The second is *wave propagation* method, where piezoelectric actuators are driven with a defined shape and frequency of a pulse signal generating guided waves in an ultrasonic range. These waves are propagating on the surface of the structure and are sensed by other sensors. The acquired responses are then compared to baseline signatures and the differences are supposed to contain information on damage [43].

Piezoelectric film sensors

An elastic lightweight plastic film possessing piezoelectric properties was invented in 1969 by Kawai [44]. It was proposed to be used as a sensor for dynamic structural measurements. The film is made of a polarized semi-crystalline fluoride polymer called polyvinylidene fluoride (PVDF) [45], [47], [47]. PVDF films are available at a range of different sizes. A piezoelectric film transducer glued to a structure is shown in Fig. 1.5. This is a good candidate for optimal sensing solution in OMA, as will be shown further.

The comparison of the effectiveness of piezoelectric PVDF films and other popular sensor choices in SHM communities, namely, PZT, accelerometers and optical FBG sensors is given in Table 1.1. The merits and shortcomings of these sensors are summarized relative to the PVDF sensors.

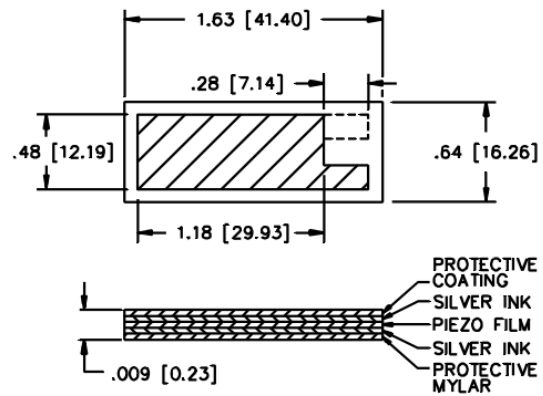
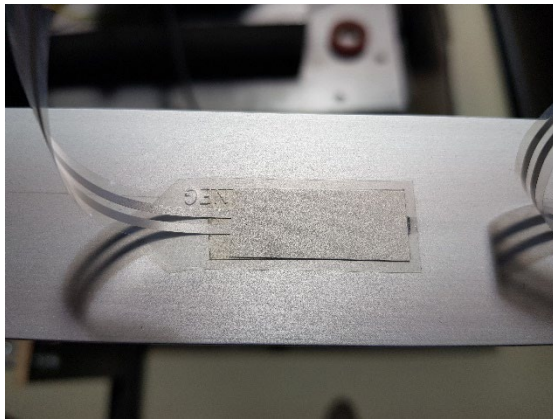


Fig. 1.5. Piezoelectric PVDF film transducer for vibration measurements [48].

PVDF material is superior to materials of other sensor types in numerous ways [47], [48]:

- Wide frequency bandwidth (10^{-3} to 10^9 Hz).
- Large dynamic range ($6.9 \cdot 10^{-4}$ to $6.9 \cdot 10^{10}$ Pa).
- High elasticity (2-4 GPa compared to 43 GPa for PZT).
- Low density (1780 kg/m^3 compared to 7500 kg/m^3 for PZT).
- High dielectric toughness – can withstand strong electric fields ($75 \text{ V}/\mu\text{m}$), where most of piezoelectric ceramic materials become depolarized.
- High mechanical toughness and impact resistance (10^9 Pa to 10^{10} Pa).
- High chemical stability – resistance against humidity ($< 0,02$ % moisture absorption), most of chemical substances, oxidizers and intensive UV radiation.

Table 1.1

Comparison of performance of PVDF film sensors and other popular sensors in SHM applications [49], [50], [51], [52].

	PZT	Accelerometer	FBG
Advantages	Better electromechanical characteristics, Higher working temperature, Static measurements possible, Well-developed calibration methods.	Better impact resistance, 3D accelerometers allow for 3D measurements, Mature technology, Possible shielding from electromagnetic interference.	Low electrical conductivity (shielding against electromagnetic interference and lightning), Corrosion and water resistance, Different geometries available, Easily embeddable into structure, High signal-to-noise ratio and low signal attenuation, Distributed sensing easily achieved with multiplexing.
Disadvantages	Higher density, Lower elasticity, Brittleness, Toxicity of lead, Expensive auxiliary equipment, Insufficient dynamic characteristic that needs to be compensated.	Lower elasticity, Mass loading reduces accuracy of modal parameter estimation, Non-negligible size may affect aerodynamic performance of a structure, Cannot be embedded into structure, Useful only for vibration measurements, Higher cost.	Fragile protective acrylate fibre coating, Temperature compensation may be needed, Operating frequency range is insufficient for most industrial applications, Considerably higher cost.

Sensing based on piezo-film sensors is a cost-effective SHM solution. They are much cheaper (about 10-15 euros/piece) than accelerometers which, for industrial applications, can cost hundreds of euros [53]. Accelerometers typically also induce mass loading to the structure and have a non-negligible size, thus affecting the structure's modal and aerodynamic properties.

This is more of an issue in aerospace sector, where lightweight structures are normally being tested. On the other hand, piezo film sensors measure deformations in longitudinal direction (compression/stretching), which is beneficial in many cases. The films are also lightweight and

can be glued tightly on the surface. Furthermore, if only a dynamic component of deformations is to be measured, advanced piezo films can be employed which don't require balancing circuits like, for example, Wheatstone bridge for resistive strain gauges. Moreover, PVDF film sensors can be produced with different shapes and attached to surfaces with commercial adhesives [48].

Shielded sensor datasheet [54] reports that PVDF films can be bonded to the surface with a double-side adhesive. This capability makes the PVDF film sensors significantly easier to mount on the structure compared to other sensors. Moreover, with this surface bonding, the PVDF films can be mounted and removed from the surface multiple times [55]. Compared to acceleration measurements, the dynamic strain measurements are proven sensitive to small local damage [56], [57], [58], which is another reason to employ PVDF film sensors instead of accelerometers in the SHM framework.

The downside of PVDF film material is [46], [59], [60]:

- Low electromechanical characteristics
- relative permittivity: 12 compared to 1200 for PZT;
- d_{31} constant: 23×10^{-12} C/N compared to 110×10^{-12} C/N for PZT.
- Lower maximum operating temperature (85 °C compared to 135 °C for a copolymer film).

Several studies compared structural response measurements performed with a PVDF thin film sensor and accelerometer [45] or strain gauge [46]. Authors concluded that spectra obtained from PVDF measurements contained more noise, particularly, in the lower frequency region. This effect may be due to poor electromagnetic shielding of the PVDF sensors. Several other sources reported the sensitivity of PVDF film sensors to electromagnetic interference [55]. The electromagnetic shielding of PVDF film sensors can be improved by folding the film and encasing it in a moulded plastic housing [54].

An important study on the sensitivity analysis of PVDF film sensors has been done by thesis authors' colleagues [61]. The results showed that an average sensitivity of these piezo films at room temperature of 25°C is 30.2 V/% or V per strain unit. In practice strain of an arbitrary vibrating structure results in tens and hundreds of mV. The 3 standard deviations of normal sensitivity spread of these sensors between 50 samples is 4.94 V/%, which is 16%. The study showed, that piezo films change their sensitivity depending on the ambient temperature. At 45°C the sensitivity was 19.1 V/%, while the spread was very similar 4.44 V/%, which constituted 23% when related to the mean sensitivity at this temperature. It was concluded that these sensors can be used for structural health monitoring purposes. However, the fact that sensors have a considerable spread of around 20% (also stated by the manufacturer) does not allow to directly compare modal shapes between different structures. It does allow SHM for an individual structure, assuming that the sensitivity of the sensors does not significantly change with time.

Embedded sensors in composites structures

In the case of composites, like glass fibre reinforced plastics GFRP, embedment of sensors has its advantages from SHM point of view. It allows to create a uniform structure, which is especially important for aerodynamic structures, like wind turbine blades or aircraft parts. Most common used types of sensors are piezoelectric, fibre optic and combination of those.

Popular examples found in literature of embedded PZT layers are SMART® layer [62], [63] and HELP® layer approaches [64], which imply the embedment of a flexible layer containing piezoelectric sensors. Scheme of SMART layer is shown in Fig. 1.6(a). Piezoelectric sensors are integrated into thin flexible polyimide dielectric FPCB (thickness 0.05 mm to 0.25 mm) with an etched copper circuit on top [65]. With the automated FPCB production process it is possible to, firstly, automatize the embedment of a whole sensor network at a time, secondly, to minimize the scatter of characteristics not only for each sensor, but also for a diagnostic layer as a whole, providing uniform sensor response. Thirdly, electrical insulation properties of FPCBs make it possible to prevent the electrical shortening of circuitry induced by carbon fibres. Lastly, the elastic properties of FPCBs allow for flexible bending without breakage [62]. Another solution is described in a study by Melnykowycz et al. in [66], where so-called active fibre composites (AFCs) were manufactured by incorporating longitudinal PZT fibres in a composite epoxy matrix situated between two electrodes (see Fig. 1.6(b)). Authors argued that this design is superior to traditional bulk PZT wafers, since this configuration optimizes crack propagation, where load is transferred from fibres to matrix. On the other hand, common PZT wafers are brittle and prone to cracking [67] rendering them unfunctional decreasing the overall

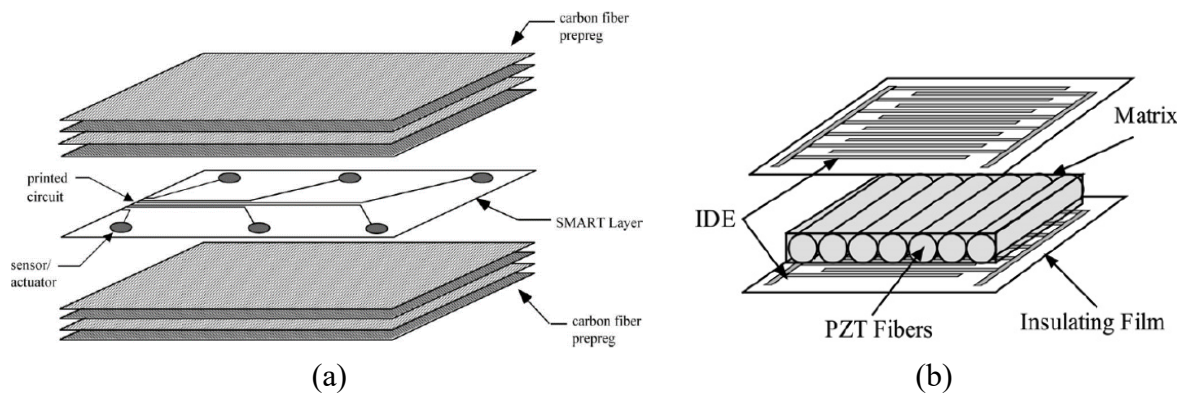


Fig. 1.6. Embedded piezoelectric sensor solutions – (a) SMART® layer [62]; (b) Active Fibre Composite setup [66].

performance of such damage monitoring system.

In [65], a 3D diagnostic SMART® layer was fabricated into a complex shape using resin transfer moulding to be applied to a portion of composite foam core sandwich automobile side frame. The layer consisted of 50 PZT sensors with an average spacing of 175 mm. First, a 2D version of the SMART layer was fabricated projecting the 3D locations of the sensors in the plane and then the mould was applied to obtain the complex 3D shape (Fig. 1.7).

Electrical connection is often realized through conductive epoxies or metals with low melting temperature (solders). Hence, compared with optical fibres, the precision required for electrical connectors is relatively low. Therefore, a connection to fully embedded electrical devices could be performed manually after the manufacturing phase of the composite itself. The electrical conductive circuitry can be machined as small channels or as blind holes, which are then filled with connecting studs [68].

Embedded fibre optic sensors

Fibre optic sensors (FOS) have gained popularity in SHM community (load monitoring and damage detection) owing to their many advantages over other techniques. For example, significantly higher signal to noise ratio and signal transmittance distance, reducing the need for localized signal amplification; safety against lightning due to very low electrical conductivity (crucial for wind turbine blade long-term monitoring), immunity to electromagnetic interference, light weight, small size, corrosion resistant and more stable performance in the long-term [69], [70], [71].

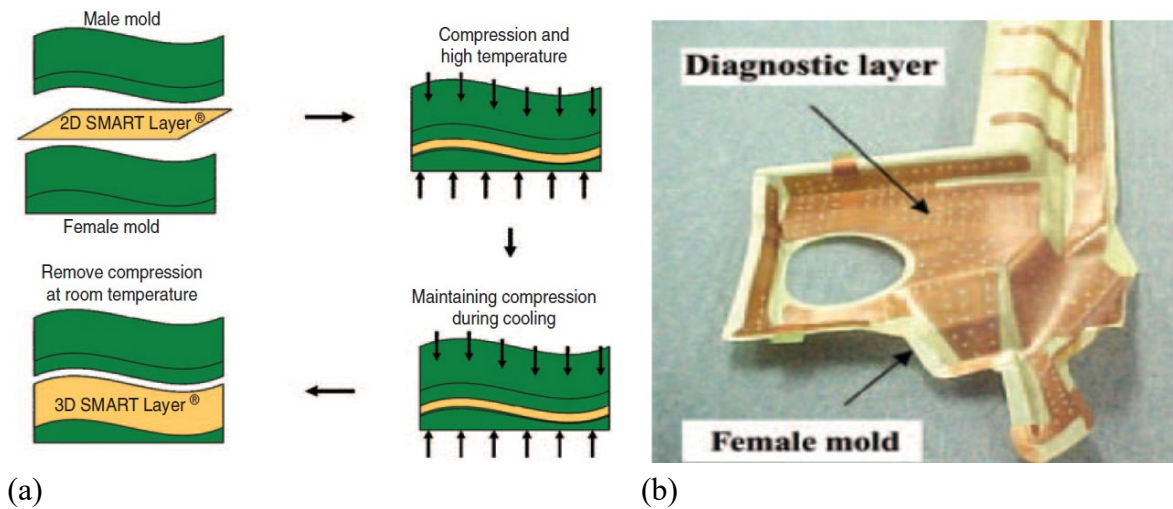


Fig. 1.7. 3D SMART® layer for diagnosis of composite structures – (a) formation process using resin transfer moulding; (b) photograph of an actual layer.

Separate category of FOS are fibre Bragg grating (FBG) sensors. For FBGs, calibration is simple because the response to strain and temperature has a wide linear range; multiplexing allows to accommodate numerous sensors into one fibre allowing for distributed strain monitoring; FBGs can either be surface mounted or embedded within the structure during the manufacturing phase [72], [73], [74], [75]. Frövel et al. in [72] argued that a strain gauge network comparable to FOS network of 15 FBGs in monitoring capacity (for strain monitoring in 6 m wing span, 40 kg of payload UAV) would weigh 10 times more – 500 g compared to 50 g. FOS are also liquid impermeable making them attractive for marine applications, which was confirmed by study of Yeager et al. in [76], where embedded FBGs were working satisfactory after 7 weeks of test article immersion into water bath at room temperature. Apart from strain and temperature, the embedded FOS can be used to monitor oven cure, external interactions and manufacturing flaws [77].

Disadvantages of embedded sensors in composites

Despite its many advantages, sensor embedment and a full sensor monitoring system may have some problematic issues. As study in [62] shows:

- Embedded sensors in general require excessive labour resources for installation.

- In the case when sensors are not integrated as a whole network, but rather individually, they might exhibit non-uniform response. Differences in sensor readings may arise due to local differences of surface roughness or boundary conditions.
- The sensor response may vary in time yielding inconsistency in sensory readings and thus failing the whole monitoring process.
- Most importantly embedded sensors can have impact on the host structure. Such effects include interlaminar stress concentrations and strain transfer from material to sensors.

Specific sensor type oriented problems for piezoelectric sensors are:

- Electrical insulation. The conductive nature of carbon fibres leads to short-circuiting of embedded sensors, which typically is the case at the stage of autoclave. High temperature and pressure (about 180 °C, 6 atm) leads to disintegration of the insulation material of panel containing piezoelectric sensors causing carbon fibres to be in contact with the sensors and shorting out the piezo electrodes [62].
- Electrical shielding. This is also an issue for non-embedded electrical sensors, but shielding adds extra bulk to the sensor system to be integrated [68], whereas non-embedded sensors shielding usually is not an issue.
- Issues of electromagnetic compatibility between host structure and electrical sensors limit the length of wire connections for embeddable electrical sensors before charge amplification is required.
- Thermal coupling. While the cure temperature of the PZT must be higher than the working temperature and curing temperature of the host composite structure by at least 100 °C, the thermal coefficients of expansion of the PZT and the host structure must be similar [39].
- In [78] authors showed that introduction of electronic components on a FPCB circuit causes cracks from resin rich pockets, primarily at the edges of the circuit boards. Semiconductors and soldered junctions are also subjected to cracks, which causes sensor failure before structural failure.

For fibre optic sensors disadvantages of embedment into composite structures are following:

- The insertion point of optical fibres into composite has to be modified. The optical wire point of entry into a laminate composite is prone to breaking [79]. This point of entry can be either at the edge or on the surface of a composite. Some solutions exist, however: either terminate the optical lead with a connector at the physical border of a composite [80] or apply a special feed-through mechanism [81].
- Optical fibres need to be either protected or strengthened. In many cases, the protective acrylate fibre coating is removed [77] either mechanically or by application of solvents [82]. Protective measures may include special supporting structures for bare optical fibres containing FBGs, which is oftentimes not possible to realize in conjunction of monitoring the actual structure [77]. Authors in [82]

argued that strengthening of optical fibre could be achieved by etching or healing. The curing process of aerospace grade composite materials requires putting the specimen into autoclave and heating to temperatures often exceeding 200 °C, which breaks down the acrylate structure of the optical fibre coating. This, in turn, damages the optical fibres and decreases the quality of coupling between optical fibre and host material [68].

- FOS are often insensitive to cracks propagating parallel to the optical fibre orientation [83].
- Some orientations of optical fibres can degrade the compressive capacity of composite laminates by about 70 % for strength and 20 % for stiffness [84]. Optical fibres should be aligned in the same direction as reinforcing fibres in a composite material to avoid resin rich “pockets”, high concentration of which decrease mechanical performance of material [68].
- Gratings are oftentimes non-uniformly strained for the embedded FBG sensors due to curing processes, leading to *chirping* – distortion and broadening of the reflection spectrum [85] causing poor signal-to-noise ratio.
- Non-homogeneous adhesion along the grating of FBG sensors contributes to non-linear sensor response leading to measurement uncertainty [86]. Surface area and shape of the optical fibre may also influence the quality of adhesion [87].
- FOS require temperature compensation [68]. Compared to surface-bonded strain sensors, it is not straightforward to introduce a reference sensor decoupled from strain sensing as all embedded sensors are surrounded by host material. Instead, extrinsic supplementary devices must be mounted over FBGs, like loose fit sleeves, which add bulk and extra joints to the whole system.

For the scope of this thesis sensor application shall be surface-mounted and sometimes with added protective layer – a hybrid between surface-mounted and embedded sensors.

1.4. Harmonics extraction

Natural excitation of structures in operation can be also harmonic in nature. This is the case for wind turbines or any machinery with engine and rotating parts. The harmonics arise from rotational movement of engine parts, bearings, shafts and so on. Recorded output responses contain both structural modes and harmonics, which quite often are indistinguishable from each other. There are methods to identify and extract harmonics to improve modal analysis.

One interesting approach for harmonics identification is presented by Brincker et al [88]. It is based on probability density function analysis of supposed modes. Normally, structural modes have a Gaussian probability density distribution, while harmonic response has two distinct peaks at the value of harmonics amplitude, as shown in Fig. 1.8.

Authors in [88] were able to successfully identify harmonics, but not computationally separate them from structural response signal. For this harmonics extraction is needed.

One of widely used harmonics extraction methods is Time Synchronous Averaging. This technique is used for obtaining periodic information from a given signal, which is widely used

for machinery condition diagnostics [89]. For structural health monitoring purposes TSA is applicable in determination of periodic component. Time synchronous averaging is a signal processing technique that extracts periodic waveforms from noisy data [29]. A tachometer signal is necessary for order tracking, although, some techniques exist, which allows production of a reference signal for TSA without direct acquisition of tachometer signal [90]. Based on the existing literature the periodic component extraction mathematical formulation was developed in the scope of the presented thesis, which is shown in Section 2.6.

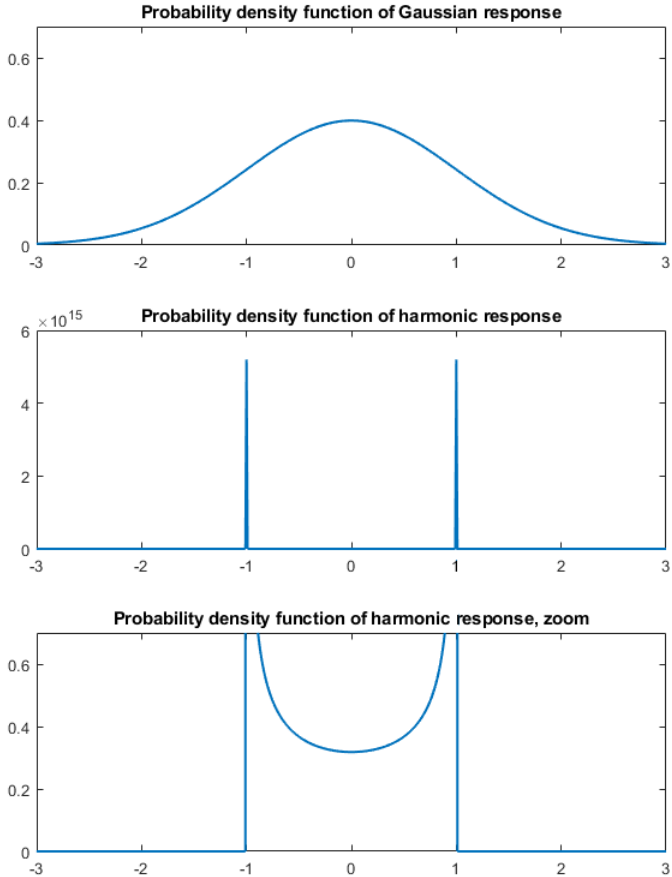


Fig. 1.8. Theoretical probability density function, top: structural response, bottom: harmonic response.

1.5. Structural damage identification

OMA based structural damage identification utilizes an assumption that the analysed system should be linear and not change with time. This allows to evaluate structural responses for potential damage. Decision on the state of structural integrity usually cannot be made by direct examination of raw measurements of structural response. Instead, the information on damage is contained in damage-sensitive features (DSFs), extracted from these responses [91], [92]. In OMA procedure, these features are modal-based. The most common modal DSFs are natural frequencies of the analysed structure. Natural frequencies and damping ratios are a global structural parameter. Hence, as opposed to accurate mode shape identification, dense sensor

network is not required to identify natural frequencies and damping ratios. However, unlike the damping ratios, natural frequencies are also more robust to noise [93]. Natural frequency analysis is also one of the most mature and cheapest approaches for damage detection. Natural frequency check is also widely applied in detecting structural deviations from the designed values. For example, in wind turbine foundations [94]. On the other hand, in [95] it was stated that the natural frequencies are not an optimal indicator for damage detection in composite WTBs. Source in [91] reported that the natural frequencies are more sensitive to environmental factors than to the actual damage.

Structural mode shapes contain spatial information on damage where high order modes shapes have higher sensitivity to damage. Mode shapes are less sensitive to the effect of temperature and humidity compared to natural frequencies [91]. DSF based on mode shapes is *modal assurance criterion* (MAC) defining the relative correlation between mode shapes (from 0 to 1), for example between shapes of the same mode in healthy and damaged states. It is calculated as [96]

$$\text{MAC}(\{\phi_i\}, \{\phi_j\}) = \frac{|\{\phi_i^T\}\{\phi_j\}^*|^2}{(\{\phi_i^T\}\{\phi_i^*\})(\{\phi_j^T\}\{\phi_j^*\})} \quad (1.13)$$

where $\{\phi_i\}$ and $\{\phi_j\}$ are different mode shape vectors. Usually, MAC is plotted as a matrix where mode shapes from one set are compared to the same mode shapes from another set. The correlation values close to unity indicate that mode shapes are similar. An example of MAC comparing simulated and experimentally identified mode shapes of a WTB is illustrated in Fig. 1.9(a). Damage assessment can be performed by comparing mode shapes of a healthy structure and the same structure containing damage using the MAC. Another widely applied mode shape based DSF is a *coordinate modal assurance criterion* (COMAC) comparing each degree of freedom i of L number of mode shape vector pairs [97]

$$\text{COMAC}(i) = \frac{\sum_{l=1}^L |\{\phi_1\}_{i,l}^T \{\phi_2\}_{i,l}|^2}{\sum_{l=1}^L \{\phi_1\}_{i,l}^2 \cdot \sum_{l=1}^L \{\phi_2\}_{i,l}^2} \quad (1.14)$$

An example of COMAC comparing two mode shapes of a WTB for all translational and rotational degrees of freedom is shown in Fig. 1.9(b).

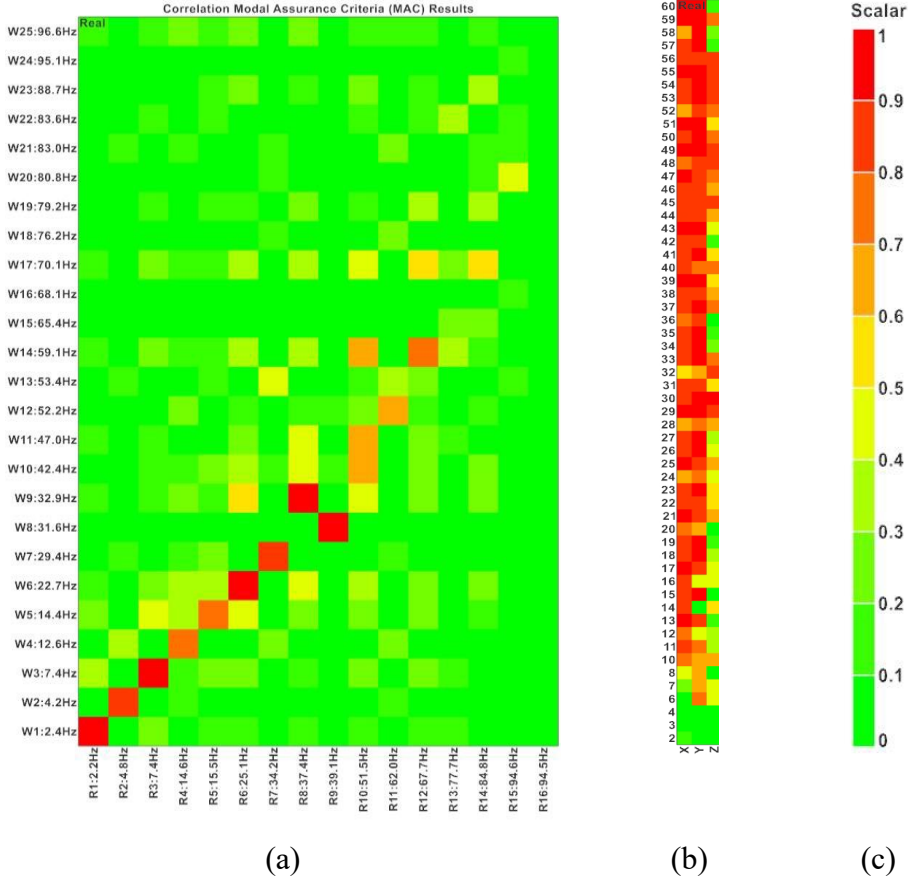


Fig. 1.9. Mode shape DSFs applied for quality check of the identified mode shape vectors of composite full-scale WTB – (a) MAC; (b) COMAC; (c) colour scale for both, MAC and COMAC [98].

The idea of using a mode shape as a DSF is to exploit the fact that damage induces changes in amplitude distribution of the mode shape, and sometimes also spurious peaks. The drawback of utilizing the mode shapes and higher order mode shapes, in particular is the high density of sensor grid necessary to achieve a sufficient accuracy of mode shape identification. Furthermore, the process of mode shape identification is not fully automatic [91].

Other modal-based DSFs reported in the literature are derived from the power spectral density (PSD), where the entire bandwidth is divided into frequency bands $[f_1, f_2]$ around each natural frequency. The width of the frequency band can be set as 10 % to 20 % of the value of the natural frequency in question. The DSFs are calculated only for the intervals $[f_1, f_2]$. These DSFs are characteristics of average value and spread of frequency in the frequency band, for example, frequency centre FC, the root variance frequency RVF and peak indicator I_{peak} were defined in [91].

$$FC = \frac{\int_{f_1}^{f_2} f \times s(f) df}{\int_{f_1}^{f_2} s(f) df} \quad (1.15)$$

$$\text{RVF} = \sqrt{\frac{\int_{f_1}^{f_2} (f - \text{FC})^2 \times s(f) df}{\int_{f_1}^{f_2} s(f) df}} \quad (1.16)$$

$$I_{\text{peak}} = \frac{\sqrt{3} \times \text{RVF}}{\text{FC} \times (f_2 - f_1)} \quad (1.17)$$

Other DSFs can be based on transmissibility. Transmissibility is calculated as a ratio of two response spectra measured at degrees of freedom i and j as [99]

$$T_{i,j}(f) = \frac{Y_i(f)}{Y_j(f)} \quad (1.18)$$

where Y denotes either displacement, velocity, acceleration or strain. No assumptions about the nature of excitation forces are necessary using transmissibility function. The forces can be arbitrary, however, the frequency band of interest has to be consistently excited [100]. DSF as a sum of transmissibility in a frequency range of interest is reported in [101]

$$ST_{i,j} = \int_{f_1}^{f_2} T_{i,j} \times df \quad (1.19)$$

The concept of selecting the DSFs only in the frequency bands around the natural frequency and not over an entire bandwidth of the PSD is beneficial in itself as a measure of data reduction. Moreover, for closely spaced modes, the number of DSFs can be further reduced by merging the frequency bands. This approach is also effective in suppressing noise in the extracted DSFs.

In the context of this thesis comparison of all three modal parameters is performed as the main tool for damage identification (see Sections 3.1 and 3.2). Also, an alternative damage identification method is introduced in Section 3.3, which utilizes modal data in the measured response, but does not require estimation of modal parameters. But first, the reader is introduced with the proposed SHM system.

2. STRUCTURAL HEALTH MONITORING SYSTEM

2.1.SHM related problems

External factors

The damage detection of an OMA based SHM system is based on the change of modal properties of a structure. But modal properties are influenced not only by the change in stiffness, mass or damping (internal factors), but also by loads, temperature and other external factors. This can create false positive alarms, thus degrading SHM effectiveness. For example, modal parameters of a bridge change due to temperature variation, as well as metal fatigue. Change of rotation velocity of a wind turbine also change modal parameter of a blade, due to resulting difference in centrifugal force.

Skilled personnel requirement

After measurements and data processing any trial OMA based system gives a set of modal parameters for some number of modes. When dealing with structures, which are more complicated than simple structures (beam or plate), number of detected modes can be quite large. For analysis and interpretation of such modes highly skilled and experienced personnel is required. Necessary skills include knowledge of physics, oscillation theory, material behaviour, modal analysis and so on. Mass application of OMA based system is complicated due to the need of subjective interpretation of results.

Methodologies for quantitative evaluation of integral modal parameters of entire structure and healthy state boundaries definition do exist, but few practical applications were demonstrated.

Sensors costs and size

Common type of sensors used in OMA are accelerometers, which are robust and precise. However, they are quite expensive (100 – 1000 \$), in some applications they require thread fixation, their size and weight (including shielded coaxial cables) are able to have influence on modal characteristics of a structure and on operations of a facility. For example, it is not feasible to put tens of accelerometers on a wind turbine blade – this will distort air flow around the blade, as well as add extra weight. Embedding the accelerometers into structures is technologically complicated and limited. Other type of sensors, deformation sensors, do not have most of the mentioned limitations – they are cheap, applied on the surface of a structure, are plain and light, together with connecting wires can be covered with protective layer, creating an integral element with the measured structure. Two types of deformation sensors can be used – strain gauges and piezo film sensors. Strain gauges are very useful for testing structures in laboratory conditions, but these are hard to apply for OMA. These sensors require bridge connection and balancing, so each sensor needs single dedicated channel in a specific data acquisition system. Large number of data acquisition channels increases SHM system costs. Utilization of accelerometers and strain gauges limits SHM system development and application diversity.

All mentioned problems have a cumulative effect, which results in high costs of production and application of SHM systems, not to mention the size and weight of sensors. High cost of an SHM system reduces interest from commercial sector, and consequently do not allow mass usage of SHM systems. Sensor's size and weight is also crucial for aerodynamic applications.

2.2.SHM problems solutions

This thesis is proposing an overall approach to an SHM system development process. This process can be divided into the following tasks:

1. Choosing the structure to be monitored, acquiring its dimensions, functional properties.
2. Selection and application of a sensors network.
3. Acquisition of healthy state vibrational data with influence factors, formation of a healthy state data base embedded in *Modal Passport* (discussed further).
4. Periodic acquisition of unknown state vibrational data during structures life cycle (monitoring), comparison of newly acquired data to the healthy state data.

Above the term of *Modal Passport* is introduced. This is a complex of methodological, algorithmic and software solutions, which includes modal description method of typical monitoring objects' structure, primarily internal and external factors influence functions on structures modal properties. Another feature of modal passport is a universal method for monitoring of an individual object, using typical modal properties and influence functions, which allows:

- Integrated estimation of structural condition as a result of a measurement,
- Structural condition healthy (reference) state boundaries definition,
- Fault detection.

As a solution to the skilled personnel requirement and to reduce the complexity of the SHM system data processing steps a Modal Field Comparison Method is introduced in Section 3.3. This method processes vibrational responses based on singular value decomposition without modal parameter estimation. This simplified method is referred to as an intermediate step for fast assessment of the structures health if needed.

The solution to the high cost of sensors is application of piezo film deformation sensors, which are described in detail in Section 1.3. These sensors lack the disadvantages that are identified for accelerometers and strain gauges, and are widely used for industrial purposes, mainly for alarms, signalization and other security solutions. Just like strain gauges, piezo film sensors are cheap, light, and can be integrated into a structure. Piezo films do not require bridge connection and balancing. Industry standard piezo films are produced with very small tolerances in geometry and size, however the accuracy of sensitivity has $\pm 20\%$ deviation [60]. The size of a piezo film sensor used in current studies is 16 x 45 mm and 28 μm thick, although other sizes are available. The weight of a single sensor is smaller than 0.1 g. Application of piezo films also allow using the same data acquisition systems (DAQ) as for accelerometers, which tend to be affordable, mobile, and robust for field use. Many industrial laboratories have such DAQ systems that may support and simplify piezo films application. Wiring between

piezo film sensors and DAQ can be done using multiplexing approach, which reduces amount of input channels and brings costs further down. Multiplexing is achieved by using switches or patch bay to connect signals from sensors to DAQ input in patches, making measurements for different zones of the structures sequentially, which is shown later in Section 4.4 and 4.6. Piezo films are produced by spraying conductive layers, which allows production of not only sensors themselves, but also sensors networks and its parts as a single product (batch). This in its turn brings possibility of integration of piezo film sensors into composite structures. Sensor batches installation on a structure is easier and faster than installation of numerous individual sensors and their wiring systems. Therefore, sensor batches are preferable for serial production and more usable for massive application on structures.

Implementation of said solutions will allow to bring SHM system costs down and simplify its application.

2.3.SHM system development steps

The proposed SHM system technology would ensure the development, serial production and application of a monitoring system for technical state of various structures for typical equipment (objects) operating under different operational conditions.

Typical objects in this context are industrial, transport or energy serial equipment, which consists of structural elements. For such structural elements, it is important to observe the technical condition for safety and economic purposes. SHM system is designed to detect damage in an individual structure from a set of measurements of this structure. Damage detection in a structure from a set of monitored structures is not pursued here, as early studies showed that the large scatter of damage sensitive parameters due to changes in mass, geometry as well as other material properties, significantly reduces reliability of the SHM system.

In order to successfully monitor structural condition, each structure must have a built-in SHM system, which reads the vibration data and sends it to the workstation (computer). Next, the operator performs Operational Modal Analysis (OMA), evaluating modal parameters of each structures sample. The resulting modal parameters, together with recorded external influence factors such as static loads or rotational velocity (blades), shall be entered by the operator into the database. This database provides application of the modal passport technique (see later in Section 3.1) storing the results of previous measurements of these structures. Such a database also stores the reference modal parameters of an intact structure and the influence functions that are typical for such structures. A special damaged sample recognition algorithm later analyses the database and recognizes measurements (data samples) that showed sufficiently different modal parameters at given external factors compared to the reference. This stage is called damage identification. Next, the operator will be able to perform an in-depth analysis of modal parameters of a particular damaged sample in order to decide on the significance of the damage, possibly localize damage from analysis of mode shapes. This allows to further plan actions with the given structure – repair, replace or perform no action, if the defect is not significant.

Based on the above description, two components can be defined for the SHM system:

- A measuring system, which in turn consists of:
 - Sensors and cables on the structure
 - Data transmission system to the computer
- Data storage, processing and analysis part:
 - OMA software
 - Modal passport with reference state data and influence functions

Modal passport formation for typical structures consists of the following steps:

1. Build an FE model of a structure.
2. Calculate modal parameters for the FE model, taking into account the real-world boundary conditions, loads, temperature regimes and other factors. FE calculation results are required to optimize sensor network, select test settings and for modal identification.
3. Create a sensor network based on the results of the FE modelling. Optionally, use optimization algorithm for sensor placement [102].
4. The real structure is to be equipped with the developed sensor network.
5. Prepare a measuring system, including cables, connectors, a data acquisition device with a computer, sensors for load, temperature and other factors.
6. Perform operational modal analysis of the structure, record the obtained modal parameters and external factor indicators in one database (modal passport). Where possible, these measurements shall be carried out in a controlled environment, gradually changing the external influence factors.
7. Obtain damaged state data with modelling approach. Damage modelling allows to foresee modifications in modal parameters due to possible future damages:
 - a. A random test situation shall be repeated on the FE model and it shall be verified that the FE model and test results are similar. In case the results do not match, necessary adjustments shall be made to the FE model.
 - b. Introduce structure-specific damage into the FE model, perform calculations and save obtained parameter sets, including modal parameters and external factors.

For further process an operator is taking estimated modal parameters from new measurements of the same structure or other structures of the same type, and, using modal passport, performs evaluation of the structural condition. The measurement results are compared to the modal passport data using one of the damage detection algorithms, presented in Section 3.2 or alternatively using raw data by the algorithm from Section 3.3. The result of the evaluation is usually a statement whether the structure is healthy or damaged.

The diagram of the SHM system prototype is shown in Fig. 2.1. The full description of the system is presented further.

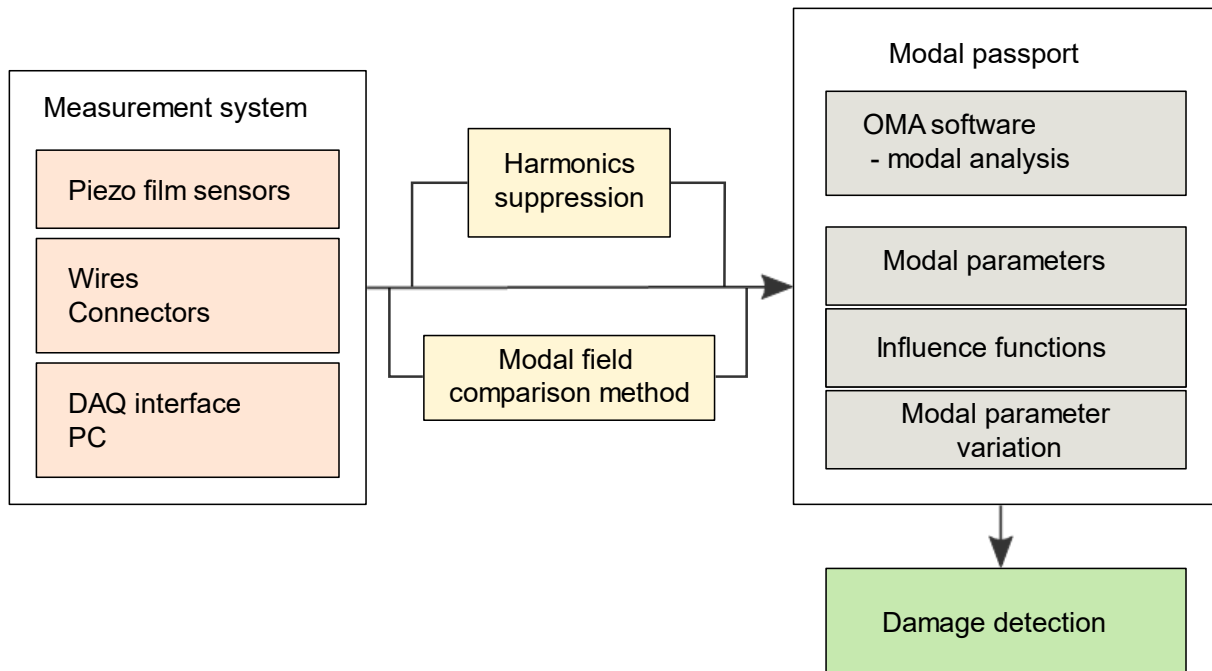


Fig. 2.1. Diagram of the SHM system prototype.

2.4. Application of deformation sensors for OMA

Available OMA applications, which determine the modal parameters of the operating object, deal with acceleration signals, but not deformation or strain. To use deformation sensor data, it is necessary to justify the relationship between acceleration and deformation parameters.

Deflection at a Pure Bending

The analysis is carried out on the example of a solid beam subjected to bending under the influence of an external load. The vibration and deformation parameters of this beam can be measured using an accelerometer and a deformation sensor both mounted on the beam surface. Displacement of any surface point of bending beam is determined by the curvature of so-called elastic or neutral line of this beam. This curvature depends on longitudinal deformation of the surface layers.

For convenience let's consider an example of a pure bending of the beam, i.e., under the action of a constant bending moment along its length. Considering relations within static bend, under certain limitations it may be applied to the bending oscillations of the beam. Bending of the beam under the bending moment leads to normal tensile stresses or compression in cross section of the beam depending on the sign of curvature of the neutral line [103], [104]. Stress diagrams for loading illustrated in Fig. 2.2(a) shows the case of a simple bending under the action of a variable bending moment along the length due to the transverse load P. Fig. 2.2(b) shows the case of pure transverse bending caused by a constant bending moment only. A more complex case of stress distribution along the beam axis with a stable oscillation in the 2nd bending shape is shown in Fig. 2.2(c).

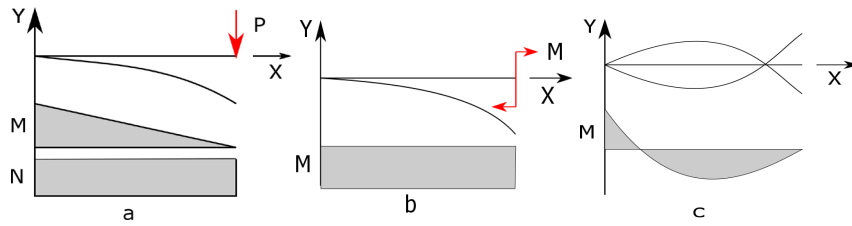


Fig. 2.2. Diagrams of bending moments of the cantilever beam in statics and dynamics: a) concentrated load; b) constant bending moment; c) inertial loads in stationary vibrations (2nd bending mode).

For a solid-state beam, as shown by experimental studies using the grid method [105], the cross sections (AA' and BB' in Fig. 2.3) that are flat without loads remain flat after their application.

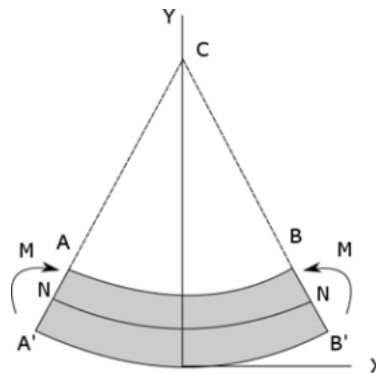


Fig. 2.3. Scheme of a beam in pure bending.

In this case, the longitudinal layers of the beam under the applied load are lengthened (A'B') or shortened (AB). The beam layer (NN) that separates the compressed layers from the stretched ones does not change in length and is called the neutral beam layer. For the case of pure bending of the beam, the hypothesis of flat sections is valid [106], according to which the longitudinal fibres do not exert pressure on each other. In the cross section of the beam, only normal tensile and compressive stresses occur in pure bending. The stresses are distributed unevenly along the height of the cross section, having zero values in the neutral layer (Fig. 2.4). Due to this unevenness, there is a curvature of the layers and the axis (neutral layer) of the beam. Based on the above, we can assume that all layers of the beam equidistant to the neutral one work under pure tension or compression, i.e., stress and strain in these layers are related by the ratio

$$\sigma_x = \varepsilon_x E_x \quad (2.1)$$

where ε_x – longitudinal deformations, E_x – elastic modulus.

Let's consider the stress distribution σ_x and deformations ε_x in layers across section in pure bending element of a cantilever (Fig. 2.4).

The relative elongation of the stretched layer located at a distance from the neutral layer will be determined by

$$\varepsilon_x = \frac{Y}{\rho} = k \cdot Y \quad (2.2)$$

where k – curvature, ρ – its radius, Y – distance from the neutral axis N to the center of the cross section of one of the stretched layers.

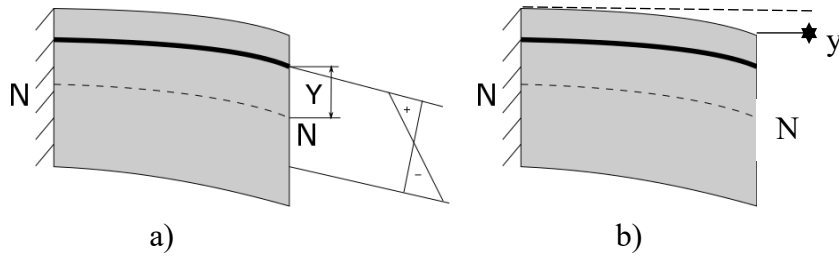


Fig. 2.4. Cantilever beam bending.

Substituting Equation (2.2) into (2.1) we obtain

$$\sigma_x = E \frac{Y}{\rho} = EkY \quad (2.3)$$

Thus, at pure bending of the beam both deformation and stress are distributed along the height of its cross-section according to the linear law, illustrated by the diagram in Fig. 2.3(a). Signs + or - correspond to strains and stresses of tension or compression in the layer. The relationship between the stress and the bending moment acting in the beam section at pure bending is established from the fact that in each cross section only the moment M acts, and the transverse forces N are absent (see diagram in Fig. 2.1(a)). Since the load in section F is determined by the stress integral over this section, we obtain

$$N_x = \int F \sigma_x dF = 0 \quad (2.4)$$

Then the moment M_y acting in the layer

$$M_y = \int F \sigma_x y dF = 0 \quad (2.5)$$

Substituting σ_x from (2.1) to (2.5)

$$M_y = \frac{E}{\rho} I_y \quad (2.6)$$

where I_y - axial moment of inertia of the section. Thus, the curvature of the neutral layer of the beam at pure bending is determined from (2.3) and (2.6)

$$\frac{1}{\rho} = \frac{\sigma_x}{EY} \quad (2.7)$$

$$\frac{1}{\rho} = M_y \frac{1}{EI_y} \quad (2.8)$$

Relation Between Displacement and Curvature

Let us consider the case when the force factors leading to a pure bend are unknown, but the distribution of transverse displacements Y along the longitudinal axis X of the beam $y = f(x)$ is known. From mathematics [107] it is known that the curvature of the curve is the limit to which the ratio of the angle between tangents to the curve at two nearby points to the length of the arc between these points tends

$$k = \lim_{\Delta s \rightarrow 0} \frac{d\alpha}{ds} \quad (2.9)$$

If the curve is given by an explicit equation $y = f(x)$, the formula relating the curvature to the equation of this curve will take the form

$$k = \frac{1}{\rho} = \frac{y''}{(1 + (y')^2)^{\frac{3}{2}}} \quad (2.10)$$

For a rigid beam its deflections in comparison with the length are very small and the value of $(1 + (y')^2)^{\frac{3}{2}}$ is close to one. In this case, approximately curvature can be determined

$$k = \frac{1}{\rho} = \frac{d^2y}{dx^2} = y'' \quad (2.11)$$

Taking into account the previously obtained equation (2.8) to determine the curvature of the neutral layer of the beam during bending, we can write:

$$\frac{1}{\rho} = \frac{M_y}{E \cdot I_y} = y'' \quad (2.12)$$

This equation establishes the relationship between the transverse displacements along the axis y (neutral layer) of the beam and the curvature of the rigid beam at pure bending. It allows to approximate the distribution of the curvature of the neutral layer of the beam by double differentiation of the deflection line equation of the curved axis of the beam. For an approximate estimation in the experimental study, the equation of the beam deflection line $y = f(x)$ can be replaced by the numerical dependence of the values of the beam surface displacement $y_s = f(x)$ on its neutral position (Fig. 2.3(b)).

Substituting the curvature value from formula (2.12) into expression (2.2), we obtain a formula describing approximately the relationship between the deformation of the surface layer of the beam and its displacement

$$\varepsilon_s = y_s'' \cdot \frac{h}{2} \quad (2.13)$$

where h – the thickness of the beam, and $h/2$ – distance from the neutral axis of the beam N to the centre of the cross-section of the surface layer.

Displacement and Deformations in Dynamics

Although deflections of vibrating bending beam and the neutral line in the static bending of the beam are similar, the use of the above expressions in relation to the parameters of the oscillating beam is limited by some restrictions.

First, the deflection of the vibrating beam is variable in time. To achieve similarity to static bending, it is necessary to measure the movements of the oscillating beam, synchronizing the moments of measurement with the phase of its extreme amplitude position. The displacements measured by such way turn out to be a time-independent function. Fig. 2.5 illustrates oscillation modes as the displacement distribution along the beam axis.

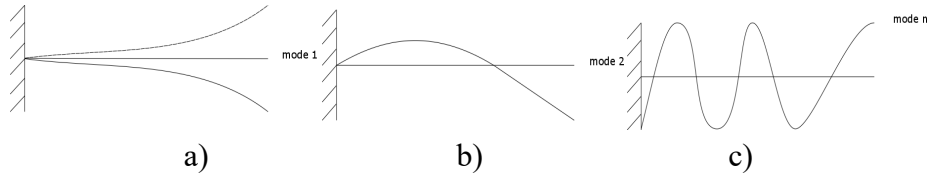


Fig. 2.5. Bending mode shapes of a beam: a)-1-st, b) – 2nd, c) – n -th.

The assumption about the equidistance of the bending lines of the surface layers and neutral layer of the beam is used. This assumption is justified by the theoretical possibility of applying to the oscillating beam such a combination of periodic transverse forces and moments, which leads to the form of oscillations similar to static bending. Based on the above assumptions it is possible to use the equations (2.1)-(2.13) for the qualitative assessment of the relationship between the deformations of tension and compression on the surface of the vibrating beam, from one side, and the curvature of its neutral line, from another.

It should be noted that the credibility of this approach for the oscillating beam is limited by zones of small gradients of the acting moments. The fact is that the diagram of bending moments in dynamics (Fig. 2.5(a)) does not correspond to the case of pure bending (Fig. 2.2(b)). The area of small gradients in this example is limited to a small area in the central part of the beam. In the work [108] experimentally on the example of the 2nd bending mode oscillation it was shown that the zone of the minimum (not more than 1%) change of the bending moment (and deformation) does not exceed 10% of the total length of the beam. Only in this zone, where curvature gradient is minimal, the stress-strain state in statics and dynamics can be considered almost equivalent and be described by formulas (2.7) and (2.8). For such zones of oscillating beam the formula (2.8) is applicable for estimation of neutral layer curvature and the formula (2.13) for its surface layer deformation. As far away from such zones, the reliability of the calculated estimates decreases.

The typical task of experimental studies of transport structures is to identify their modal properties. One of the approaches to bending modes identification of vibrating beam structure is based on application of so-called half-waves to the neutral line of the beam. The mode order is classified by the number of such half-waves along the oscillating beam. The presence of a half-wave is fixed by the antinode, near which the gradients of the bending moment are small. In this approach, the beam zones for which the above assumptions are valid, have been used to identify the mode. Thus, for the problems of identifying the bending modes, it can be assumed that the strain of tension or compression measured on the surface of the oscillating beam is determined by the second derivative of the distribution function of the transverse displacements of the neutral line of the beam and the distance from it to the surface layer. In the case of experimental studies, it makes possible to use the values of the measured surface deformations for natural modes identification of the beam.

If the thickness of the structure is negligible compared to other dimensions, then deformations are directly proportional to the second derivative of displacements.

Modal parameters estimation results in mode shapes which show not acceleration (although acceleration is the measured signal), but displacement. So the obtained mode shapes using

deformation signals from piezo film sensors would be simply 180° out-of-phase compared to displacement shapes.

2.5.Measurement system

The measuring system is a part of the SHM system, which is individually and permanently installed on the structure to be tested throughout its life. The measuring system consists of deformation transducers, wires, connectors and a data reading device together with a computer and software.

Sensors

The type of sensor used for the proposed SHM system is a polyvinylidene fluoride (PVDF) sensor, described in detail in Section 1.3. These films are elastic, light and have piezoelectric properties. Thanks to these properties, the deformation of the film leads to a change in voltage. Piezo film is located between two printed silver electrodes, forming a capacitor-like structure. Due to this design, the sensor is not able to measure static deformations, but this is not an issue for SHM. The particular sensor shown in Fig. 2.6 is 40 mm long, 16 mm wide and only $28\ \mu\text{m}$ thick.

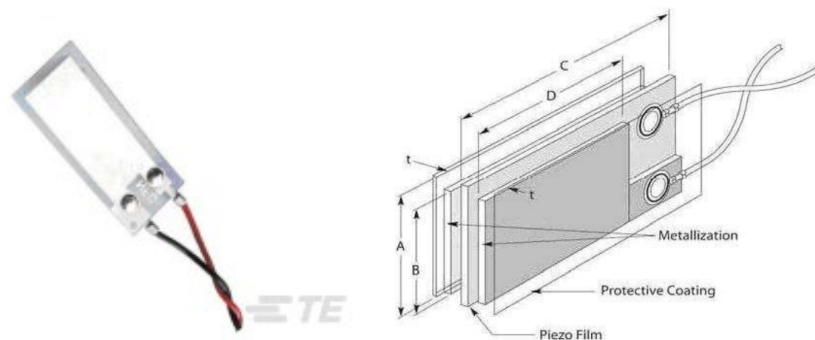


Fig. 2.6. PVDF film deformation sensor from TE connectivity [53].

The sensors are glued with the help of a double flexible adhesive tape (Fig. 2.7(a)). Other types of adhesives are suitable, as long as the adhesive is elastic after curing. The size of the piece of adhesive tape must coincide with the size of the transducer surface to ensure full adhesion to the surface of the structure.

Wires and connectors

Wires used for the SHM system are small diameter (0.25 mm or similar) enamelled copper wires (Fig. 2.7(b)). Wires are glued to the transducers using special two-component epoxy glue. The wires are applied to the surface of the structure using a narrow double-sided elastic adhesive tape and are soldered to a wire hub at the boundary of the structure (Fig. 2.9).

Piezo film sensor has a positive and a negative voltage output. Positive output is considered to be a signal output, negative one is connected to ground. All negative outputs are thus joined. The cable hub can also be realised as a cable connector, for example D-SUB type.



a)



b)

Fig. 2.7. a) Adhesive double-sided tape; b) Enamelled copper wire.



a)



b)

Fig. 2.8. a) Piezo film sensor with attached wires; b) two-component epoxy glue.

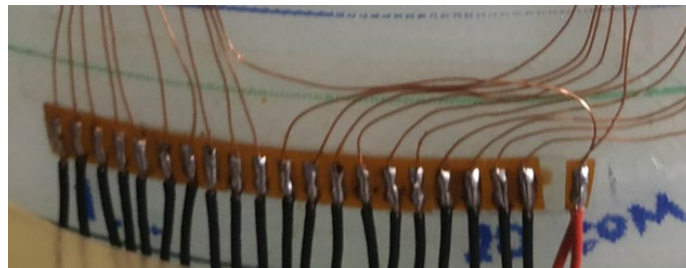


Fig. 2.9. Wiring hub at the boundary of a structure.

Data acquisition (DAQ) device

The primary role of a DAQ device is to perform analog-digital (AD) conversion of deformation signals. Most commonly, prior to the AD conversion, there is also a conditioning step – signal amplification and frequency filtering. *Brüel & Kjaer's LAN-XI Type 3053* or a similar type of *LAN-XI* module can be used as a DAQ device. The number of modules depends on the number of sensors. For example, with four *Type 3053* modules it is possible to measure 48 channels at the same time. Other manufacturers like *National Instruments*, *Siemens*, etc., also offer DAQ systems.



Fig. 2.10. DAQ devices: a) *LAN-XI Type 3053*; b) *CompactDAQ*.

2.6. Periodic component suppression

Problem formulation

It is important to eliminate periodic components (harmonics) before performing modal analysis, because these can be mistaken for identification of structural modes during signal analysis. Also, periodic components can mask structural modes in frequency range where the former dominate. Of course, the best way to deal with harmonics is to block them from being measured. Generally, it means shutting down rotating machinery on the structure. Obviously, this is undesirable, especially in energetics (power plants, electric motors) or navigation (airport and naval radars). So there must be a post-processing tool to suppress or extract harmonics before performing analysis of vibrational data.

Theoretical basis

Let systems frequency response be presented as $H(\omega)$, in which all necessary information about a system (e.g., any type of structure) is stored. The stochastic part of a response can be shown as

$$X(\omega) = H(\omega)F(\omega) \quad (2.14)$$

where $F(\omega)$ is the excitation force and $X(\omega)$ is the measured signal, without presence of any deterministic components. Note that in case of traditional OMA force function $F(\omega)$ (and its inverse Fast Fourier transform $f(t)$) is not measured nor controlled and it is assumed that the excitation force is spectrally uniform (white noise) and evenly distributed around the system. Often in reality this is not the case, which constitutes one of the limitations mentioned in Section 2.1.

Deterministic part in a simplified way, can be presented as

$$D(\omega) = \sum_{n=1}^N D_n e^{j\omega_n t + \phi_n} \quad (2.15)$$

where n denotes one of N deterministic components ($n = 1, 2, \dots, N$), and ω_n is the rotation speed of rotor or fundamental frequency of a periodic component. It is important to have periodic components frequency time function $\omega_n(t)$, e.g., recording of a periodic component,

as it can fluctuate and influence further signal processing. In reality this is supported with tacho probe signal.

Further extension of Eq. (2.14) is

$$D_n(\omega) = D_{n1}e^{j\omega_{n1}t} + D_{n2}e^{j\omega_{n2}t} + \dots + D_{nK}e^{j\omega_Kt}$$

$$D_n(\omega) = \sum_{k=1}^K D_{nK}e^{j\omega_Kt} \quad (2.16)$$

which basically means that periodic part is superposition of numerous harmonics. In case there is more than one periodic part then these parts can create intermodulation that results in extra harmonics,

$$D_n(\omega) = \left(\sum_{k=1}^K D_{nK}e^{j\omega_Kt} \right) e^{j\omega_0t} \quad (2.17)$$

Altogether, the periodic component of a vibrational signal on a structure with different machinery and/or EMI noise consists of separate polyharmonic periodic parts and their intermodulated harmonics, as shown in Eq. (2.16).

Combining Eq. (2.14) and (2.17), the true equation for harnessed signal is given as

$$X(\omega) = H(\omega)(F(\omega) + D_n(\omega)) \quad (2.18)$$

as deterministic periodical excitation is part of the excitation forces.

Now assume there are some experimentally obtained $D_{na}(\omega) \approx D_n(\omega)$. Extracting $D_{na}(\omega)$ from (3) will result in

$$X_p(\omega) \approx H(\omega)F(\omega) \quad (2.19)$$

and

$$x_p(t) = \frac{1}{2\pi} \int_{-\infty}^{\infty} X_p(\omega) e^{j\omega t} d\omega \quad (2.20)$$

where index p means ‘‘processed’’. Note that $X_p(\omega) \neq X(\omega)$ since the structure is responding to the forced periodical excitation and this response remains in the signal. Hence when one is referencing to extraction of a periodic component, this means suppression of the said component with sufficient efficiency.

Most commonly the signal enhancement technique is applied to suppress periodic components. The enhancement process based on fundamental frequency like rotation speed or other allows detection of all signal components related. As typical machine has more than one fundamental frequency enhancement process is repeated for each one of it. The resulting accumulated vector $d_{na}(t) = d_{na}^1 + d_{na}^2 \dots$, with the same length as $x(t)$, is subtracted from $x(t)$ and $x_p(t)$ is obtained.

2.7.Data processing and analysis

As was previously mentioned, the life cycle of the SHM system for a series of structures is divided into two parts:

- Formation of modal passport
- Monitoring

The formation of a modal passport is the process of creating a database in which the characteristics of the typical structure and dependence on external factors are measured and evaluated. By its very nature, it is the process of creating the content of the system, when the engineer performs OMA measurements for standard structures with a healthy state, also called the reference state. OMA measurements result in a set of modal parameters, which are retained in the modal passport. The measurements and the calculation of the modal parameters shall be repeated under different characteristic external conditions (operating temperature, standard or expected loads) in addition to the modal passport. This way a modal passport of a typical structure is formed.

Next, the monitoring itself is carried out, which is based on a comparison of the modal parameters and external factors measured for the particular structure to its reference state considering influence functions, which are typical for structures of the same type.

The data processing and analysis part is divided into the following steps:

1. Recording
2. Estimation of modal parameters
3. Addition of new parameters set to the modal passport / comparison with the modal passport.

The stages of recording and estimation of modal parameters are the same for both modal passport formation and structures consecutive monitoring. Stage 3, on the other hand, depends on whether it is the formation of the modal passport or monitoring. The modal parameters and external factors obtained during monitoring shall be compared with the modal passport, from which it is concluded on the condition of a particular structures sample.

Data recording

OMA is performed on each physical sample of the structure. First, it is ensured that the structure is subjected to mechanical excitation (by natural forces or artificially) and begins to fluctuate. Then the wireless measurement system turned on and signals are recorded from the sensors in the computer memory. The time length of a single recording will depend on the type of excitation. For example, when the excitation is provided without disruption (heavy traffic, regular hammer impacts, windy weather), then it can be sufficient to have a one minute recording. When the excitation consists of rare irregular impacts (low intensity traffic), sufficient amount of such impacts is needed, at least 100, which can take hours. It possible of course, to pause the recording while no excitation is observed.

Modal parameters estimation

Deformation signals recording and estimation of modal parameters can be performed in a single piece of software – *ARTEMIS* from *Structural Vibration Solutions*. The following steps are performed:

- Make a structure’s geometric model with nodes as sensors locations,
- Import data recordings into the program, attach sensors signal to a designated node,
- Select the frequency range to analyse, processing methods and other settings.

When the estimation is started, the program generates a mathematical model of structural vibrations that matches the measurement data as close as possible. The computing algorithm then solves the mathematical equations from which the modal frequency, shape and damping coefficient are obtained. Detailed description of the mathematical basis for estimation procedure is given in Section 1.2.

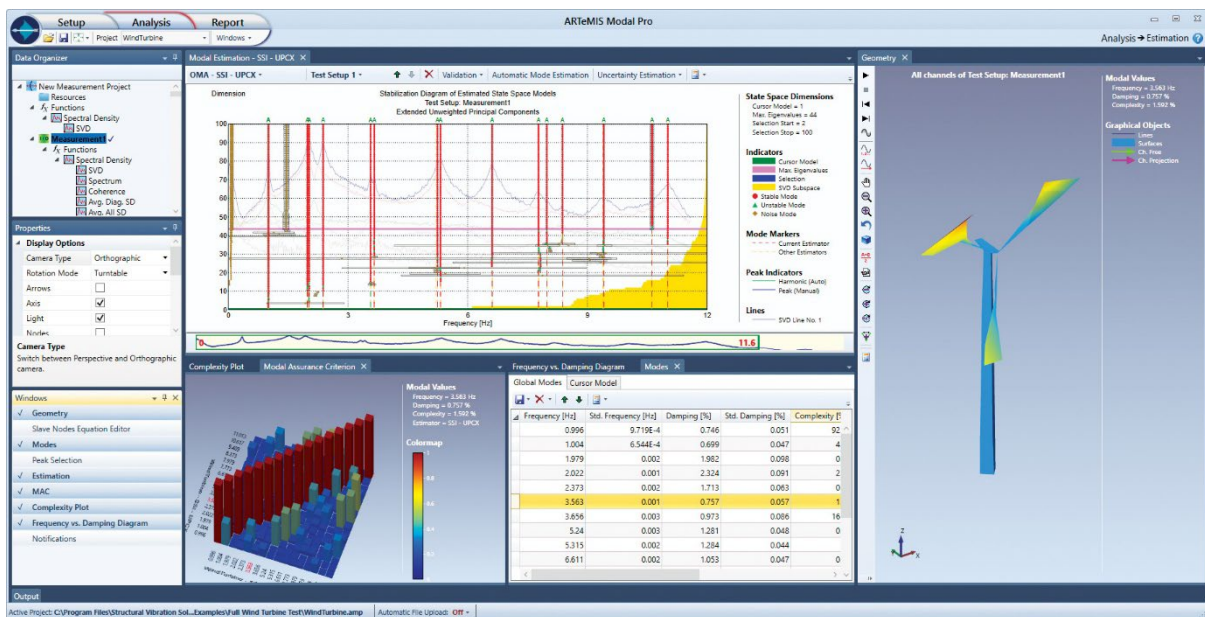


Fig. 2.11. *ARTEMIS Modal* software screenshot.

As a result, the engineer acquires modal frequencies and shapes of recognized modes. These modal parameters are exported as a matrix in a text file. Frequencies are recorded as separate values, shapes are recorded as vectors with curvature/deformation values at each position of the transducer.

3. DAMAGE DETECTION AND EVALUATION

This section introduces the theoretical and mathematical basis for damage detection and evaluation algorithms of the SHM system prototype. The description starts with Modal Passport architecture and implementation steps. Next, Modal Parameter Change Assessment is shown. This is an assessment method that allows to compare combination of different modal parameters (frequencies and shapes together and separately) vividly and conveniently between different measurements, aiding the engineers in analysing structural condition. Finally, the so-called Modal Field Comparison Method is shown, which evaluates structural states without modal parameter estimation techniques.

3.1. Modal Passport

Modal passport is a combination of measurement technique, modal data storage and processing methods in order to perform structural health monitoring. MP is based on the common knowledge that modal parameters represent structural properties and that modal parameters can be used for structural health monitoring. MP considers application for a series of structures of the same type, e.g., wind turbine blades or towers. The set of modal parameters which are common for the structures of the same type is the core of the MP [109].

Modes which are typical for a series of structures of the same type are selected to form *typical modal passport*. The typical modal passport is valid within wide range of operating factors, such as operational loads and temperature. Description of typical modal passport includes matrices of modal parameters: frequency, damping and shape, over different operating factors.

The referred values of modal parameters are the expected means (i.e., average values) of modal parameters for structures of the same type. In addition to averaged values, a typical modal passport also contains confidence intervals, which show the variance of modal parameters around the mean value.

It is well anticipated that modal properties vary significantly under the influence of external conditions and operational factors, like temperature and loading. Typical passport is multidimensional, as it describes dependence of modal parameters from different operational factors. This description is realised in the form of influence functions. For example, Fig. 3.1. shows influence function of helicopter blade modal frequency against rotor rotation speed. Some modes (particularly of bending type) are more influenced by rotation speed than others (of torsional type). Sometimes modes even change their frequency sequence order, i.e. modes swap positions between each other in frequency.

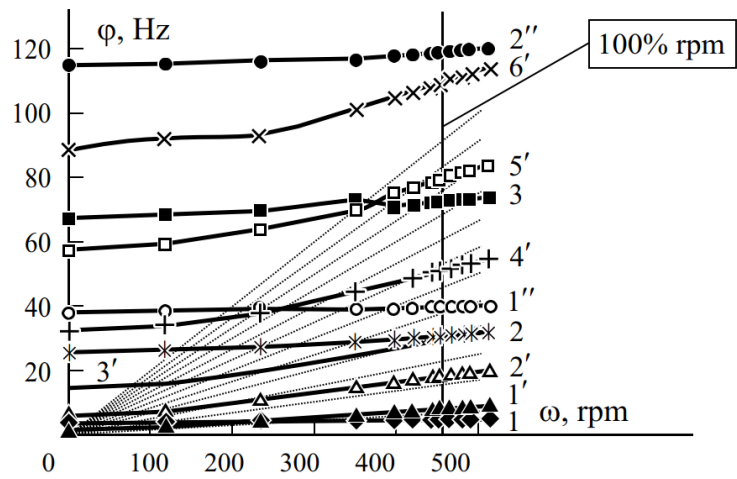


Fig. 3.1. Different modal frequencies as a function of rotational speed (revolutions per minute, rpm) for a composite helicopter blade. Numbers at curves are modes type: 1-3 – bending in the rotation plane; 1'-6' – bending in the thrust plane; 1'' and 2'' – torsional [110].

Typical modal passport serves as a template for *individual modal passport* of a certain structure. Typical modal parameters, which are carefully selected (as shown further), serve as guiding references for selecting modal parameters when processing data from individual structures. Individual modal parameters of a certain structure are obtained during arbitrary operational conditions. Using influence functions of a typical modal passport these modal parameters are recalculated from arbitrary conditions to reference conditions. The health monitoring is then done in reference conditions. Reference conditions are usually the same for a number of individual structures, but this may not be true for full set of typical structures. For example, a wind turbine tower in the North Sea would have a reference temperature of 10°C, but at the African coast it would be 25°C. Variance of individual modal parameters values is compared to the reference confidence intervals of individual passport. An indication of a damage is when measured variance exceeds reference confidence intervals.

Fig. 3.2 shows the components/procedures of a typical modal passport that includes full process of operational modal analysis (signal measurement, algorithms for modal parameters estimation) and the resulting modal parameters, stored in a data base.

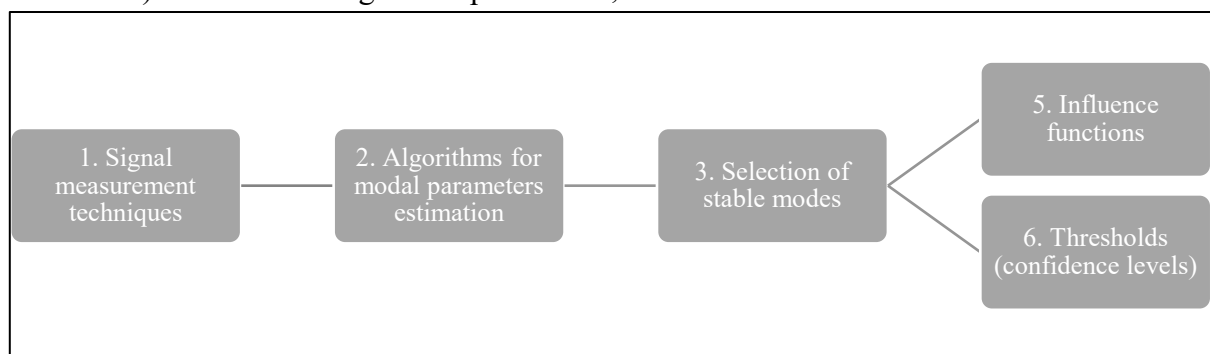


Fig. 3.2. The components of typical modal passport.

For SHM purposes a typical passport of a healthy (reference) state is formed, which includes modal parameters of healthy structures obtained under a variety of environmental and

operational conditions and then brought to common reference state. The composition of a modal passport for a structure with variable load and environmental temperature is shown in Fig. 3.3. It consists of modal frequency and shape and corresponding external factors values. For each influence factor there is a set of n frequencies and corresponding mode shapes. The upper half of the Fig. 3.3 shows modal parameters for changing load p and constant temperature of 20°C. The lower half of the Fig. 3.3 shows modal parameters for constant load p and changing temperature. Modal passport is realised either manually in *MS Excel* or semi automatically in *Matlab* software, however it can be realised in any data processing software. For each state modal parameters tend to differ, i.e., external factors are influencing modal parameters.

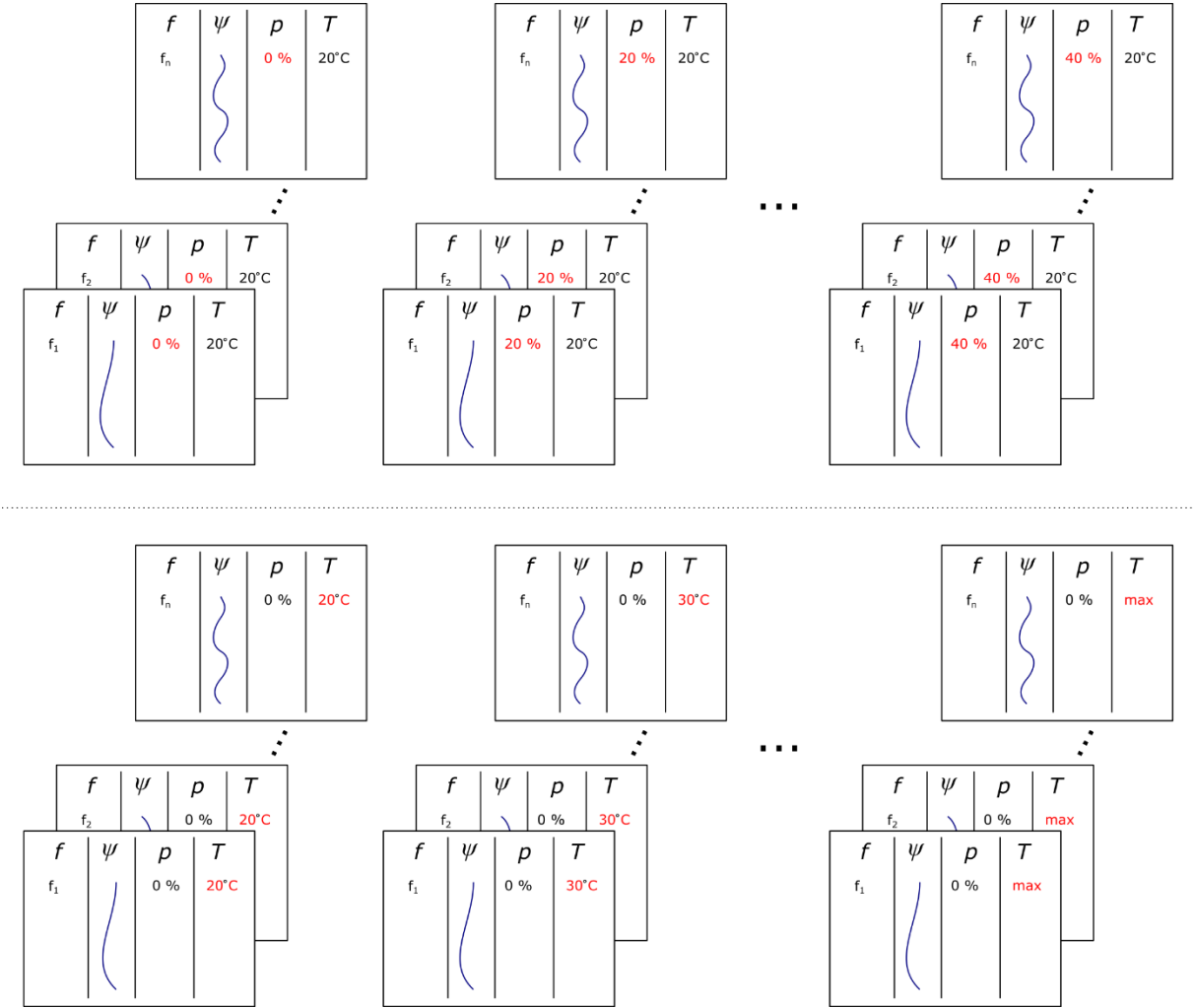


Fig. 3.3. Example of a modal passport composition – modal frequency and shape under variable operating conditions.

Typical modal passport formation

The use of the modal passport is based on the assessment of changes in modal parameters of the operating structure as a sign of a change in the state of this sample. The analytical model for modal passport is defined using Eq. (1.1) and applying changes induced by external factors:

$$[M + \Delta M]\{\ddot{x} + \Delta\ddot{x}\} + [C + \Delta C]\{\dot{x} + \Delta\dot{x}\} + [K + \Delta K]\{x + \Delta x\} = f(t) \quad (3.1)$$

In practice change of mass can be attributed to an attached (or detached) element on the body of the structure, change of damping – due to changes in boundary conditions, and the stiffness changes mostly because of defects like cracks. These changes influence the FRF of a measured vibrational signal from the structure, which leads to modified modal parameters:

$$H_{pq}(\omega) + \Delta H_{pq}(\omega) = \sum_{m=1}^M \frac{A_{pqm} + \Delta A_{pqm}}{j(\omega + \Delta\omega) - (\lambda_m + \Delta\lambda_m)} + \frac{A_{pqm}^* + \Delta A_{pqm}^*}{j(\omega + \Delta\omega) - (\lambda_m^* + \Delta\lambda_m^*)} \quad (3.2)$$

The influence factors should be identified for each type of structure. Most commonly, as is mentioned in this thesis numerous times, the influence factors are operational loads and temperature, however other factors may be present.

Modes should be stable and typical for the given structure to recognize changes in the state. Stable modes (in the context of modal passport) are considered to be repeating modes of similar shape between different measurements and/or samples. Stable modes are also more robust to slight variation in operational conditions. There are 3 criteria (verified in practical tests) for stable modes:

1. Repeating of the similar mode shape and frequency at least for 50% of estimators of T tests, for example at least 3 times out of 5 estimators of T tests. The number of tests should be at least 3, but 5 or more tests are recommended.
2. Limited frequency deviation. An acceptable frequency deviation is usually in the region of few percent.
3. MAC value (Eq.(1.13)) between stable mode shapes at least 0.9, but smaller than 1. MAC value can be higher than 0.9 if necessary.

The assessment of modal stability is carried out in two stages. First, a comparative analysis of modal parameters is carried out between modes, which are obtained by five different modal parameters estimation methods (EFDD, CVA, UPC, PC, UPCX, further in text – estimators) within one measurement (see Section 1.2 and [36]). If the same mode is recognized by at least three methods, it is flagged as relatively stable. The selected modal shapes are used for modal enhancement to reduce uncertainty, due to random differences in excitation (which is sporadic and unknown) and differences in estimators. Enhancement is explained in detail further.

When the modal parameters of relatively stable modes meet requirements 2 and 3, then they are recognized as stable modes and their parameters are averaged, thus a typical mode of modal passport is calculated.

Sequence of steps to create a typical modal passport:

Step 1

OMA of a structure in the s state. Initial state for typical passport requires structure to be undamaged (healthy).

Step 2

Acquired data processing using five modal parameters estimation methods. Selection of relatively stable modes estimated with at least 3 estimators. There might be situations, where a mode is estimated by 3, 4 or 5 estimators. As the result, one obtains a set of relatively stable modes.

Mode shapes given by different estimators have different scale. To bring them to a common (-1.0... 1.0) range, each n element of eigenvector ψ_m^n of the m mode is normalized to the square root of the sum of squares of all N elements:

$$\hat{\psi}_m^n = \frac{\psi_m^n}{\sqrt{\sum_{n=1}^N (\psi_m^n)^2}} \quad (3.3)$$

This step is naturally called *normalization* and it allows to select stable modes in the next step.

Step 3

Selection of stable mode from relatively stable modes using above mentioned criteria of limited frequency deviation and $0.9 \leq \text{MAC} < 1$. If more than one relatively stable mode is estimated in the limited frequency region of interest, then the mode with higher MAC is selected as a stable mode for further analysis. Each such mode is represented by $2N + 4$ data vector:

- shape and its standard deviation ($2N$ elements)
- frequency and its standard deviation (2 elements)
- damping coefficient and its standard deviation (2 elements)

N is essentially equal to the number of sensors on the structure, as the shape is represented by as many DOFs as there are sensors.

In this way, a $M \times (2N + 4)$ matrix is formed from a set of tests, where M is the number of stable modes. Steps in 1-3 are repeated for each of T tests. Naturally, for each test number of resulting modes may differ. But using the three criteria mentioned above a selection of modes is performed and a full set of stable modes K is acquired for T performed tests. This way a $T \times M \times (2N + 4)$ matrix is obtained.

Step 4

Different estimators may reflect the same mode shape in opposite phases so, the *phase alignment* procedure is required. The procedure involves the check of phase compatibility between modes of the group and inversion of eigenvectors with the opposite phases. To check phase compatibility, the correlation is calculated between the reference and other eigenvectors. Eigenvector values with negative correlation (~ -1) are considered as opposed and are inverted. Once the eigenvector phases in the group have been matched, the modal enhancement can be performed.

Step 5

Calculation of the mean and variance of the modal parameters. Typical frequency and damping for m mode is

$$\bar{f}_m = \frac{1}{K_m} \sum_1^{K_m} f_m^k, \quad (3.4)$$

$$\bar{\zeta}_m = \frac{1}{K_m} \sum_1^{K_m} \zeta_m^k, \quad (3.5)$$

Analysis of experimental data, for example in [111], shows the distribution of modal estimates close to normal. The uncertainty of enhanced modal parameters with 99,7% probability is characterized by triple standard deviation of its K estimates based on the assumption of a normal distribution:

$$\delta f_m = 3 \sqrt{\frac{1}{K_m} \sum_1^{K_m} (f_m^k - \bar{f}_m)^2} \quad (3.6)$$

$$\delta \bar{\zeta}_m = 3 \sqrt{\frac{1}{K_m} \sum_1^{K_m} (\zeta_m^k - \bar{\zeta}_m)^2} \quad (3.7)$$

Mode shape averaging is done for each element of the mode shape vector:

$$\bar{\psi}_m = \frac{1}{K_m} \sum_{k=1}^{K_m} \hat{\psi}_m^k. \quad (3.8)$$

The uncertainty of the enhanced eigenvector is estimated for each n^{th} element of enhanced eigenvector by triple standard deviation in the group of M_k modes and is presented as a vector:

$$\delta \bar{\psi}_m^n = 3 \sqrt{\frac{1}{K_m} \sum_1^{K_m} (\hat{\psi}_m^k - \bar{\psi}_m)^2} \quad (3.9)$$

For the purpose of simplifying the analysis and reducing amount of processed data an integral estimate of the m mode eigenvector uncertainty is introduced:

$$\delta \bar{\psi}_m = \frac{3}{N} \sqrt{\sum_1^N (\delta \bar{\psi}_m^n)^2} \quad (3.10)$$

After the 3-5 steps were performed for the reference state of the tested sample (structure, specimen), the trials are repeated for structures' other states. A state is represented with external influence factors. For rotating blades, the applied forces are centrifugal forces during rotation, so state is defined by the rotation velocity (Fig. 3.1). Influence function of the m^{th} mode frequency f_m against rotation velocity v is described using the 2nd order polynomial:

$$f_m(v) = \beta_0 + \beta_1 v + \beta_2 v^2 \quad (3.11)$$

This is a rotation velocity influence function of a typical structure, common for all structures of this type with some degree of uncertainty. It is not feasible to determine individual influence

function for each structure, so a simplification is made. Coefficient β_0 for this influence function is the natural frequency in static modes, i.e., without rotation, and each blade will have individual value of this coefficient. The 2nd order polynomial is chosen as a close enough approximation for typical influence functions, as empirical data shows.

The process of determining the influence function is the process of regression for 2nd order polynomial using least mean square method, which is done by setting a set of equations in a matrix form:

$$\begin{bmatrix} v^4 & v^3 & v^2 \\ v^3 & v^2 & v \\ v^2 & v & n \end{bmatrix} \begin{bmatrix} \beta_2 \\ \beta_1 \\ \beta_0 \end{bmatrix} = \begin{bmatrix} f_m v^2 \\ f_m v \\ f_m \end{bmatrix} \quad (3.12)$$

and is then solved for coefficients β .

The set of test states depends on external and internal factors that typically have influence on samples in natural conditions. The scale of influencing factors and requirements to accuracy define the number of test states.

Individual modal passport

Creating a typical modal passport requires resources, however once it is done, it simplifies assessment of modal properties of the specific structures of this type. The *individual modal passport* inherits from the typical one the computational procedures and the set of stable modes, each with an influence function and a threshold. The set of stable modes is used as a guide for individual modal parameter estimation for each structure. For the individual passport to function properly it needs healthy state data, which are obtained by testing the particular structure (sample) in its healthy state under arbitrary conditions. Testing under arbitrary conditions allows to avoid inconvenient and expensive testing in laboratory conditions. Influence functions of the typical passport are used to recalculate obtained modal parameters to the reference conditions. Further measurements of the particular structure are also being subjected to recalculation to the reference conditions, so that the monitoring of damage sensitive features is being done for these conditions.

As an example, temperature influence functions for frequency $f(t)$ and damping $\zeta(t)$ are shown in Fig. 3.4. Some dependencies are linear (mostly for frequency), some are not. These functions allow to approximate modal parameters for other temperatures.

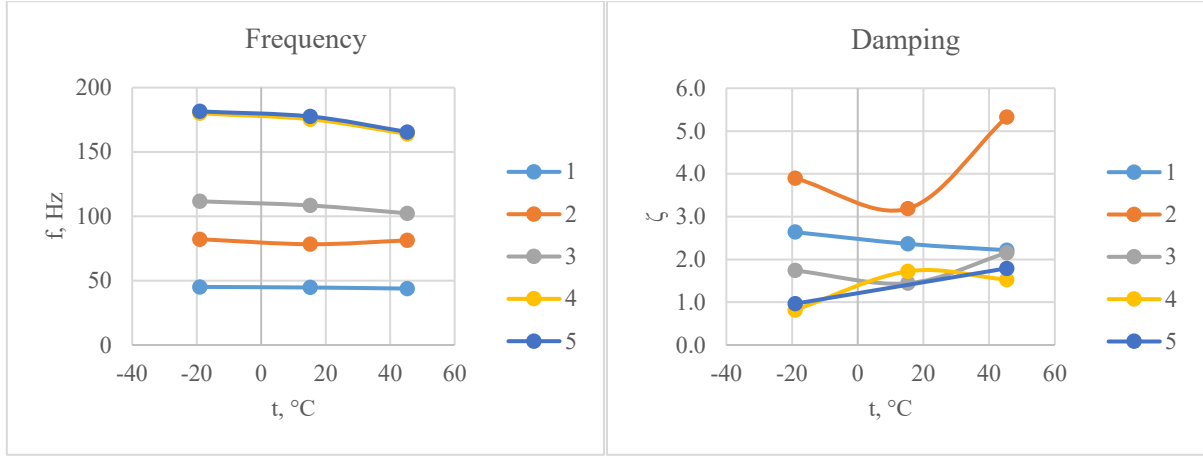


Fig. 3.4. Temperature influence functions for a glass fibre composite cylinder for first 5 modes.

Individual MP considers possibility to detect damage. Detection of the damaged state (if one occurs) is performed using damage detection algorithm. An estimation of damage severity can be done using Modal Parameter Variation (MPV). An alternative approach to damage identification, which is out of scope of modal passport concept, is called Modal Field Comparison Method (MFCM) and is introduced in the Section 3.3.

3.2. Modal Parameter Variation

Above mentioned MFCM allows monitoring of structure's state using damage identification, but not damage localization. For latter case a comprehensive evaluation of object's modal parameters modification is required. There are examples and some experience in evaluation of modal parameters variation in [112]. This thesis offers a mathematical formulation of modal parameters variation evaluation.

To estimate modification of m^{th} mode from a structure test, which has not been used for formation of the typical modal passport, the Modal Parameters Variation (MPV) is used as a parameter, which considers modal frequency, damping and shape modification from its reference state (baseline). MPV is an integral part of modal passport, a simple algorithm for evaluating possible damage in a set of typical structures.

A modal test i of a structure is considered. First, a modal test of the structure in a healthy state is performed and a set of individual modal parameters – $\bar{f}, \bar{\zeta}, \bar{\psi}$ – is obtained. It is possible to perform the modal test for any operational condition, as the influence functions allow to recalculate obtained modal parameters to another operational condition, for example to a reference one. In the case of rotating blade, a reference condition is when the blade is static.

Next, modal tests are performed on the same structure at later time. It is assumed, that the structural condition of it is unknown. Individual modal parameters – $\bar{f}^i, \bar{\zeta}^i, \bar{\psi}^i$ – are estimated using the standard approach, as in the typical passport formation steps 1 and 2. Normalization and phase alignment is also performed to match new modal shapes $\bar{\psi}_m^i$ to the typical ones.

Typical modal parameters serve as guides for selection of the newly obtained parameters. When the set of individual modal parameters

For frequency and damping the normalized modal difference for mode m is:

$$\Delta \bar{f}_m = \bar{f}_m^i - \bar{f}_m, \quad (3.13)$$

$$\Delta \bar{\zeta}_m = \bar{\zeta}_m^i - \bar{\zeta}_m, \quad (3.14)$$

The shape deviation $\Delta \bar{\psi}_m$ compared to the typical shape is calculated as geometrical sum of all the shapes elements deviations $\delta \bar{\psi}_{m,n}$:

$$\Delta \bar{\psi}_m = \sqrt{\sum_{n=1}^N (\bar{\psi}_{m,n}^i - \bar{\psi}_{m,n})^2}. \quad (3.15)$$

With modal shapes of cylindrical shell objects, it is common to see that mode shapes from different measurements from different structures, or even of the same structure, are angularly shifted. When this happens one has to match the two shapes manually, which is similar to phase alignment, only the phase is not equal to 180° .

It is advantageous to estimate an integral deviation of tested structure where deviations from all modes are considered. For this purpose, parameters of integral deviation of frequency $\Delta \bar{f}$, damping $\Delta \bar{\zeta}$ and shape $\Delta \bar{\psi}$ are calculated:

$$\Delta \bar{f} = \sqrt{\sum_{m=1}^M (\Delta \bar{f}_m)^2}; \quad \Delta \bar{\zeta} = \sqrt{\sum_{m=1}^M (\Delta \bar{\zeta}_m)^2}; \quad \Delta \bar{\psi} = \sqrt{\sum_{m=1}^M (\Delta \bar{\psi}_m)^2}. \quad (3.16)$$

Integral modal deviation is referred to as Modal Parameters Variation. When it is necessary to perform an overall modal assessment of the structure using a single value, then Modal Parameters Variation (Integrated) can be used:

$$MPVI = \sqrt{\Delta \bar{f}^2 + \Delta \bar{\zeta}^2 + \Delta \bar{\psi}^2}. \quad (3.17)$$

The practical application of MPVI is shown in Section 4.4.

3.3. Modal Field Comparison Method

Modal field comparison method is a vibration signal processing method, which allows to obtain structures condition numerical assessment. Modal field here is a term to describe matrix of singular vectors $\Phi(\omega)$ and values $s(\omega)$. The assessment is relative, meaning it requires a reference condition to be defined, which serves as a baseline. This baseline can be a modal field of a single measurement of a healthy state, or a modal field averaged between several measurements. In order to objectively compare modal field, the presented modal field comparison method (MFCM) was developed.

High energy filtering

Singular values $s(\omega)$ frequency function (or simply SVD plot) shows power spectral density for the whole system. Frequencies, where power spectral density is low, fall between resonances, meaning that no mode is present at those frequencies. It is worth to select only those $\Phi(\omega)$, which are represented with enough energy. This is done by forming a threshold line s_t that follows the trend of SVD plot. The threshold line s_t is defined as p^{th} order polynomial. The red line in the Fig. 1, has a polynomial of order 10. Modal peaks will lift up above the threshold, whereas low energy region will remain under the threshold, as shown on an example in Fig. 1. For further calculations, only $\Phi(\omega_k)$ are selected, where ω_k is an array of frequencies for $s(\omega_k) > s_t(\omega_k)$.

Singular vector phase alignment

Next issue to deal with when comparing singular vectors is their phase. Quite commonly modal parameter estimation for the same system gives almost identical mode shapes, but with inverse phase. This is also relevant for singular vectors, obtained after SVD. For objective assessment these vectors should be phase-aligned, otherwise MFCM parameter will show high difference between modal vectors, which will cause a false detection of condition change.

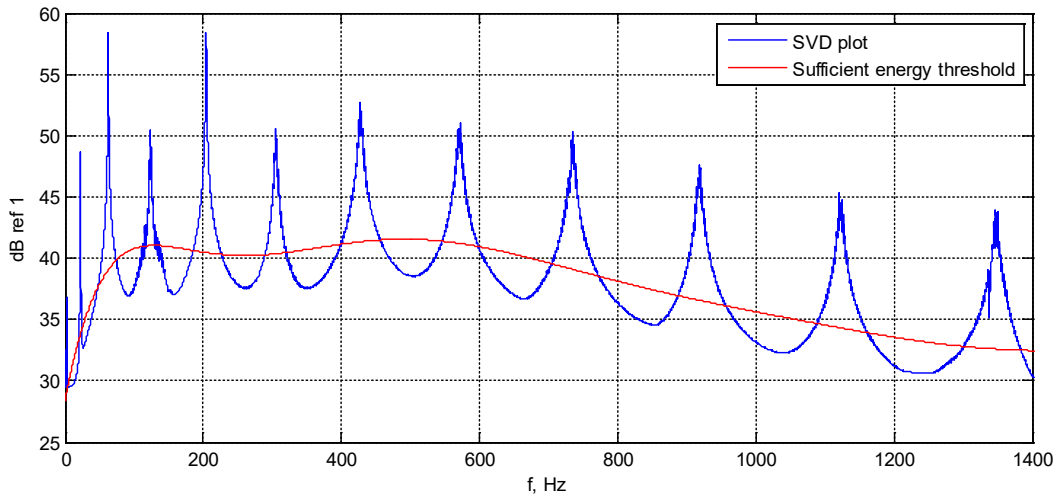


Fig. 3.5. SVD plot of the aluminium beam.

As a reference vector, the very first singular vector is chosen, denoted as $\Phi^1(\omega_k)$. For every frequency line singular vector from measurement m is being compared to $\Phi^m(\omega_k)$ using Pearson correlation coefficient

$$\rho(\Phi^1(\omega_k), \Phi^m(\omega_k)) = \frac{1}{N-1} \sum_{n=1}^N \left(\frac{\phi_n^1(\omega_k) - \mu^1}{\sigma^1} \cdot \frac{\phi_n^m(\omega_k) - \mu^m}{\sigma^m} \right), \quad (3.18)$$

where N is the number of entries in Φ , which is basically the number of DOFs, and where μ^1 and σ^1 are the mean and standard deviation of $\Phi^1(\omega_k)$, respectively, and where μ^m and σ^m are the mean and standard deviation of $\Phi^m(\omega_k)$. For every singular vectors pair, where ρ is negative, the vector $\Phi^m(\omega_k)$ is inverted, which makes it phase-aligned with the first vector.

Baseline

The similarity assessment between singular vectors is done frequency by frequency. The baseline to compare all measurement results to is defined as an average between M singular vectors of a healthy state

$$\Phi_{avg}(\omega_k) = \frac{1}{M} \sum_{m=1}^M \Phi^m(\omega_k). \quad (3.19)$$

In practice it is recommended to have around $M = 20$ reference measurements, from which the baseline is obtained.

Singular vector difference coefficient

The next step involves singular vector difference coefficient calculation. For each frequency line a correlation coefficient $\rho^m(\omega_k)$ is estimated between singular vector of m^{th} measurement $\Phi^m(\omega_k)$ and the baseline $\Phi_{avg}(\omega_k)$ using the same formula as in Eq. (3.18).

Correlation coefficient is an efficient tool to estimate similarity between variables (vectors in this case). However, correlation coefficient does not take into account the amplitude of the vector. For example, Fig. 3.6 shows two pairs of modal vectors. Both Fig. 3.6(a) and Fig. 3.6(b) pairs have a correlation coefficient close to 1, as both pairs are similar. But the Fig. 3.6(b) pair is obviously different in amplitude. To take this feature into account, a weighting coefficient should be implemented.

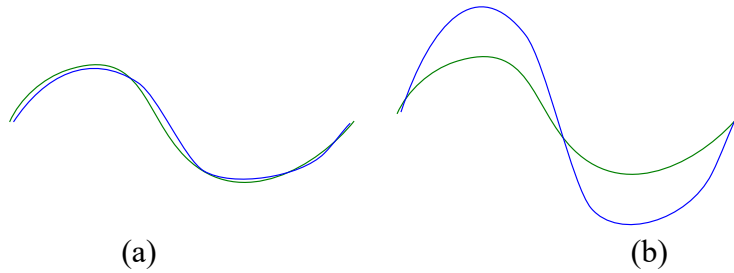


Fig. 3.6. a) Shapes pair example 1; b) shapes pair example 2.

A vector of absolute difference z in each point is calculated first. Then the sum of standard deviation of this absolute difference vector and the mean of this vector is regarded as the weighting coefficient

$$w^m(\omega_k) = \sigma(z) + \mu(z), \quad (3.20)$$

where $z = |\Phi^m(\omega_k) - \Phi_{avg}(\omega_k)|$. This way, the higher the weight w^m , the larger is the difference in amplitude.

Next, difference coefficient frequency function is calculated as

$$c_{\Phi}^m(\omega_k) = \frac{w^m(\omega_k)}{\rho^m(\omega_k)}. \quad (3.21)$$

Difference coefficient function is directly proportional to the weight and inversely proportional to correlation coefficient, meaning that if modal vectors are similar in both shape and amplitude, the difference coefficient function will be low and vice versa.

Frequency function represents detailed difference between modal vectors. For detection, however, such a detailed information is not necessary. It is more convenient to have a single number, which represents the structural state. These numbers can be easily compared with each other. One way to obtain this number is to estimate median value of the difference coefficient function. Median value advantage is that it is not influenced that much by extreme values opposed to a mean, for example. Median is more accurate in describing a typical value of a population (or function in this case). So singular vector difference coefficient for measurement m is

$$C_{\Phi}^m = \text{median}(c^m(\omega_k)). \quad (3.22)$$

Singular values change coefficient

Singular vector difference coefficient shows how modal shapes have changed, but it omits change of modal frequencies. To consider modal frequencies, singular value frequency functions or SVD plots are used. The change in structural characteristics will result in alteration of SVD plot peaks frequency, sharpness, in its slope and magnitude. In order to detect this change a comparison between SVD plots of different measurements and an average should be done. One way to compare functions is to get cross correlation of these functions, which is given by

$$R^m(\tau) = \int_{-\omega_{max}}^{\omega_{max}} (s^{avg}(i))^* s^m(i + \tau), \quad (3.23)$$

where s^{avg} is an averaged SVD plot between M measurements and τ is lag. Usually cross correlation is performed for time sequence data, however, the principle works for SVD plots as well.

The resulting $R^m(-\tau \dots 0)$ will be symmetrical to $R^m(0 \dots \tau)$ if s^{avg} and s^m are identical. Structural change will cause SVD plots to change, so structural change affects the symmetry of $R^m(\tau)$ function. This symmetry is assessed with yet another cross correlation function between $R^m(-\tau \dots 0)$ and flipped $R^m(0 \dots \tau)$. The resulting cross correlation function R_{R^m} shows how much of signal energy is dissipated due to asymmetry of two halves of $R^m(\tau)$. Simply put, the sum of all points of the resulting function R_{R^m} will be higher for symmetrical $R^m(\tau)$ and lower for asymmetrical $R^m(\tau)$. This way it is possible to estimate the difference between two SVD plots in a single number

$$C_f^m = \sum_{n=1}^N R_{R^m}. \quad (3.24)$$

Finally, it is more convenient to normalize C_f^m to its maximum value to get singular values change coefficient

$$\hat{C}_f^m = \frac{C_f^m}{\max(C_f^m)}. \quad (3.25)$$

MFCM parameter

Modal field comparison method parameter is calculated by equation

$$C^m = \frac{C_{\Phi}^m}{\hat{C}_f^m}. \quad (3.26)$$

This gives a scalar number for every measurement m . For convenience, it is better to normalize the parameter by the average MFCM value for previously selected M reference measurements

$$\hat{C}^m = \frac{C^m}{\frac{1}{M} \sum_{m=1}^M C^m}. \quad (3.27)$$

Eq. (3.27) gives values for a range of measurements that correspond to the condition change relative to the mean value $\mu(\hat{C}^m)$, which is 1. For unchanged condition, MFCM values will variate around 1. Variation is caused by random physical factors like subtle changes in environmental conditions, boundary conditions, excitation irregularity. For a definite structural modification \hat{C}^m will give a number significantly higher than 1. This approach depends on correct choice of reference measurements, i.e. an engineer must be confident that M measurements have steady state.

Condition threshold

Finally, the MFCM parameter threshold level, above which the condition is considered modified, is given as three standard deviations of MFCM parameter $3\sigma(\hat{C}^m)$ for M reference measurements. All later measurements are related to the mean $\mu(\hat{C}^m)$ from Eq. (3.27) and compared to the threshold value. If the given MFCM parameter value exceeds the threshold, then this indicates that structural condition is changed. Note, that MFCM parameter is dimensionless.

The above principle of three standard deviations is taken from 68-95-99.7 % rule [113]. This is widely used in statistics for normal distribution problems. It is assumed that MFCM estimation is a subject to normal random data variability. The rule states that 99.73 % of the values lie within 3 standard deviations from the mean. Of course, there is a 0.27 % probability of false alarm, however, if at some point parameter exceeds the threshold just once (within a reasonable range), and the following parameter values fall within healthy state range, then this event can be neglected.

To recap, Fig. 3.7 shows the flowchart for calculation algorithm for modal field comparison method parameter.

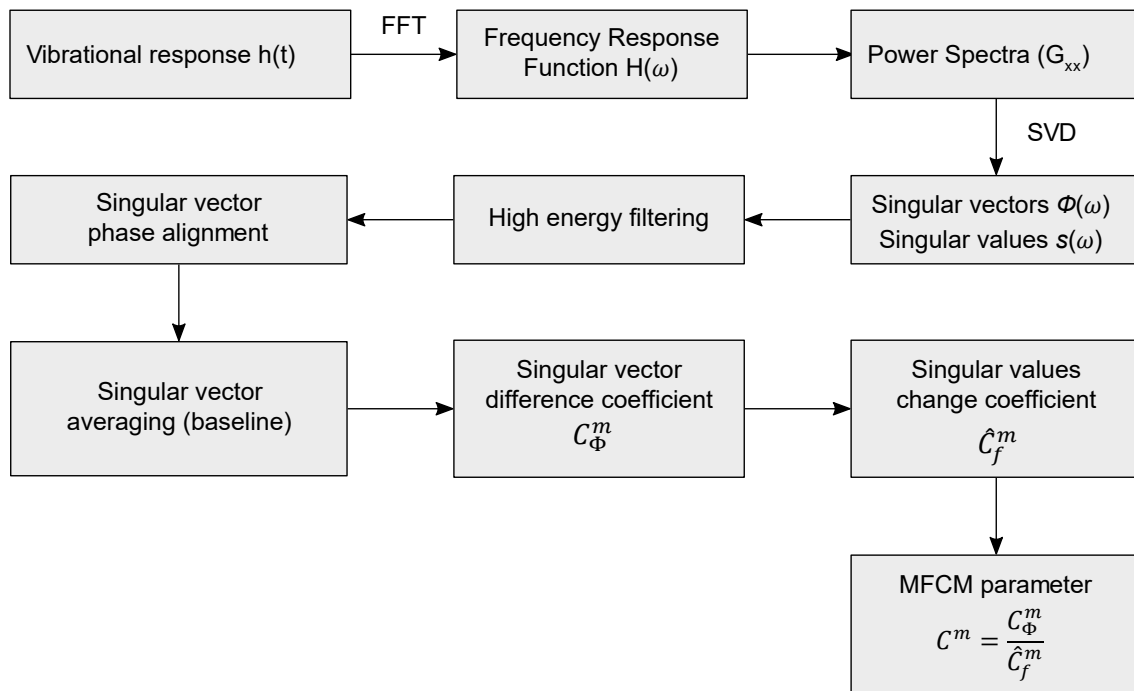


Fig. 3.7. MFCM parameter calculation algorithm.

The MFCM is an optional technique and can be used as a separate tool for structural health monitoring. The main advantage of MFCM is that it does not require modal parameter estimation. This saves a lot of processing time. On the other hand, this method is not as robust as modal passport approach.

4. CASE STUDIES

This section covers proposed SHM system application cases. Experimental verification of described approaches is based on both existing methods, mainly OMA and established modal parameter estimation techniques, and several novel solutions:

- Use of PVDF piezo film sensors for OMA
- Application of wireless data transmission solutions for OMA of rotating blades
- Estimated modal parameters evaluation methods for damage detection and identification.

Concepts and theories presented in this thesis are tested using the following objects: 85 cm long aluminium beam, a 1.5 m high model of a wind turbine, 20 m high airport radar tower, and a 2 m small helicopter composite blade.

4.1. Application of deformation sensors

Typical approach for modal properties identification considers measurement of vibrations. For this purpose, the sensor array, for instance accelerometers, is distributed over the surface of the object. Alternatively, non-contact measurement methods may be used, for example, a scanning laser interferometer [114]. Double integration of acceleration measured at DOFs of the object's surface provides displacements of the surface. Assuming the tested body as solid, the calculated displacements are considered as equivalent to displacements of the neutral layer. Based on the assumptions and conclusions, which are justified in Section 2.4 and measuring the surface deformations as an alternative approach, we may also estimate the neutral layer curvature. Thus, both approaches use similar assumptions and provide a similar error level. However, the technical implementation of these approaches has significant differences.

The findings obtained in Section 2.4 need experimental validation – a comparative analysis of vibration and deformation shapes of a testing object, which is one of the goals of the thesis. Additionally, this study aims for validation of piezo film sensors application without preamplifiers.

The trial sample of the composite blade was chosen as an object for experimental research study. Two modal techniques provide experimental estimation of this blades modal parameters: experimental modal analysis (EMA) and OMA. Within the EMA the blade was excited by dynamic hammer with force transducer while response measurements were carried out by two accelerometers. OMA technique uses 10 piezo film sensors that measure blade deformations. The measurement setup for both methods is shown in Fig. 4.1. The blade is connected to the rotor through the adapter and the torsion. There are 10 piezo film sensors on the surface of the blade in five sections along its axis and in two lines: one near the front and the second near the rear blade edge. At the blade tip and at its root two 3-component accelerometers are fixed for reference vibrations measurement. On the picture (Fig. 4.1), colored arrows indicate the degree of freedom (Degree Of Freedom – DOF): acceleration measurement (blue), deformation measurement (green) and the direction of impact (red).

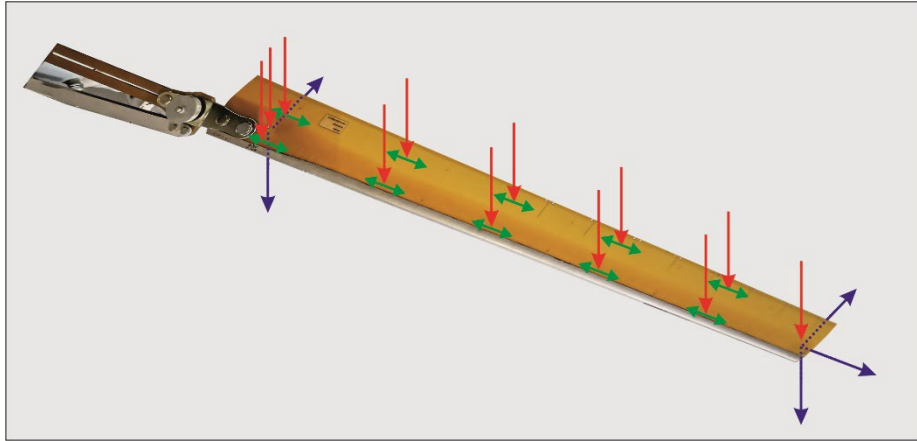


Fig. 4.1. Measurement set up for blade vibrations and deformations.

Piezo film deformation sensors integrated into the structure

For advanced composite structures, piezo film sensors provide an important advantage due to their ability to be integrated in the structure. As an example, in Fig. 4.2 an experimental sample of a composite blade with film sensors integrated on its surface is presented. The sensors are glued on to the surface of the blade (as described in Section 2.5) and covered with a glass mat, which is then soaked with epoxy resin. This creates an extra protective layer on the blade, which copies the aerodynamic shape of the blade and keeps the sensors intact and in place.

An alternative option is sensors embedment into the core of the composite structure. This has a major disadvantage – the locations of sensors would have delamination, which might cause serious structural integrity issues. This approach is not attempted in this thesis.

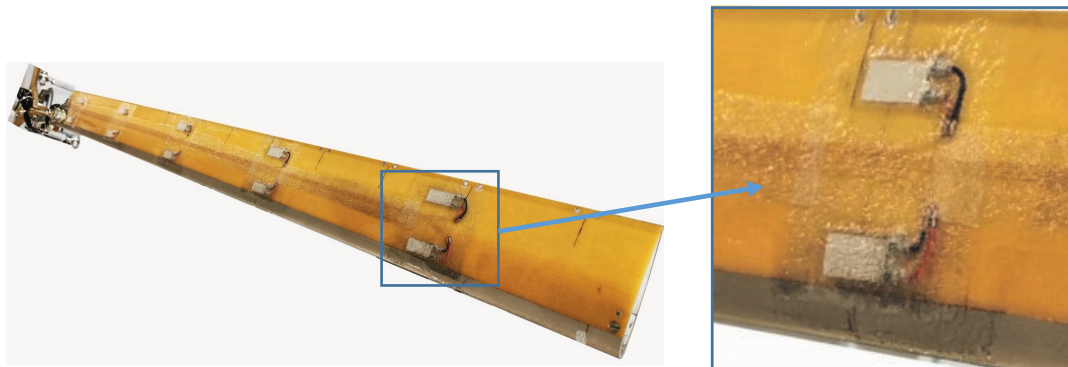


Fig. 4.2. Piezo film sensors on the composite blade surface.

Processing of mode shapes

Only the bending modes similar to pure bending were used for the comparative analysis of experimentally estimated vibration and deformation mode shapes. Blade flapping modes can be considered as similar to pure bending, so only flapping direction (vertical) was used for blades excitation.

The EMA technique involves measuring both: the testing impacts in all indicated DOFs and the responses to it at the reference points. The hammer with a built-in force sensor was the controlled actuator and Fig. 4.1 illustrates places and directions of excitation (red arrows) along the front and rear edges of the blade. Blade responses to excitation were measured by two

accelerometers (at the tip and at the root). During the tests, both impulse force and acceleration signals were recorded synchronously. The data obtained during the experiment was processed using the software *Modal Consultant* of *Pulse Labshop* platform, which estimates modal parameters in frequency range of interest.

OMA techniques do not require measurement of excitations and consider multiple responses only. The array of 10 piezo film sensors is insensitive to the static component of deformation and measure dynamic deformations signals only. The blade is excited with ordinary hammer hits to the metallic details fixing the blade's root to a test stand, similarly to wind turbine model base excitation in Section 4.4. Such excitation way provides more global impact on the entire blade avoiding direct impact to its surface. The frequency and strength of the impacts varied providing arbitrary excitation that is consistent with the limitations of OMA. Modal shapes obtained using OMA provide the eigenvector of each mode $\bar{\varepsilon}(x)$ in the relative scale normalized to the maximum value of the blade deformation in this mode ε_m

$$\bar{\varepsilon}(x) = \varepsilon(x)/\varepsilon_m \quad (4.1)$$

To compare curvature and deformations two conditions are to be met. The parameter of curvature has to be normalized to its maximal value. As measured deformations are the function of surface height (from neutral layer) the coefficient C (height consideration) is applied

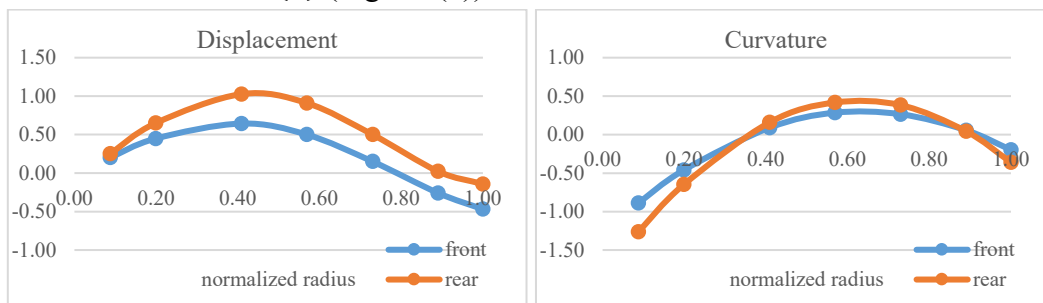
$$\bar{k}(x) = \bar{\varepsilon}(x)/C \quad (4.2)$$

where C is the relation between height of front h_f and rear h_r edges.

As the curvature of the surface layer at an arbitrary point is proportional to the tensile-compression deformation in this layer $k_i = C\varepsilon_i$, so the normalized curvature $\bar{k}(x)$ corresponds to the normalized deformation of the blade with a coefficient of proportionality C , reflecting the height of the blade profile at measured DOF.

Comparative analysis of curvature and deformations

To compare blade mode shapes of displacement and deformation, diagrams are used to illustrate distribution of curvature or deformations along the longitudinal axis of the blade, i.e., the eigenvector. Blue dots on the diagrams show the eigenvector, calculated using measurements in DOFs along the leading edge of the blade, red – along the rear edge. Diagrams on Fig. 4.3 allow to compare shapes of the 2nd bending mode reflected by: the mode shape computed using EMA (displacement) (Fig. 4.3(a)), the curvature derivative from the said mode shape (Fig. 4.3(b)), deformations $\bar{\varepsilon}(x)$ measured by piezo film sensors (Fig. 4.3(c)) and normalized deformations $\bar{k}(x)$ (Fig. 4.3(d)).



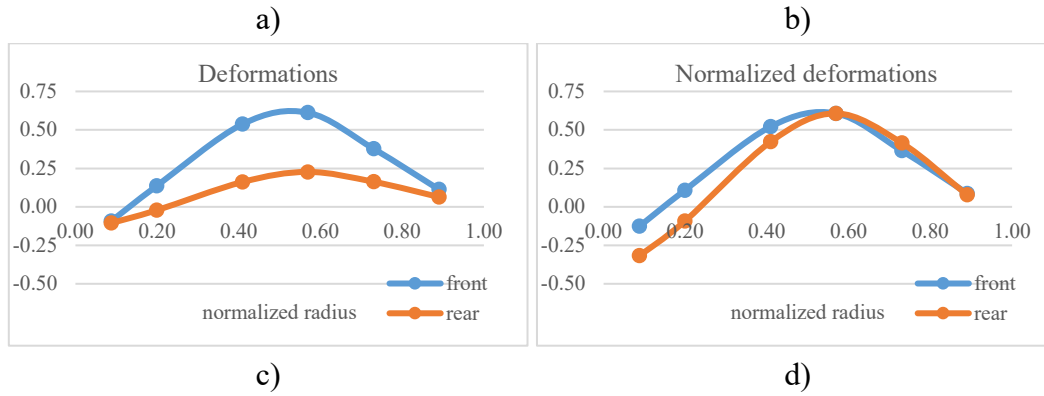


Fig. 4.3. Diagrams of eigenvectors: a) – displacement, b) – curvature, c) – deformations measured, d) – normalized deformations.

Analysing the above diagrams, it is necessary to consider that the blade vibrates together with the torsion connecting it to the rotor. That means the diagrams show only the part of mode shape that is located on the blade; another small part located on the torsion is not visible. The displacement shape is presented on Fig. 4.3(a). There are some specialties of the considered mode. This shape is similar to the classical 2nd mode of bending beam with maximal values (on the leading edge) in the area of 0.4 radius and at the blade tip. Vibrations of blade's front edge differs from the rear one, having larger magnitude in central part and smaller ones at the tip. Such behaviour is due to the asymmetry of blade cross section, which has a lower mass and moment of inertia in the rear part. Fig. 4.3(b) presents a curvature diagram calculated as the 2nd derivative of the FRF distribution along the axis of the blade (as considered in Section 2.4). As a second derivative shifts the phase on 180°, the curvature diagram in Fig. 4.3(b) is inverted so that its phase coincides with the shape of the oscillations.

Deformation diagram of the vibrating blade (Fig. 4.3(c)) differs from the shape of oscillations (Fig. 4.3(a)). First, the maximum deformations are shifted to 0.6 radius, not 0.4, as in the vibrations shape. Second, at the blade tip deformation is almost zero, in contrast to significant vibrations, especially along the leading edge. Third, the deformation of the rear edge of the blade is much less than the front, due to the lower height of the rear edge in accordance with the Equation (2.13). For ease of comparison of vibration and deformation shapes, the values of the rear edge deformations are recalculated taking into account the difference in the profile height along the front h_f and rear h_r edges

$$\bar{\epsilon}(x)^c = \bar{\epsilon}(x) h_f / h_r \quad (4.3)$$

The diagram in Fig. 4.3(d) illustrates height-adjusted deformations with difference between front and rear edge in root part only, where the blade is bevelled at the attachment to the torsion bar. Comparing the curvature in Fig. 4.3(b) and corrected deformations in Fig. 4.3(d), one can see similarity – in both diagrams, the maximum is located at 0.6 radius of the blade, and the values at the end of the blade converge to zero.

Resuming consideration above and applying half-wave approach to bending mode identification we can consider the curve in Fig. 4.3(a) as 2nd bending mode, which lacks the left side, located on invisible torsion. Curvature diagram (Fig. 4.3(b)) has 180° shifted phase

compared to the displacement curve. Since the deformations must be similar to the 2nd derivative, the phase shift must also be 180° relative to the shape of displacement. This shift is observed between the curves of the diagrams in Fig. 4.3(a) and Fig. 4.3(d). Thus, similarity of experimentally obtained estimates of the displacement and deformation shapes of the 2nd bending mode confirms the validity of the above assumptions.

To verify these findings, the data of other bending modes of the same blade was used. Fig. 4.4 illustrates the diagrams of displacement and deformation shapes characterizing 4th bending mode of the same blade. There are 3 half-waves in these diagrams (the 4th is not visible, because it is located on the torsion) that indicates that this is a 4th bending mode. There is noticeable similarity of displacement shape (Fig. 4.4(a)) and deformation shape (Fig. 4.4(b)) with a shift between them of approximately 180°.

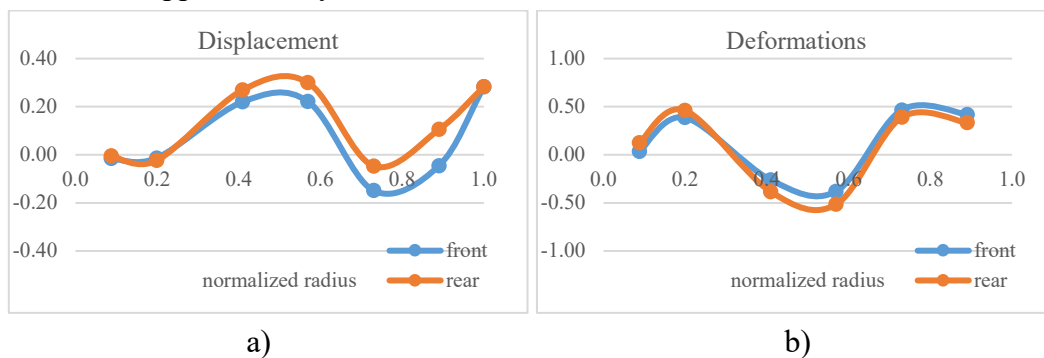


Fig. 4.4. Normalized eigenvectors: a) – acceleration, b) – deformation.

Based on all bending (flapping) modes it was found that the deformation shape of the blade is shifted by 180° in relation to the shape of displacement, having the same number of half-waves. Thus, the experimental verification confirms the validity of the assumptions made in Section 2.4 on the relation between 2nd derivative of displacement and the deformation shape of the surface layer. This linear dependency allows using the measurement of deformations of beam-like structural element to determine its modal parameters.

4.2. Harmonics extraction

Multiple experiments were conducted on glass fibre composite small helicopter blades of similar type. The experiments included dynamic rotation tests on a special testing rig. The task of this study is to validate harmonic extraction method, formulated in Section 1.4 and to evaluate methods effectiveness on an operating structure.

Measurement system

The measurement system is integrated into the blade itself and consists of piezo film deformation sensors (Fig. 4.5), thin conducting wires and data acquisition (DAQ) module on the rotating shaft. Sensors are fixed to the blades surface via double sided adhesive tape, which correctly transmits deformations in the frequency region of interest. Sensors and wires are covered with a layer of low-density glass fibre mat and epoxy resin. This layer holds the measurement system parts on the blade surface, prevents hazardous impact from fast airflow

and centrifugal force, which tends to rip off the sensors and wires during rotation. Epoxy resin is chosen accordingly to the properties of the blade's material, so that both layer and the blade pair together successfully.

The DAQ is Bruel & Kjaer LAN-XI 12 channel module. It is transmitting acquired signals wirelessly onto PC nearby at the control desk.

There are 5 sections with 2 sensors in each, parallel to the axis of the blade, 10 sensors in total. Additionally, a tacho probe is installed on the shaft, which records the speed of rotation, giving impulses as output.

Presented signals of blade deformations are obtained for measurements with angle of attack of 8 degrees, which allows the air flow to effectively excite structural vibrations of the rotating blade.

Data processing

Measured signals are 60 seconds long with 4096 Hz sampling rate. Time synchronous averaging was applied to measured vibrational signals for harmonic component enhancement. Fig. 4.6 shows 3 graphs for the measured signal, where the upper one has both periodic and random components ("mixed signal"), the middle has periodic signal, accumulated using tacho impulses and the lower – the resulting signal ("corrected signal"), which is received by subtracting periodic component from mixed signal. The time domain is shown on the left and frequency domain is shown on the right, using Fast Fourier Transform. The phase alignment of mixed and periodic is very important and is achieved by careful usage of tacho signal.

Time Synchronous Averaging application allows determining periodic component, which has its fundamental frequency at 17.1 Hz. Periodic component also has multiple harmonics, which is normal for complex rotary machinery.



Fig. 4.5. Blade with piezo film sensors and measurement system.

The magnitude of the 2nd harmonic at 34.2 Hz for mixed signal is 57.5 mV. The signal correction reduces this harmonic sixteen times – down to 3.5 mV. This scale of reduction is not the same for each harmonic, but it shows the effectiveness of extraction for some. It should be noted that this type of correction is able to extract periodic component coming from excitation. Algorithm is not able, however, to extract forced responses of the structure itself. This should be kept in mind, while performing modal parameter estimation.

The efficiency of periodic extraction cannot be directly measured. If a spectral magnitude is considered, there is not much of a difference between mixed and corrected signal, but this is not entirely objective, because FFT spectrum is largely dependent on conditioning properties, like time windowing, overlap, sampling rate and others. Additionally, the purpose of extraction is to obtain more correct results of modal parameter estimation. Thus, it is more practical to compare modal parameters instead of FFT spectra (or time domain functions for that matter).

Modal parameters estimation

The procedure of modal parameter estimation was performed using enhanced frequency domain decomposition (EFDD) analysis. EFDD transforms vibrational responses into frequency domain.

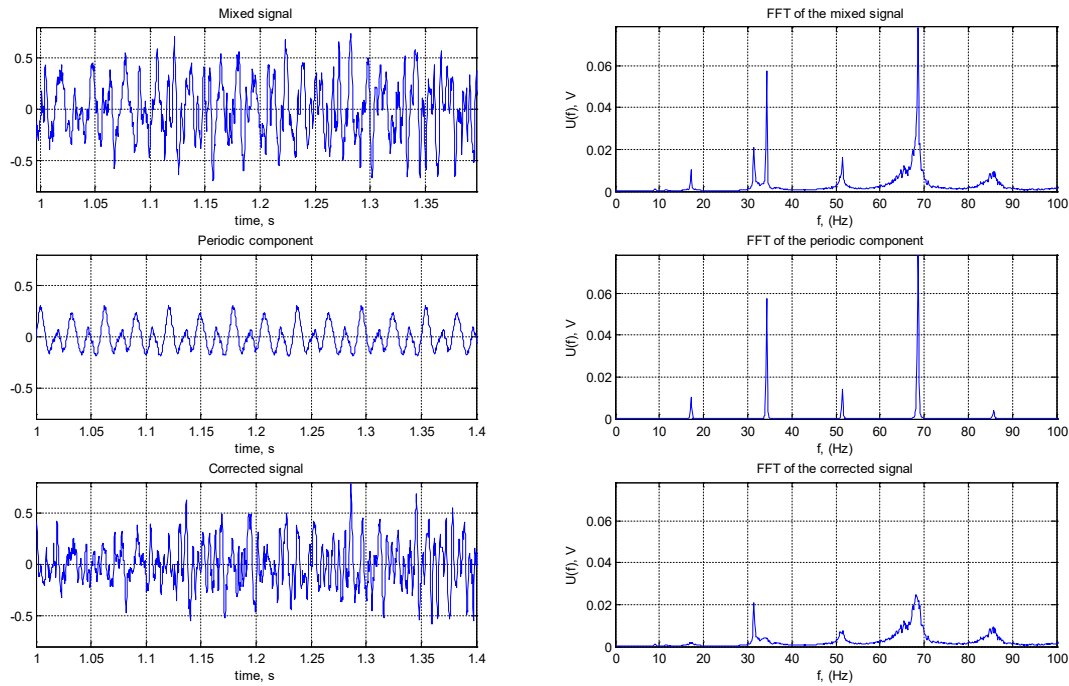


Fig. 4.6. Example of TSA extraction for vibrational signal.

The operator chooses a peak from a power spectrum or SVD plot (Fig. 2.11), which presumably belongs to a mode. The *Artemis* software then takes the corresponding singular vector of the chosen peak as a reference vector and compares other singular vectors on both sides of the singular value plot using Modal Assurance Criterion (MAC). This is a correlation coefficient based criterion and is set to be 0.8. Singular vectors, which have MAC value 0.8 or more compared to the reference vector are taken into account. These singular vectors together with the reference vector are averaged out to form a representation of particular mode shape. Averages are weighted by multiplying to corresponding singular values. Corresponding singular values, when plotted, form a characteristic single degree of freedom (SDOF) spectral bell, which is then inverse Fourier transformed into time domain, giving an SDOF correlation function. This, in turn, can be used for natural frequency and damping ratio estimation (Section 1.2).

The resulting modal frequency, mode shapes and damping coefficients for 10 estimated modes are shown in Table 4.1 It has been observed that the highest change of frequency and damping after harmonics extraction appears at harmonic frequencies, which is expected, because these frequencies were affected by the extraction algorithm. It is assumed that degradation of harmonic presence allows to better evaluate response of the blade itself, even though it is forced.

As the result of extraction, it was possible to estimate two additional modes, one of which lies on 2nd harmonic frequency (34.29 Hz) and another mode (137.27 Hz) is a high order mode.

In order to quantifiably evaluate difference between the same mode shapes before (original) and after (extracted) processing, again MAC is used (Fig. 4.7). Modes can be regarded as similar when MAC is > 0.8 . It is a good indication that same modes pairs (before and after

processing) show MAC values close to 1. That means that processing did not alter modal information in the signals in significant way.

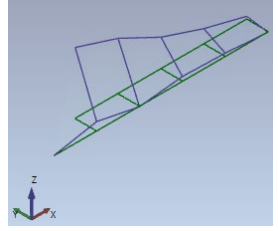
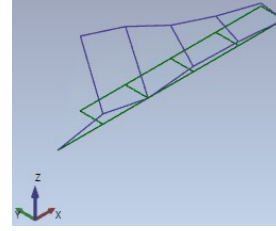
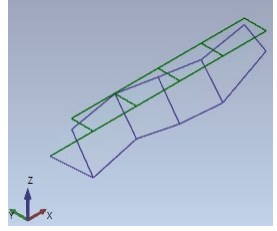
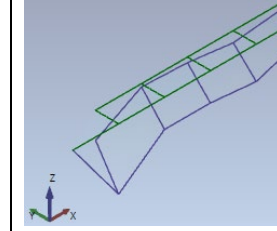
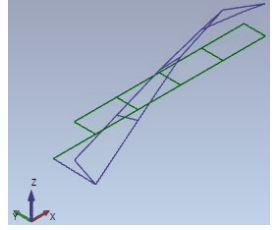
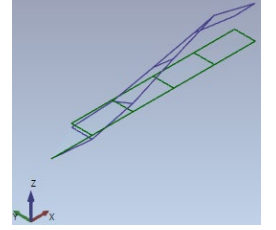
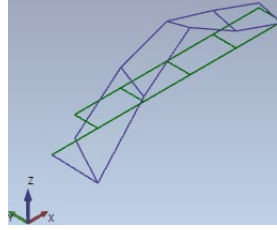
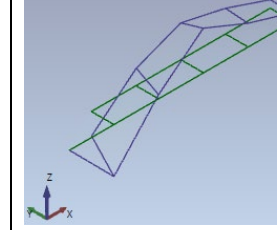
Table 4.1

Modal frequency and damping of a composite blade. Estimation without and with periodic extraction.

Nr.	<i>f</i> , Hz		damping		complexity		Mode shape description
	<i>original</i>	<i>extracted</i>	<i>original</i>	<i>extracted</i>	<i>original</i>	<i>extracted</i>	
1	9.06	9.06	1.756	1.755	15.4	14.9	1 st bending Y axis
2	17.14	17.27	0.337	0.864	14.3	37.4	forced bending (1 st rotor harmonic)
3	31.44	31.44	0.234	0.235	21.2	21.3	1 st bending Z axis
4	-	34.29	-	1.058		4.0	forced bending Z axis (2 nd rotor harmonic)
5	51.46	51.32	0.368	1.394	99.2	94.2	(3 rd rotor harmonic)
6	68.59	68.58	0.921	1.321	10.3	13.7	3 rd bending Z axis (4 th rotor harmonic)
7	84.80	84.83	0.118	0.166	70.7	66.9	2 nd bending Y axis
8	118.75	118.71	1.284	1.293	0.8	0.7	4 th bending Z axis
9	-	137.27	-	0.072		48.2	
10	153.59	153.54	0.546	0.557	42.6	35.0	3 rd bending Y axis

Table 4.2

Mode shapes of a composite blade. Estimation without and with periodic extraction.

original		extracted		original		extracted	
9 Hz				17 Hz			
							
51 Hz				84 Hz			
							

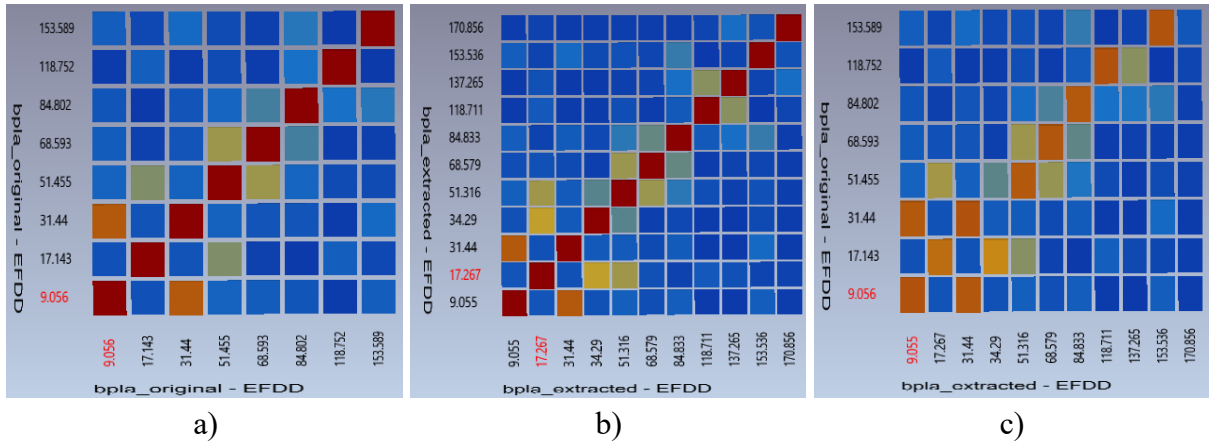


Fig. 4.7. MAC values for mode shapes between original and extracted mode sets: a) autoMAC for original; b) autoMAC for extracted; c) MAC between original vs. extracted.

The original mode shape set shows some correlation between shapes, with MAC values > 0.5 , estimated at frequencies falling to different harmonics, for example between the 1st bending mode in Y axis (9 Hz) and 1st bending mode in Z axis (31 Hz) (values are rounded up). This is an indication that there is some kind of physical connection on these frequencies, which is rotor excitation in this case. Another common reason for higher MAC between different mode shapes is aliasing shapes for high order modes, which is most probably not the case here. For the pair of modes at 17 and 51 Hz MAC is 0.523; for 51 and 68 Hz MAC is 0.601. When comparing same pairs of modes between original and extracted sets, MAC value is 0.618 and 0.583 respectively, showing no significant anticipated reduction of MAC values. This shows that harmonics extraction (suppression) does not change existing correlations between different modes.

Another approach to evaluate difference between before and after processing is to use modal complexity and its measure – Mode Complexity Factor (MCF). A complex mode can appear due to several reasons: non-proportional damping, bad measurements or poor modal parameter estimation and inconsistent data due to e.g. time variant conditions [26]. Complexity close to 0 % means that the mode is real, which is a good sign of a natural mode. Complexity close to 100 % means that the mode is complex. The composite blade is not homogenous and its inner structure changes between sections, so some modes are complex due to non-proportional damping.

As can be observed in Table 4.1, the harmonic extraction decreases the influences of periodic parts. This results in a decreased complexity for modes Nr. 5, 7 and 10 – 5.5 % improvement in average. On the other hand, modes Nr. 2 and 6 obtained higher complexity after processing. This might be explained by the fact that mentioned modes are basically a superposition of several modes (most probably of two modes), one of which is a forced harmonic mode, and another is a natural one. Decreasing the harmonic part in ensemble brings the natural mode to a higher relative presence. This might lead both to a higher or lower complexity, depending on the initial presence of the harmonic part. Modes that are not in vicinity of harmonics (Nr. 1, 3, 8) did not show serious modification of MCF parameter.

Case study conclusion

A method for harmonic components suppression/extraction in a vibrational response is developed. The influence of harmonic components extraction algorithm on modal parameters is rather low, which means also low influence on the response and therefore – low error. The effectiveness of the processing depends on the initial overall presence of harmonics in the given signal. The processing gives possibility to estimate some extra modes, which might be hidden by harmonics. There has been reduced complexity for some modes, although for others it was increased. Nevertheless, the extracted harmonics dataset shows some improvement in the quality of modal parameter estimation. The ability to compare original and extracted versions provides more insight on the structural response and the impact of harmonics in the response, which leads to better understanding of oscillations of the specific object and allows better judgement on the latter. This feature can be used by engineers and researchers for a more precise evaluation of dynamic behaviour of vibrating structures under harmonic excitation conditions.

4.3.Modal Passport application

The presented study aims to validate OMA techniques and modal passport application to a rotating blade. The work considers comparative analysis between vibration and deformation sensors and of data transmission system, as well as validation of the formation of modal passport for composite helicopter blades.

There are two stages of composite blades modal testing. At first stage, the blade is tested in a static position using EMA and OMA, and the second stage – only OMA techniques application to rotating blades.

Static testing

Typical EMA approach based on calculation of Frequency Response Functions (FRFs) allows testing the blade in static position. The set of FRFs is calculated based on measured excitation and response in multiple DOFs allocated around the blade. Depending on testing goals, excitation could be periodic or of impact nature. The testing procedure considers consequent actuation and measurements in DOFs according to geometric model of the blade. Then all FRFs for all DOFs are computed and after the FRF curve fitting the modal parameters are estimated.

Periodic excitation allows higher credibility of modal parameters using step-by-step frequency sweeping in defined frequency range. This approach is most appropriate, for instance, to determine modal damping, as sufficient energy for excitation of steady-state vibrations ensures a high accuracy in estimation. The measurement set-up, including the DOFs number and allocation, depends on the resolution requirements. At the same time, the periodic excitation method is quite time consuming.

Where accuracy of damping determination is not so important, the Roving Hammer (RH) technique is more appropriate for static tests. Using this approach, the transducer with fixed DOFs measures the responses of the single impact made by the hammer “roving” all DOFs consequently around the blade. The equipment required are the impact hammer having an

embedded force sensor and one or more transducers providing DOFs measurement in three directions. RH requires significantly less time than the periodic excitation technique. Fig. 4.8 illustrates the typical measurement set-up for blade RH technique; the hammer icons indicate DOFs (places and directions) of hits, and three coloured arrows indicate measured DOFs of the transducers.

3-axial accelerometers and vibration deformation sensors (piezo film sensors) are used in these tests. Fig. 4.9 shows samples of both sensor types application on the blades models. The blades models are specifically designed for series of different experiments and not intended for actual operation on an aircraft. These blades have inner stiff structure and the outer shell made of aviation grade plywood. Measuring the response simultaneously in three directions is an

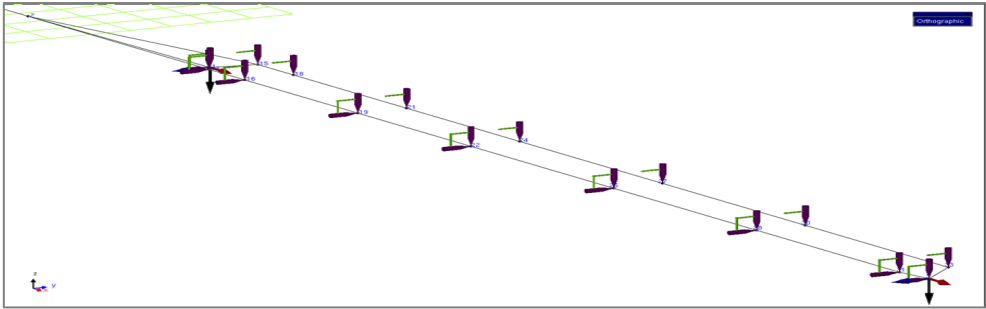


Fig. 4.8. Measurement set-up for blade test with a hammer.

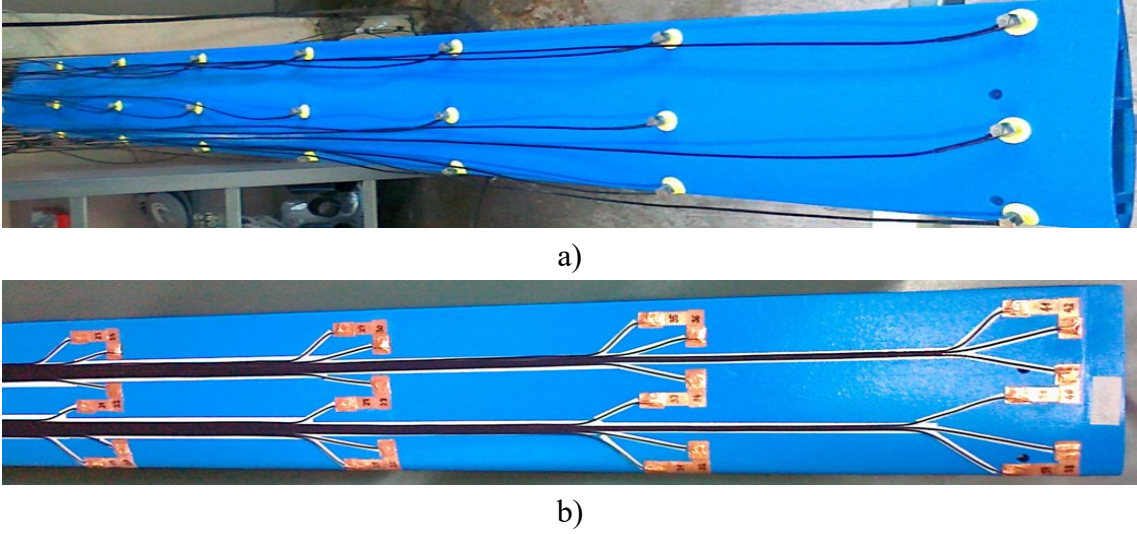


Fig. 4.9. Vibration accelerometers (a) and vibration deformation sensors (b) on similar blades.

advantage of three-axial accelerometers (Fig. 4.9(a)) that is acceptable for medium and large blades. Even though these sensors are lightweight, they may affect modal properties of the tested blades, especially considering coaxial cables and washers/fasteners. Piezo film deformation transducers (Fig. 4.9(b)) are more acceptable for this kind of structures.

The advantage of vibration deformation sensors is especially evident for rotating blades testing, where accelerometers may modify modal parameters of the blade and cause

aerodynamic distortions. That is why vibration deformation sensors were chosen for testing rotating blades.

There are two stages of static tests of blade modal properties in discussed case. First, the RH technique is applied for testing using 3-axial vibration transducers (accelerometers) and then software estimates modes of blade vibrations. To verify modal properties the mode shape analysis and identification is required. For a beam like structure, such as blade, the diagram of dependence on the relative deformation radius of the respective DOFs is a useful tool for mode shape identification. For convenience, coloured lines relate to mode shape values along the blade axes. As an example, Fig. 4.10(a) shows a diagram of mode shape for the third bending (flapping) mode, where blue line illustrates mode shape vector distribution along the front edge of the blade and the green line – along tailing edge. As deformation sensors characterize dynamic behaviour of rotating blades it is necessary to define the compatibility between deflection and deformation shapes of the same mode. So, at the second stage of static tests, the modal parameters of the same blade are determined using OMA techniques based on the signals of deformation sensors.

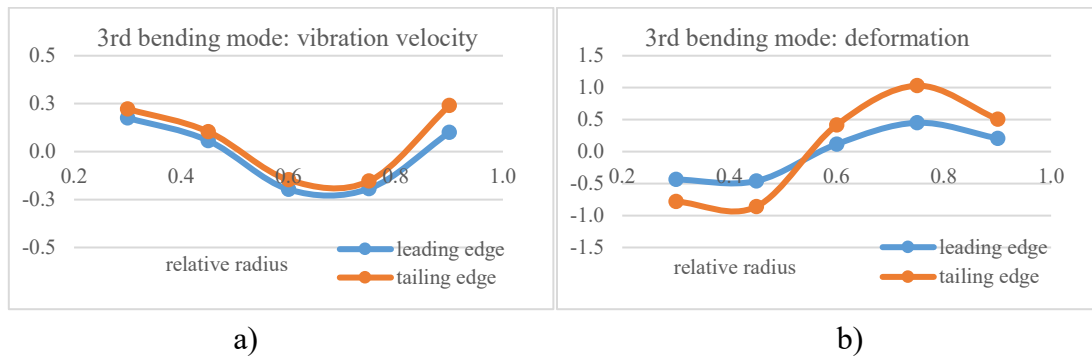


Fig. 4.10. Diagrams of vibration velocity (a) and deformation velocity (b) shapes of third flapping mode.

The rubber hammer (without force transducer) is used for blade excitation by hitting on the support of fixed blade with randomly varying force, direction and frequency. Then, using signals of deformation sensors, the modal parameters are computed using *ARTEMIS* software platform in terms of the vibration deformation magnitudes. Based on the blade geometric model, which reflects the location of DOFs, *ARTEMIS* provides processing of the measured response signals and resumes the set of modal parameters.

Identification and classification of vibration modes is carried out based on the modal parameters obtained from both static tests. When identifying vibration and deformation modes, standard methods (such as MAC, COMAC, etc.) are not appropriate, since, even if they reflect the same mode, their curves are different. Therefore, an analytical approach shall be used for modes matching and identification, concerning the nature of vibrations and deformations distribution along the length and chord of the blade for each vibration mode, considering findings of the study in Section 4.1. Classifying the modes of composite blades typically bending (flapping and chord wise) as well as torsional modes are defined. Aiming for test results validation after initial modal identification the static tests are repeated. The number of re-tests may vary depending on the tasks. From plurality of modes detected in a given frequency range,

the only modes selected for further consideration are those who have passed the test for repeatability (as described in Section 3.1).

Rotating Blades Testing

The testing is performed on a different type of blade. The technology for rotating blade testing includes methodical and measurement parts. The advanced multichannel system measures and transmits signals of vibration deformation sensors. Fig. 4.11 shows the measurement set-up of rotating blades with deformation sensors as in Fig. 4.9(b), and Fig. 4.12 shows multichannel data acquisition unit (DAU) with wireless data transmission device on top of the propeller.



Fig. 4.11. Integrated array of deformation sensors and wiring.

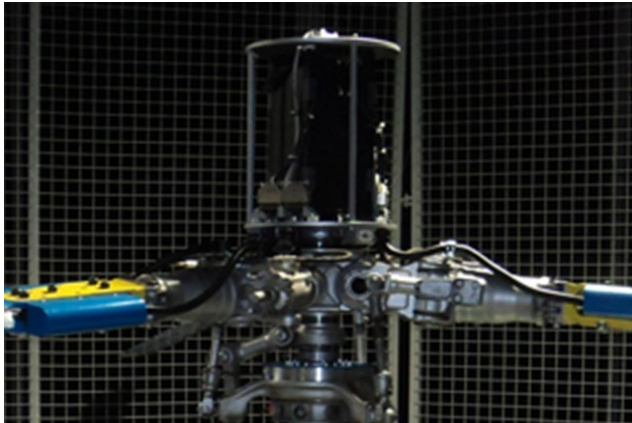


Fig. 4.12. Multichannel wireless DAU with connecting cables from blades rotates together with the whole propeller.

To minimize the influence of sensors and their cables on the aerodynamic properties of the rotating blade, they are coated with the additional protective layer of glass fibre veil and epoxy resin (Fig. 4.11), similarly as in previous case studies. Thin deformation sensors and its wiring (less than 1 mm) allows the protective layer to repeat the blade profile shape, excluding significant aerodynamic disturbances. The system providing measurement data and transmission complies with the harsh environment at rotation speeds of up to 1200 rpm. The wireless router rotating with DAU transmits the data to the workstation that ensures receiving, storing and further processing of data.

Modal properties of rotating blade are influence by test conditions, like rotation speed and pitching. The loads affecting the blade in rotation is a sum of constant and variable components. Variable loads (can be related to as random excitation) play useful role actuating vibrations and

surface deformations used for determination of modes. Since blade vibrations affected by these loads remain elastic, such loads practically do not affect modal properties. In opposite, constant component of loads affect the mechanical properties of the blade, and, respectively, change its modal parameters. This effect has to be taken into account when testing rotating blades, since under the impact of centrifugal force and the constant lifting force, the internal pressures in the blade structure change, which in turn affects modal parameters.

Different factors determine operational mode of the rotor, so its influence on modal properties should be studied separately. For instance, to study rotational speed influence on blade modal properties a zero pitch (angle of the blade relative to the rotating plane) of the blade first is arranged. This reduces lifting force so that modal parameters are only insignificantly affected by it. The effect of centrifugal force is remained. To study the impact of lifting force on modal properties, the tests are performed at the same rotation frequency, altering the main rotor pitch.

Modal passport formation

As an example, let us consider the dependence of blade modal parameters on the rotor speed, which has the most significant effect. Tests on the rotating blade are conducted in operational range from static to the maximal rotation speed that exceeds the nominal speed by 20-30%. The modal parameters are computed separately for each rotor speed. As a result of data processing, parameters of vibration deformation modes are computed, including frequency, damping coefficient and deformation shape for each mode at a given rotation speed. Identifying deformation modes, only those would be considered that conform to the typical modal passport. The combination of modal parameters computed in all operational modes constructs an additional dimension of typical modal passport. This dimension reflects modal properties dependence on rotation velocity, as shown for modal frequency in Table 4.3 and Fig. 4.13. The mentioned figure shows the data from the Table 4.3 and the respective 2nd order polynomial approximation – influence function.

Table 4.3

Modal frequencies (Hz) of the blade at different rotation velocities for 6 bending modes.

RPM	Bending mode					
	1	2	3	4	5	6
0%	2.6	12.2	41.3	75.8	143.5	209.5
29%	4.9	19.1	37.8	80.2		215.1
58%	9.7		47.3	92.0	160.1	229.0
67%	11.6	28.8	55.9	98.1	165.3	234.0
77%	13.0		54.4	101.7	167.8	240.3
86%	14.6		58.3	101.9	174.9	246.9
91%		30.6	61.5	107.8	181.1	250.7
96%	16.4	31.5	64.3	112.7	181.3	255.8
101%		34.0	67.4	117.1	185.1	260.1
106%		35.5	70.2	122.3	191.3	263.9
115%		40.3	76.5	128.9	193.5	271.6
120%	19.2	41.3	79.5	131.2	201.2	279.4

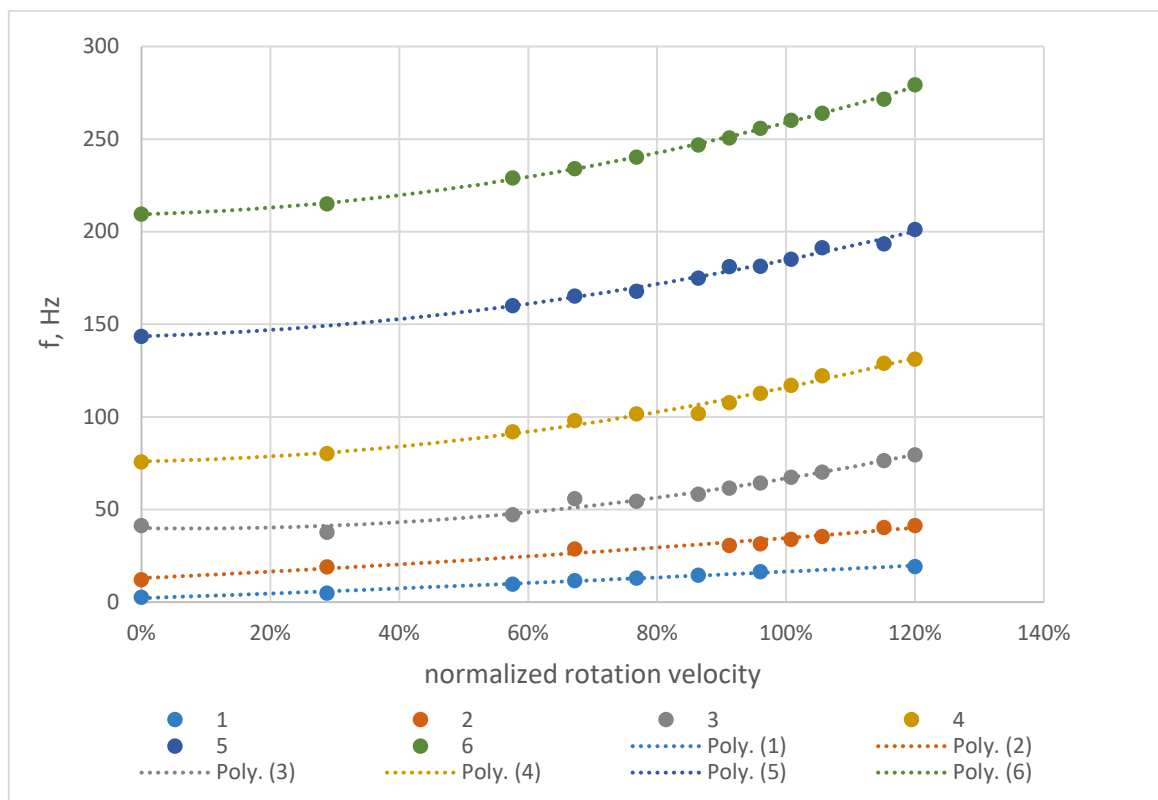


Fig. 4.13. Rotation velocity influence function on modal frequency.

The influence function for 6 bending modes of the blade (Fig. 4.13) can be used further for monitoring purposes. It is possible to perform OMA on the blade during rotation at any rotation velocity, then recalculate estimated modal parameters to the reference state, which is 0% or no rotation, static position. Recalculated modal parameters are then compared to previously obtained individual healthy modal parameters.

As one can see from Table 4.3 and Fig. 4.13, parameter values of the same mode vary for different rotation velocities. For instance, the 3rd bending mode significantly changes its properties under the impact of centrifugal load. The modal frequency increases from 41 Hz in a static position to 64 Hz at the nominal rotation speed, and the damping coefficient drops from 4.1% to 0.6%. At the same time, the modal deformation shape is modified as it is illustrated on Fig. 4.14. Due to applied centrifugal forces the blade becomes stiffer, which increases the modal frequencies.

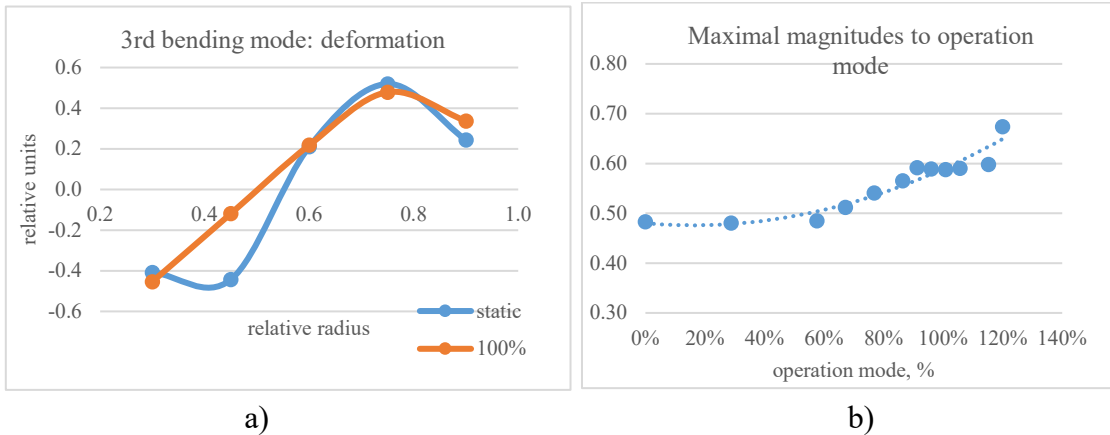


Fig. 4.14. (a) Modal shape deformation with rotation speed increase; (b) magnitude of 3rd flapping mode as a function of operation mode.

Another important factor influencing modal parameters is the pitch of a blade. The pitch is the angle between the propeller blade chord line and the plane of rotation of the propeller. In case of rotor testing with blade pitch variations, the modal passport gets a fourth dimension, which reflects the modal parameters dependence on a pitch. For any other operational factors, like ambient temperature, flight speed, blade loading, etc. additional dimensions of modal passport are formed based on blade tests under corresponding conditions. For full SHM purposes an additional dimension should be added to relate modal parameters modifications depending on damage scale (like delamination or other). Ultimately, the size of typical modal passport is not limited and can be increased by adding results of additional types of tests. The list of typical factors which influence modal properties of operating blade should be evaluated within preliminary study of operation conditions. Fig. 4.14(b) illustrates the dependence of third flapping mode deformation magnitude to operational mode (rotation speed).

Case study conclusion

This study was aimed at validation of modal passport application for typical structures. First, a typical modal passport was created for a healthy composite helicopter blade. The modal passport creation included – experimental modal analysis tests of the blade in static mode, and operational modal analysis of the blade in dynamic mode with different speeds of rotation. This allowed to obtain modal parameters for a reference state and external influence factor (centrifugal force) dependency functions for the modal parameters.

4.4. Wind turbine laboratory model

There are many types of industrial objects like energy towers, bridge supports, dams, etc., which functionality requires its health monitoring. The most damageable group includes those industrial objects, which on top of ambient excitation may suffer additional dynamic loads from its own functioning. For instance, wind turbines, going ships or flying aircrafts, operating pipeline parts next to pump station etc.

The current study sets forth the following task:

1. Validation of OMA methods applicability for detection of modal parameters modifications.
2. Testing of multi-patch OMA approach for reduction of necessary measurement channels.

The laboratory model of a wind turbine designed for validation of SHM techniques must have typical features of industrial structures:

- a massive foundation capable to simulate stable ground of the model,
- a structure similar to industrial one,
- functional unit generating both periodical and random excitation.

The measurement system of the model must provide:

- collection of dynamic signals from the whole structure,
- signals commutation to multichannel measurement system

Next sections reveal in detail what is the wind turbine model, how the measurement network is designed and is functioning along with some measurement setup.

Model structure

The laboratory scaled model of wind generator (Fig. 4.15) that is high as an adult human was built up to conform to the above requirements. The model includes three structural parts: the base (1), the tower (3) and the rotor head (4). The base is a massive 1 by 1 m concrete slab weighting approximately 70 kg. It rests on the floor via rubber pads. This base acts as an immovable mass that separates the rest of the model from the floor and vibrational noise.

The base bears the tower (3 on Fig. 4.15(b)) and the commutation box (2 on Fig. 4.15(b)). The tower is a frame made out of 20 by 20 mm aluminium angle beams. The tower has outer walls, riveted to the frame from three sides and a removable panel is screwed on the fourth side. The rotor unit (4 on Fig. 4.15(a)) is equipped with three rotating blades driven by electric motor and transmission inside a housing part. The electric control unit is mounted on the back of the housing to turn power on/off and adjust rotation speed. When operated, the motor, the transmission and the rotor provide periodic excitation to the tower, but blades also generate air turbulent excitation of the tower structure. Electric noise shielding is provided for the cables in such way that could be used as prototype in industrial conditions for other studies. Fig. 4.15(d) illustrates the shielded ribbon cable connecting deformation transducers to commutation unit.

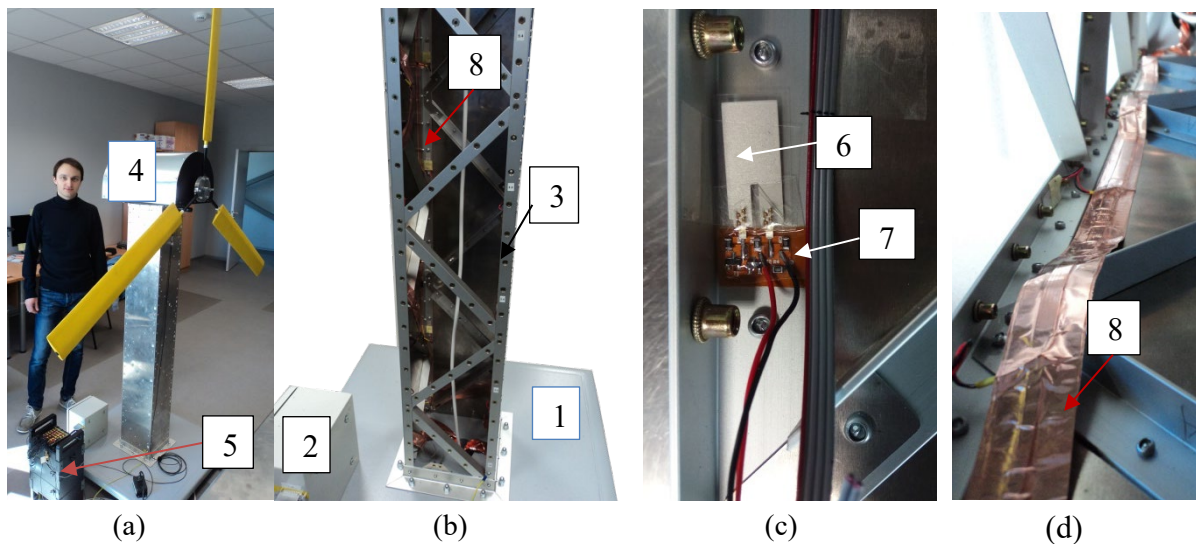


Fig. 4.15. Wind generator model: (a) overview (person for reference), (b) view on the tower structure without front panel, (c) measurement unit (film sensor with preamplifier), (d) harness cable. 1 – base; 2 – commutation box; 3 – tower; 4 – head; 5 – DAQ; 6 – piezo-film; 7 – preamplifier; 8 – cable.

The measurement and data processing system

The model is equipped with 32 deformation transducers allocated around the model's structure. Each transducer includes piezo-film sensor (6 on Fig. 4.15(c)) and preamplifier (7). Such sensor type was successfully used for OMA application for pipeline condition monitoring in [115] and rotating blade models [112]. Each sensor is attached to the surface of the frame beams using adhesive tape. Transducer leads are soldered to the flat ribbon cable 8 (Fig. 4.15(d)), stretching along the tower, curving around obstacles. There are four cables, one cable for each tower edge. Cables are terminated in the commutation box allowing signals grouping by patches.

All sensors are allocated vertically along each beam axis. There are seven vertical levels and one diagonal group with four sensors in each. Each set of four sensors is grouped into single connector in the commutation box and can be freely connected to any set of 4 input channels on the data acquisition system (DAQ). Sensors are numerated from 1.1 to 8.4. First digit stands for the group position (1-7 are horizontal, 8 is diagonal), with 1 being the lowest to the ground and 7 is the highest, just under the rotor unit. Second digit denotes one of four edges where sensor is located on. In this study diagonal group of sensors (8.1 – 8.4) was not used.

Data processing system includes DAQ that is Brüel & Kjær PULSE 48 channel frame and processing unit that is PC with *ARTEMIS* software platform.

Study of the model's dynamic characteristics

FEM analysis

To support modal identification of experimentally obtained results, Finite Element Analysis using *NeiNastran* was performed on the 3D model of the wind generator tower. However, even after careful modelling FEM results had large discrepancy with experimental data. Still, FEM

analysis of an approximate wind generator model allowed evaluating principal mode shapes that are expected in the experimental results.

Physical experiments

Principal tasks of experimental stage are:

- Adaptation of the modal testing technique for the given object,
- Experimental study of natural modes of the object, towers modes identification and comparison with modelled ones,
- Evaluation of estimated modal parameters uncertainty in simultaneous tests,
- Experimental study of natural modes of the object using multi-patch approach,
- Evaluation of estimated modal parameters scatter (uncertainty) in multi-patch tests.

Final section will also include study of damage detection approaches for the tower.

Excitation

The scaled model is designed to provide periodic excitation to the studied structure, as it is often a case in real life scenarios. OMA requires excitation close to white noise (flat in frequency domain). Obviously periodic excitation contradicts this requirement and poses a problem for OMA. For the purpose of this experiment it is assumed, however, that one can overcome this problem and even use periodic excitation for SHM. This assumption is not dealt with in this paper and is left for other studies. Some preliminary results of these studies showed (as was anticipated) that purely random excitation is not enough to excite all necessary modes. What is more, the current model's structure is rather stiff and deformations are relatively small, so considerable input force is needed, which was not provided solely by rotating parts.

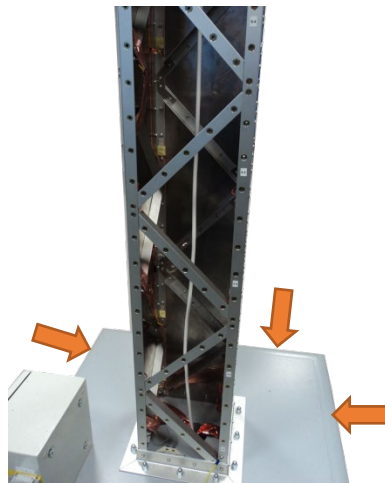


Fig. 4.16. Illustration of sledgehammer impacts on the base of wind generator model.

For the current study only random impacts were used to provide excitation of the model. Impacts by the plastic head hammer on to different points of the model excited the structure. To optimize excitation technique three types of actuations, including points, impacts force and frequency have been tested. Number of discovered modes and its repeatability were the criteria of excitation technique suitability.

Impacts with a sledgehammer on the base, powerful enough to excite certain modes. Impacts fall normally on four sides of the base (red arrows in Fig. 4.16) in horizontal plane, simulating earthquake effect on the structure. Occasional impacts are varied around the base to fulfil OMA requirement about random spatial distribution of excitation.

Impacts with sticks on the walls. The hammer impacts in this case overload the sensors so researcher hits the walls of the tower with wooden stick. Hits are made in random locations.

Impacts on the top of the model with a sledgehammer. The hits were made across the perimeter of the rotor unit (header), frequently, in the same manner as with the first excitation case.

As it turned out, impacts on the walls and on the top did not provide satisfactory excitation because of weak modes emanation and repeatability. With the second case (hits on the walls) it appeared that the walls reacted to the excitation more than the frame. As can be seen on Fig. 4.15(c), the sensors are placed on the frame and walls vibration does not excite the structure well enough. Energy from impacts on the top did not distribute around the structure well, and hits overloaded the sensors (measurement channels).

After examination of excitation types, it was decided to continue with impacts on the base for the study. By this way of actuation, the base acts as a buffer and impacts provide sufficient energy to the structure to excite natural modes. Single hit energy is being provided to a point on the base, which dissipates this energy and provides spatially even distributed energy to the frame as opposed to the hits on the frame itself, where all energy of the hit is dissipated closely around the impact point.

Simultaneous measurements

Each modal test of the model is a 120 seconds simultaneous measurement of 28 sensors (only horizontal sections are used; 4 diagonal sensors are excluded). Test output is deformation data collected from 28 sensors.

The first test session of five repeated tests is made (*Base 1*) with the same duration and similar impact parameters using simultaneous measurements. Measured data is processed in frequency range up to 1600 Hz using Enhanced Frequency Domain Decomposition (EFDD) and Stochastic Subspace Identification Unweighted Principal Components (SSI-UPC) techniques in *ARTEMIS* platform. Resulting modal parameters (frequency and shape) were compared to FEM computed parameters. After investigation of estimated modes using EFDD and SSI-UPC technique it was found that EFDD provides sufficient and stable estimation of modes, especially those of higher interest. It is decided to further use only EFDD for the sake of consistency.

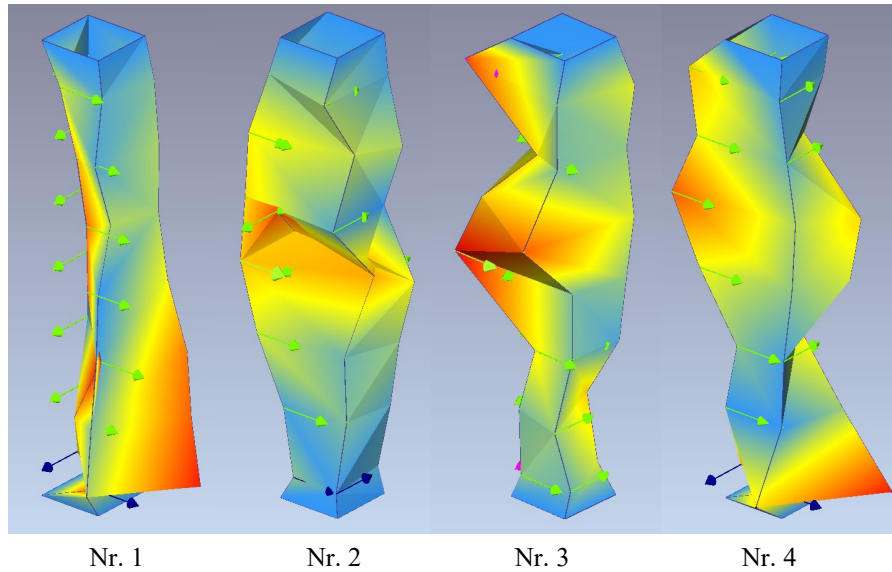


Fig. 4.17. Experimentally obtained mode shapes. Left – 66.1 Hz (1st bending mode); center left – 206.1 Hz (1st axial mode); center right – 323.7 Hz (1st torsional bending mode), right (combined mode) – 534.6 Hz.

Fig. 4.17 shows those shapes of the modes, which demonstrated the best shape and frequency stability and repeatability. These modes were estimated consistently for all 5 tests. There were other modes estimated as well, but they were not consistent from test to test, so it is decided to select only the presented ones. As was mentioned earlier, FEM analysis helped in identifying several mode shapes and labelling them accordingly, as written in the caption of the Fig. 4.17.

Uncertainty of estimated modal parameters in simultaneous tests was evaluated using scatter of MPV parameters. Repeated set of 5 OMA tests (*Base 2*) was done with the same conditions as for *Base 1*. Scatter estimates of two test series are presented in Table 4.4 in columns titled *Base 1* and *Base 2*.

Multi-patch measurements

There were 5 multi-patch OMA measurement sessions performed. Each session consisted of 6 consecutive tests-measurements. Each test was done by measuring two groups of channels, where one is the 1st sensor group (next to base) and the 2nd is one of the other channel groups. These two groups of 8 sensors form a patch, which gives possibility to measure the structure with 28 sensors using only 8 channels. The group pairing sequence was: {1-2}, {1-3}, {1-4}, {1-5}, {1-6} and {1-7}. To repeat – each group has 4 sensors on the same vertical level. Each measurement was 120 s long. 1st level group sensors are taken as reference sensors. Careful reader might question this choice of reference sensors, as they are not evenly distributed across the structure. This choice is dictated by 1st group being positioned on an actuation path and technical limitations of the measurement setup. As practice showed, modal parameter estimation quality did not suffer from this. It also is assumed that this choice will not influence the quality of damage identification. Fig. 4.18 shows comparison of SVD plots of the power

spectra matrices (regarded here as output spectra) between simultaneous measurement and multi-patch approach.

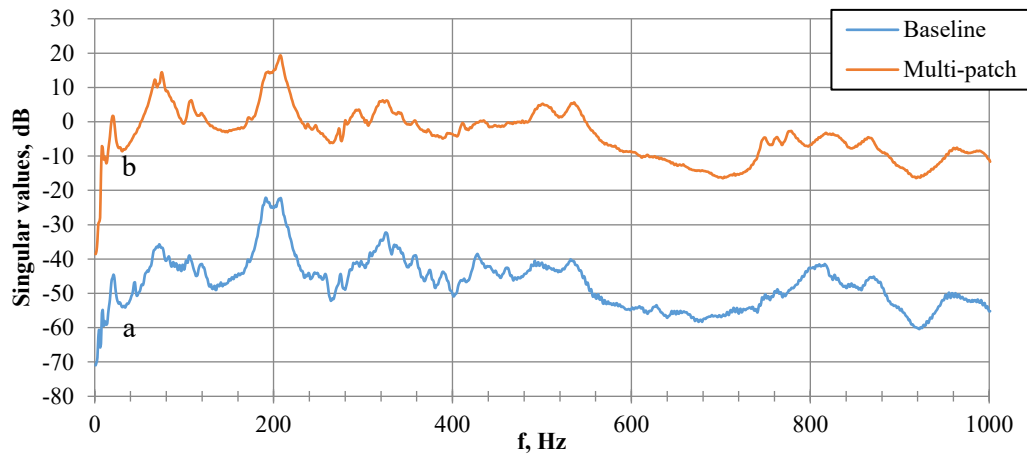


Fig. 4.18. SVD plots of output spectra: a) – simultaneous measurement, b) – multi-patch measurement.

The scatter (uncertainty) of modal parameter estimates between 5 multi-patch sessions is given in Table 4.4 (columns titled as *Multi-patch*).

Modal parameters variation for a single condition

Variation of modal parameters in all tests was estimated using MPVI. Table 4.4 and Fig. 4.19 illustrate separate (frequency and shape) MPVI values as well as combined ones.

Combined MPVI values were calculated as an average value between frequency and shape scatter. In Table 4.4 scatter of combined parameter for *Base 1* and *Base 2* for different modes vary within 2.6%, however common (average) scatter does not exceed 1.2%. Table 4.4 also allows comparison of the scatter between modal parameters of repeated tests performed with simultaneous OMA and for multi-patch OMA. It is evident that multi-patch cases have scatter 1.5-2 times less than for simultaneous cases.

It is important to note that the scatter of estimated modal parameters in multi-patch testing appears to be smaller than in simultaneous measurements. Multi-patch reduces uncertainty of modal parameters estimation thanks to more averaging (more measurement time) used from reference sensors perspective. More measurement time results in a higher energy transmitted to the system which can be observed in Fig. 4.18.

MPVI here was used to estimate uncertainty in modal parameters estimation for two types of OMA, but this parameter can also be used to determine condition change, hence indicate possible damage.

Table 4.4.

Modal parameter scatter obtained with MPVI.

mode	f, Hz	Base 1			Base 2			Multi-patch		
		freq.	shape	comb	freq.	shape	comb	freq.	shape	comb
1	66.6	0.8%	1.37%	1.06%	0.2%	1.66%	0.92%	0.5%	0.51%	0.50%
2	205.8	0.4%	1.26%	0.85%	0.2%	1.43%	0.83%	0.1%	1.06%	0.58%
3	323.4	0.3%	2.95%	1.61%	0.0%	5.24%	2.63%	0.4%	2.38%	1.39%
4	533.4	0.7%	0.72%	0.68%	0.2%	0.61%	0.40%	0.4%	0.52%	0.44%
Average		0.52%	1.58%	1.05%	0.16%	2.23%	1.20%	0.34%	1.12%	0.73%

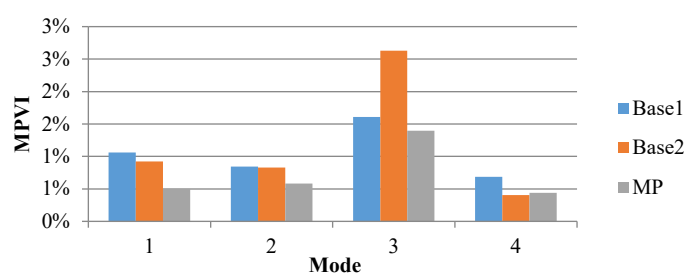


Fig. 4.19. Modal Parameter Variation Integrated (MPVI) in three test series.

Damage detection

For monitoring purposes any damage indication is enough, but for diagnostical purposes damage identification and localization is also necessary. Both above mentioned are considered: first – using MFCM as the tool for monitoring of structure's health, second – applying MPVI as the parameter for damage identification and localization.

Experimental validation of above techniques includes consequent implementation of two defects into the structure (defects are not mixed). First – unscrewed nuts on the base fixation on one side of the tower (Fig. 4.20(a)), referred here as Defect 1. This can be classified as a global defect because it alternates the boundary conditions of the system. Another defect is of a local nature – four unscrewed screws in one joint in the middle of the tower (Fig. 4.20(b)).

These screws serve as connection between the frame and the panel, which means that local stiffness becomes alternated. This defect is referred as Defect 2. Tests aimed for damage identification were done using simultaneous OMA measurements only.

MPVI application for structural diagnostics

Both defected test data were processed through *ARTEMIS* software and modal parameters variation were estimated. Table 4.5 shows MPVI parameters comparison between baseline measurements (also shown in table 1 as *Base 1*) and faulted states of the structure. Defects caused different changes in modal parameters. Fig. 4.21 displays combined MPVI values for all three states.

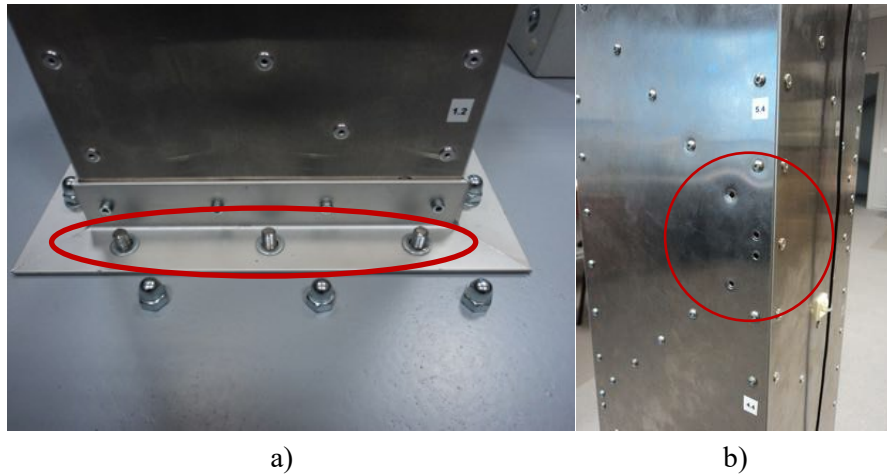


Fig. 4.20. Artificial defects. (a) – defect 1; (b) – defect 2.

In Fig. 4.21 one can notice that first defect causes MPVI increase for all modes, which shows global nature of the defect. Further analysis shows that first mode frequency has changed by 4.4% and the shape differs by 2.49% (MPVI parameter), which is significantly higher than reference values of 0.8% and 1.37% correspondingly. Second mode also has significant frequency shift – 2.3% whereas the scatter is only 0.4%. Similar discussion is right for other modes that have highly pronounced global behaviour, so one can deduce that boundary conditions or other global properties have changed. Taking into account that the first mode shape resembles 1st bending mode, it can be also supposed that the defect is in the lowest area of the tower or on the base. In practice it means that structure’s modification could be identified close to the base and an inspection is needed for that part of the structure.

It is necessary to note that analysis of mode shapes modification also includes mode shape comparison. This means that the mode estimated from the first state is verified (by Modal Assurance Criterion as well as visual examination) to be a modified version of the first state estimated mode. Otherwise, there is a risk of comparing two different modes, which obviously will give incorrect result.

Table 4.5.

Modal parameter scatter obtained with MPVI for baseline and defected conditions.

Mode	f, Hz	Base 1			Defect 1			Defect 2		
		<i>freq.</i>	<i>shape</i>	<i>comb</i>	<i>freq.</i>	<i>shape</i>	<i>comb</i>	<i>freq.</i>	<i>shape</i>	<i>comb</i>
1	67.0	0.8%	1.37%	1.06%	4.4%	2.49%	3.44%	0.6%	1.66%	1.11%
2	205.7	0.4%	1.26%	0.85%	2.3%	2.03%	2.18%	0.1%	1.73%	0.93%
3	324.1	0.3%	2.95%	1.61%	0.4%	5.16%	2.76%	0.2%	6.50%	3.32%
4	532.1	0.7%	0.72%	0.68%	1.3%	2.78%	2.04%	0.5%	1.51%	1.01%
Average		0.52%	1.58%	1.05%	2.10%	3.11%	2.61%	0.33%	2.85%	1.59%

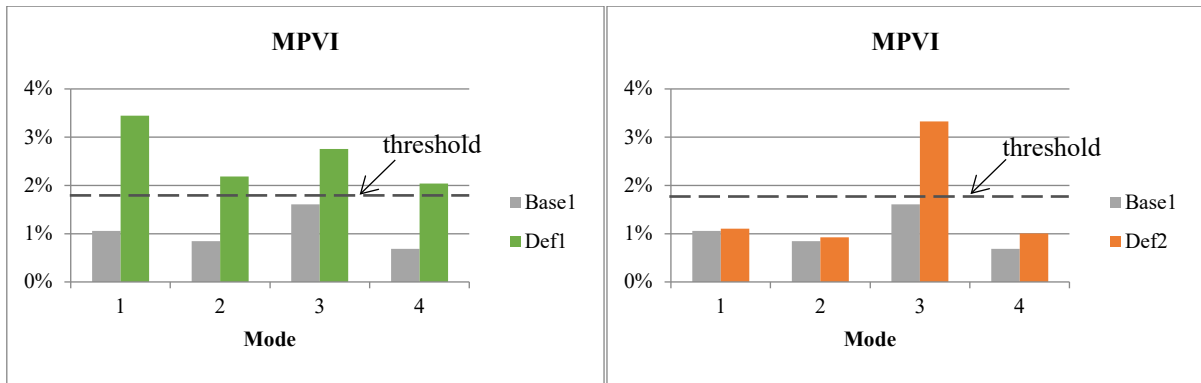


Fig. 4.21. MPVI parameters estimated for baseline and defected measurements.

Defect 2 was applied in the middle of the structure, only on one of four edges. That is why frequency MPVI (average 0.33%) as global parameter does not signalize any change in the structure and remains within reference scatter (0.52%). However, the shape MPVI of the 3rd mode (6.5%) clearly indicates there is a problem with the structure. As MPVI value exceeds threshold only for the 3rd mode, it means most probable damage location is tower's central section, where maximal deformations were found (Fig. 4.17(c)). Obviously, higher spatial resolution and more modes will bring up accuracy of this approach.

These examples clearly show that MPVI is a handy tool for diagnostics of structural condition. With some adjustments and more estimated modes it is even possible to accurately locate the defect using MPVI.

Case study conclusion

The laboratory scaled prototype of operating industrial structure was developed for study of structural health monitoring and diagnostics techniques. Optimization of technological and methodical aspects was addressed, i.e. selection of an object for modelling, measurement network and system, type of transducers, signal processing technique, etc. Selected solutions were evaluated, analysed and validated both computationally and experimentally. As the outcome, wind generator scaled operating model was designed with integrated network of deformation sensors. Experimental testing with OMA application was performed on the model in different states, establishing confidence in possibility to perform damage detection for industrial structures using OMA approaches.

It is necessary to stress the fact, that not only multi-patch OMA modal parameter scatter is lower than for simultaneous OMA, but also modal parameter estimation is more stable, thanks to higher integrated energy provided to the system in multi-patch OMA.

Modal Parameter Variation Integrated together with mode shape visualisation are very handy for diagnostic purposes. An engineer with adequate understanding and experience can identify and localize defects by analysing MPVI and mode shapes or additionally use more advanced algorithms, i.e. implementing Wavelet Transform Analysis [116].

It is presumed that multi-patch OMA results will not differ significantly from simultaneous OMA results, based on the scatter estimates comparison.

MPVI can be a convenient tool for SHM. When structures are measured with OMA technique, modal parameter estimation performed and MPVI parameter obtained, then this allows to analyse frequencies and mode shapes to potentially localize the damage. However, the severity of the damage can be evaluated only by careful inspection of a skilled and experienced engineer.

4.5. Aluminium beam

The goal of the experiment is to validate Modal Field Comparison Method. Experimental methodology:

1. Verify parameter stability for a single healthy state. Significant number of measurements for unchanged state is performed, at least 20. If the chance of false detection is lower than at least 5 %, it can be stated that MFCM is a reliable tool for SHM. Simply put, there should be no MFCM value indicating faulty condition for healthy state measurement.
2. Validate MFCM ability to detect condition modification. Test object must be modified and MFCM value should indicate this modification.
3. Results repeatability. For the experiment to be completely reliable, it is necessary also to restore initial reference healthy condition before modification and obtain MFCM parameter that falls within normal variance of other healthy values.
4. Sensitivity check. Finally, a glimpse into sensitivity of the method should be done, by starting with a small structural modification and gradually increasing it until the parameter is able to detect the change.

Experiment description

The test object is an aluminium cantilever beam with rectangular cross section 3x40 mm. The length of the mounted beam is 850 mm, the weight is 275 g. Piezo film deformation sensors are chosen as vibration transducers (Fig. 4.22).

The beam is firmly fixed on a stiff frame. Above the beam a tube is placed, which supports the shielded flat ribbon cable. This cable connects sensors to the data acquisition unit inputs. There are 12 sensors equally distributed on the upper surface of the beam. A CAD model of the beam has been studied using FE analysis.

Deformations are directly proportional to strain, so FE strain shapes describe the actual measured deformations quite well. The beam can vibrate in 3 directions – vertical, horizontal and axial, however, during the experiment, only vertical direction is excited, so it is expected to obtain modes with vertical shapes. Sensor's placement allows only vertical mode shapes to be detected.

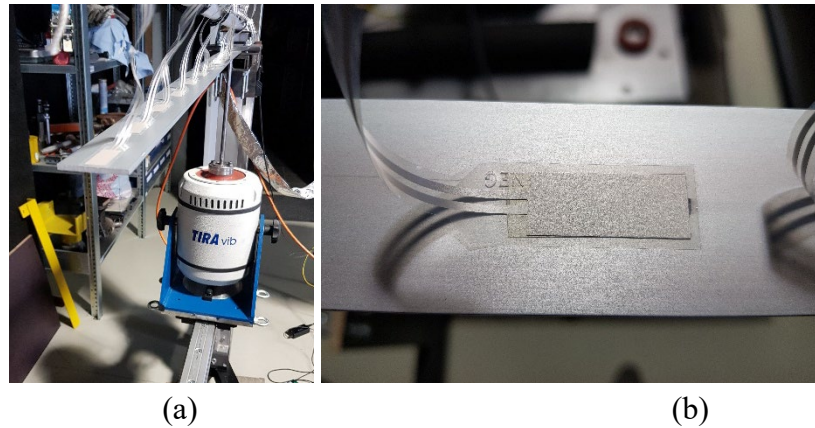


Fig. 4.22. a) Experimental setup; b) Piezo film deformation sensor.

FE analysis shows 20 modes in frequency range from 0 Hz up to 1270 Hz. There are 12 vertical classical bending modes, which shapes mimic sine function, and 8 horizontal and torsional modes. An issue one has to be aware of is mode shapes spatial aliasing. This happens when experimentally obtained modes of high order cannot be correctly displayed due to limited amount of sensors. This can lead to similar or even identical experimental shapes for different modes. A good practice is to avoid spatial aliasing, so with 12 available sensors it is possible to fully show first 6 vertical modes.

Environmental and boundary conditions stayed the same for the entire experiment, with slight temperature deviations from 10°C to 14°C. Data acquisition is done using Brüel & Kjær Pulse system with 12 input channels and 1 output generator channel, which drives the shaker through a power amplifier. The input channels have a high pass filter set to 0.7 Hz.

The excitation is 1.6 kHz wideband white noise delivered to the beam through a stem. In steady state this stem is approximately 1 mm away from the beam, so when shaker is oscillated, the stem hits the beam in random fashion. The stem is hitting the very base of the beam. Reader with experience in modal analysis can note that this is not the most efficient way to excite bending modes. Ideally, the point of excitation should be at the point of maximum displacement, which is of course the free end of the beam. However, this would alter the boundary conditions, because the free end would not be “free” at the moment of hitting. For this reason, excitation through the base is optimal in this case. It was taken into account that first order mode might not be excited efficiently. Still, practice showed, that first mode is excited, and the oscillation can be visually seen during test.

Measurement sessions

Vibrational data was recorded in frequency bandwidth of 1600 Hz, which is sampled at 4096 samples per second. Each recording is 2 minutes long. There were 23 recordings of reference state of the beam, done at different times and even on different days. Then a washer was glued on the lower surface in the middle of the beam (Fig. 4.23(a)) that simulates fault changing structural properties. Washer’s weight was 23.83 g. Two measurements were made with this added mass. After that, the washer was removed, thus reference state was restored. This was done to check if the resulting parameter will restore its reference value. Five extra

measurements of initial reference state were performed to validate MFCM consistency and stability.

After that a sequence of sensitivity tests was done. Washers of different masses (Fig. 4.23(b-e)) were sequentially and separately glued in the middle of the beam (on the lower part, because the upper one had sensors installed). Three measurements with each mass were done, which is 12 measurements for added masses. In total there were 42 measurements done on the beam.

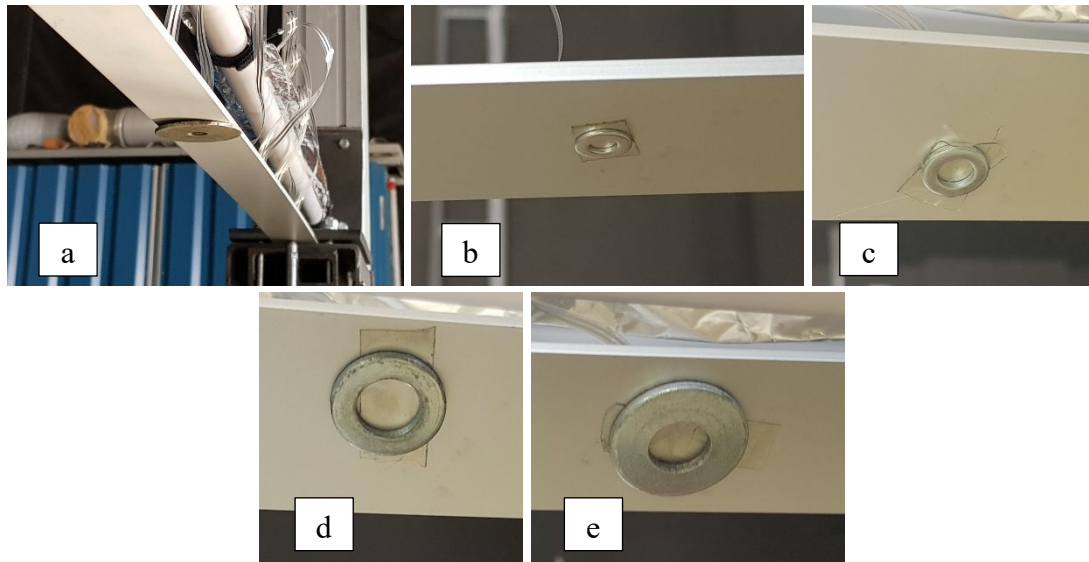


Fig. 4.23. Added masses, in order of application. a) 24 g; b) 0.3 g; c) 0.8 g; d) 2.9 g; e) 9.8 g.

Results and discussion

The MFCM parameter (3.27) is calculated relatively to baseline, which in this case was an average between first twenty measurements without added mass. Each of 42 measurement results is related to the baseline and plotted in a bar plot, shown in Fig. 4.24. The green horizontal line is the mean MFCM parameter value for first 20 measurements. The mean value is 1, as the plotted parameter is normalized as in Eq. (23). The red line is three standard deviations value above the mean, which serves as damage detection threshold. MFCM values higher than the red line are considered to represent modified state.

It is obvious from a glance, that heavy washer (Fig. 4.23(a)) makes a considerable impact on the structure. This is shown as two bars with value above 25 for measurement 24 and 25. The fixed washer does not only increase mass by approximately 9%, but also increases local stiffness. Sensitivity tests resulted in increased parameter only for 9.8 g washer (Fig. 4.23(e)). From this one can conclude that random factors, which influence modal characteristics, mask the impact that small washers (Fig. 4.23(b-d)) make on the structure.

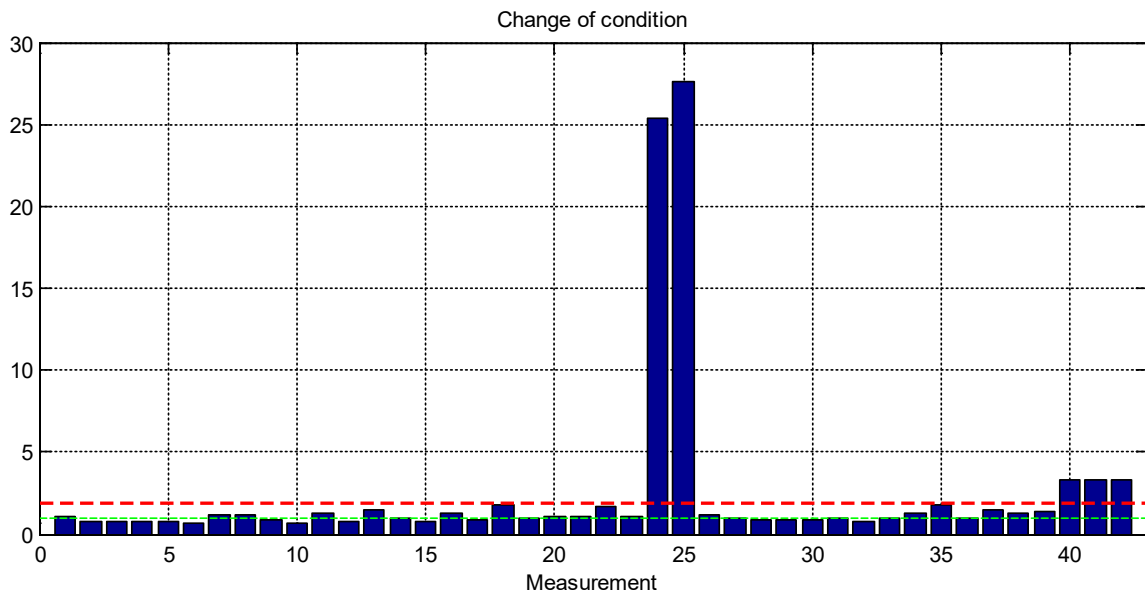


Fig. 4.24. MFCM parameter values for 42 experimental measurements.

All healthy condition MFCM values lie below the threshold, including values estimated for measurements 21-23 and 26-31, which were not used for baseline calculation.

It can be observed that washers weight increase in 2.5 times resulted in parameter value increase approximately 8 times. This shows non-linear nature of damage development and can be supported by Eq. (1.3). Linear relationship would be possible if the mass M change did not influence stiffness K and damping C change. In practice it is not true, because larger washer dimensions also change local stiffness, as mentioned before, and larger piece of adhesive tape also changes damping. Note also, that Eq. (1.3) refers only to a single DOF, but in practice multiple DOFs are affected by introduced washer.

A notable parameter change has been achieved for mass change of approximately 3.6 % of the total beam mass and some undefined stiffness change.

Case study conclusion

This experiment considers approach for structural damage detection called Modal Field Comparison Method. The method compares decomposed power spectra densities of measured reference healthy state and possible damaged states. By utilizing singular value decomposition, the method separately compares singular vectors and singular value frequency functions. The result is presented as a single parameter called MFCM parameter (Eq. (3.27)).

The method has been experimentally validated on a cantilever aluminium beam. There were no false detections and parameter showed consistent values. The method shows sensitivity to mass changes larger than 3.6 % of a total mass. The MFCM parameter has a potential to be implemented into an automated SHM system, because the method does not require modal parameter estimation.

This algorithm, however, does not take into account influence factors like load and temperature. Further study is focused on damage identification using estimated modal

parameters, as this approach is better established. Also, usage of modal parameters allows to use modal passport, which takes influence factors into account.

4.6. Radar tower

The goal of this study is to validate SHM application possibility for a full-scale industrial structure using the Operational Modal Analysis based SHM system.

The structure under test is a radar tower in Riga airport (Fig. 4.25). It is 24 m high, with a rotating antenna on the top. The platform with the antenna is not supposed to be monitored, so the monitoring area is decided to be from the bottom of the tower to the fifth red frame section, which is 18 m high. There are 20 measurement points on the tower placed in corners of 5 horizontal sections (Fig. 4.25(b)). Fig. 4.25(c) shows the middle of the section corner, where sensors are installed. The placement is chosen on each side of the corner, to register deformation in both directions.

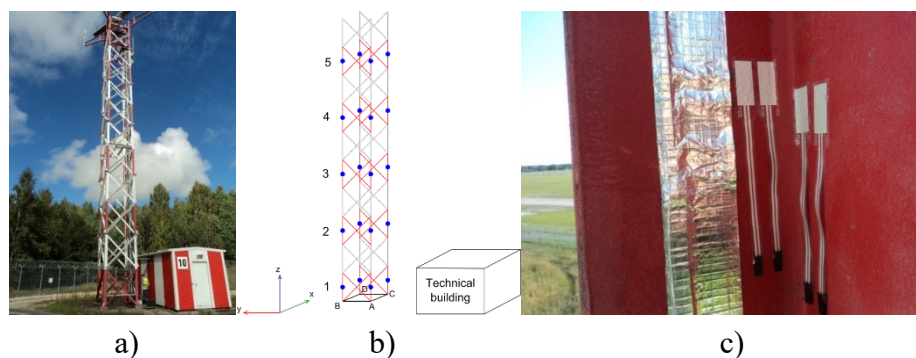


Fig. 4.25. a) Radar tower; b) point locations (blue dots); c) single measurement point.

There are two sensors on each side, one is the main sensor, another is a reserve, in case the first one fails. There are 80 sensors on the tower, from which 40 can be used for simultaneous OMA measurements.

Measurement cables and patching panel

Measurement cables connect deformation sensors to DAU inputs. Each sensor requires 2 wires – signal and floating ground. The cables used are flat ribbon cables (FRC). FRC cables are installed on each tower's leg along its length. At designated places FRC wires are soldered to the preamplifiers placed next to the sensor positions. FRC with preamplifiers on both sides are covered with aluminium fibre reinforced shielding tape that protects wiring from electromagnetic interference (EMI) noise. The shield is grounded together with DAU and PC. When cables are installed properly, piezo films are connected to the preamplifiers. The ends of the FRC cables are terminated by D-sub connectors, which are connected to the patching panel (Fig. 4.26(a)). The panel itself has 80 SMB outputs, one for every existing sensor. This simple approach allows easily changing patching cables between sensors, if one fails or for multi-patch OMA purposes. Patching cables are then connected into designated input channels on the DAU (Fig. 4.26(b)).



Fig. 4.26. a) Patching panel; b) data acquisition unit.

Installation

The process of installation requires the weather conditions to be dry and not too windy. There are 4 shielded FRC cables, one for each tower side. The cables have double sided adhesive tape on one side. Using mobile lifter, engineers go up to the height of 18 m, close to the 5th level, with the cables and sensors ready. First, the tower surface is cleansed with cleaning solution. Then engineers start to glue cables and sensors at designated locations. When sensors are glued on the surface and connected to the preamplifier inputs, the remaining open part of the sensors is covered with aluminium adhesive tape, which serves as protection from EMI and bad weather conditions. This process continues for every level on each side. After all cables and sensors are installed, the ends of the cables are connected to D-sub connectors on the patching panel (Fig. 4.26(a)). The principal schematic of the measurement system is shown in Fig. 4.27.

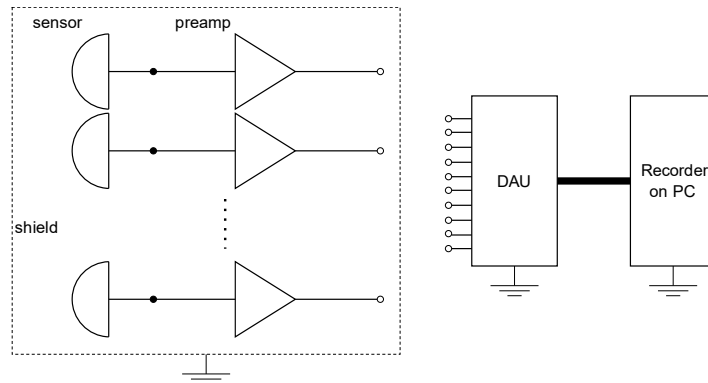


Fig. 4.27. Measurement system principal schematic.

Multi-patch OMA measurements

After the system, which included sensors, cables, patching panel and other necessary equipment, was installed, multi-patch OMA measurement session was performed. Weather conditions play a significant role for these tests – it should be windy enough, as wind is the main random excitation source. The wind speed during the experiment was slow, thus the main excitation source was periodic – rotating antenna.

The measurement setup was the following. One patch consisted of 16 channels, 8 of which are reference channels, thus another 8 are moving channels. The full session takes 4 measurements, 5 minutes each. Between the measurement the patching cables were reattached to the next measured channels.

Finite element analysis

Finite element (FE) analysis based on *NeiNastran* software package was done for a digital tower model for the purpose of obtaining analytical modal parameters. Some of modal frequencies are shown in Table 4.7. Based on these results the frequency range for measurement recordings was defined to be 200 Hz, thus the sampling frequency is 512 Hz. Some modes have identical shapes, but in different directions. For example, Modes 1 and 2 are both 1st bending shapes, but in mutually perpendicular axes.

Experimental results

Vibration recordings were processed using *SVIBS ARTeMIS* software for OMA. Artemis performs estimation of modal parameters by building mathematical models that fit the experimental data. Some of the approaches can be found in [117]. The result is a set of experimental modal parameters.

Fig. 4.28 shows modal shapes for the 1st bending mode. In Fig. 4.28(a) one can see analytical 1st bending displacement shape in Y direction, Fig. 4.28(b) is the tower geometry in steady state for comparison, and Fig. 4.28(c) shows experimental 1st bending strain mode shape. The latter is a combined shape for bending shapes in X and Y direction. The shape is estimated as combined, because the frequency resolution in OMA estimation is not fine enough to be able to separate two closely spaced modes. Also, due to periodic antenna excitation, the tower oscillation shape has torsional movement around its axis. This is observed for most shapes, not only the 1st bending one. Note, that experimental shapes show local deformation (strain) caused by stress, which is inversely proportional to displacement in the analytical results (see Section 4.1). Due to this it is impractical to quantitatively compare the analytical and experimental shapes, but it is possible to analyse similarities and differences visually or in reference domain.

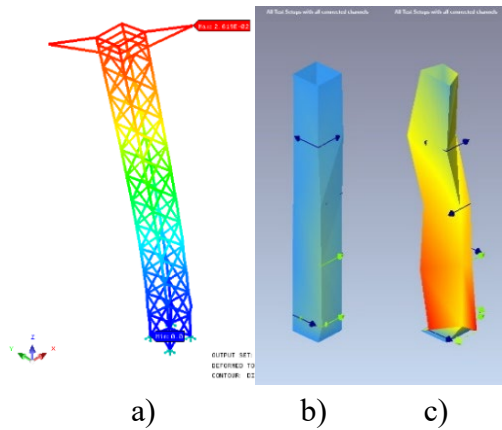


Fig. 4.28. a) Analytical 1st bending (displacement); b) Experimental steady state; c) Experimental 1st bending (strain).

Table 4.6 shows experimental modal frequencies. The first experimental mode correlates well with the analytical one (2.21 Hz and 2.14 Hz correspondingly) (Table 4.7). The first mode correlation between FE and test data is a good indication that the FE model is adequate. It is possible to compare mode shapes as well, using the Modal Assurance Criterion. In order to do this, FE model displacements can be transformed into deformations as a second derivative.

Table 4.6.

Experimental modal frequencies

Nr.	1	2	3	4	5	6	7	8
f , Hz	2.21	5.75	9.16	12.84	13.99	16.93	59.24	76.88

Table 4.7 shows comparison of modal frequencies between the experimental and analytical results. It is observed that the mode order is different for the analytical result. Analytical console (the top part of the tower) modes do not create significant vibrational response in the tower, so these are not identified. Other differences can also be explained by the fact that frame sections in the technical project were 4 m high. The measurement of the real section showed 3.6 m. Full measurement of the real tower dimensions was not feasible, so the difference between the model and the object remained.

Table 4.7.

Comparison of modal frequencies

Analytical			Experimental	
Mode Nr.	f , Hz	Shape	Mode Nr.	f , Hz
1	1.92	1 st bending	1	2.21
2	2.14	<i>pair</i>		
5	12.11	2 nd bending	4	12.84
6	12.76	<i>pair</i>		
8	16.47	1 st torsional	6	16.93

Monitoring prospects

Modal frequencies (Table 4.6) and shapes describe dynamic behaviour of the tower in its current state or condition. Once the condition of the tower is modified (local corrosion, loose bolts, base problem caused by earth erosion, added mass etc.), the dynamic behaviour changes and the modal parameters also change. By monitoring the modal parameters, it is possible to detect the condition modification. By analysing how modal parameters changed it is then also possible to identify and localize defects.

Discussion on experimental SHM system in industrial environment.

The developed experimental measurement system has turned out to be cost-efficient, as the used materials are widely accessible and inexpensive. Multi-patch OMA approach has proven to be applicable using the measurement system. The shielding was efficient, and EMI related noise was largely masked by the vibration signal.

One month after the experiment the system was checked, and OMA measurements were repeated. Unfortunately, some of the system channel signals were corrupted. There was either low and noisy signal transmission, or no vibrational signal at all. Measurement network troubleshooting was done, which did not reveal connectivity problems. It is believed that environmental conditions had a strong impact on transducers preamplifiers. Two particular causes are:

- humidity can create short circuit in the preamplifier,
- strong electromagnetic field could damage field-effect transistors (FET) in the preamplifier.

Condensed water was observed around the preamplifier after opening that area, which means that the cable was not sealed well enough. In laboratory conditions it was also observed that preamplifiers sometimes failed after touching them with bare hands, which could lead to static voltage discharge and FET damage. It is obvious, that the weakest part of the prototype is the preamplifier. Other studies done in the scope of this thesis showed that preamplifiers are not needed for applications of 3-4 m long, or even more. It remains uncertain, however, whether piezo film sensors can provide strong signal on tens of meters without preamplification.

Case study conclusion

The goal of the study was to validate SHM application possibility for a full-scale industrial structure using the Operational Modal Analysis based SHM system. For that a cost-efficient OMA measurement system prototype for 20 m airport radar tower was designed. Cost-efficiency was gained by utilizing inexpensive deformation piezo film sensors and by reducing the amount of input channels in the measurement system by switching to multi-patching. The design and installation process were done. Measurement procedures were developed and applied. The resulting modal parameters provide enough description of the tower dynamic behaviour. Modal parameters can be later used for monitoring purposes. The study has shown that for real objects, especially the ones with strong electromagnetic fields, the use of preamplifiers makes the SHM system unreliable. Based on this conclusion it was later decided to perform tests on other structures using the same piezo film sensors without preamplifiers.

5. CONCLUSIONS

The aim of the presented thesis was to develop SHM technology for structures during their operation. The technology is based on the system identification using operational modal analysis, taking into account the conditions of structures operation. In the scope of this thesis these conditions were different forces in form of loads, acting on the structure, e.g., different rotation speed for a helicopter blade model. As the result, a novel SHM system was developed and tested on 4 structures of different complexity and size.

The presented thesis includes scientific literature review that covers such topics as overall concept of structural health monitoring, basic theory of operational modal analysis and examples of modal parameters estimation methods, piezo film deformation sensors, harmonics extraction algorithms, as well as structural damage identification. The review has been useful in identifying applicable methods and techniques for the development of SHM technology prototype. The theory in the literature review is used as a background for this thesis.

A process of SHM system development and usage for a selected structure is shown in Section 2 in a form of a road map. It includes description of steps to be made to get the SHM system ready for monitoring purposes. These steps include:

- Technological procedures: sensors' installation, wiring, setting up data acquisition system and computer with OMA software.
- Measurement procedures: performing measurement of vibrational responses and registering operational conditions – loads, rotation velocity.
- Methodological procedures: harmonics extraction, modal parameters estimation, application of modal passport and damage detection.

The main technological solution presented in this thesis is application of piezo film deformation sensors, which successfully substitute accelerometers as sensors for measurement of vibration signals. When measuring vibration with accelerometers the transducers have to be mechanically fixed to the surface, which may have influence on objects properties. For aviation structures there is also the problem of transducers mass and size that may affect the structure's modal properties and its aerodynamics. Also, as was mentioned earlier, high cost of accelerometers must be considered. Even more restrictions are imposed in case of a laser scanner, not counting the costs.

Piezo film deformation sensors directly measure the stretching/compression longitudinal deformations of the surface layer. These sensors are very thin (only 28 μm), they have negligible mass and low costs that allows using large number of sensors to obtain modal data, while making much smaller distortions in mechanical and aerodynamic properties of the object. Sensors and wiring allow to be wrapped by a thin protective layer, making a homogenous entity with the structure.

Additional advantages are provided when using film piezoelectric sensors that measure only the dynamic component of deformations – they do not require balancing as conventional resistive strain gauges. Due to the low cost and practically no influence on the researched object,

the grid of film piezoelectric sensors is able to provide high enough resolution in identifying mode shapes.

The comparison of mode shapes obtained using accelerometers and piezo film sensors proved the validity of theoretical foundation, that surface deformations, arising during vibration of the structure, are related to the vibration displacement, and thus also to acceleration, which is conventionally used in OMA. Tests on a beam like structure (helicopter blade) showed that for bending modes the deformation shape of the blade is shifted by 180° in relation to the shape of displacement, which shows that the 2nd spatial derivative of displacement shape correlates with deformation shape.

It has been proven that even though deformation is not the same as vibration acceleration or velocity, it is still a valid input signal for Operational Modal Analysis methods.

Harmonics extraction algorithm from vibrational responses of a structure with periodical excitation component was proposed and experimentally validated on composite helicopter blades. This algorithm filters out periodical components, which are often induced from the shaft rotation. Extraction of these components cleared out the structural responses, decreased the influence of periodic parts of the signal, allowing to expose hidden modes, which increased overall quality of the modal analysis. There was an improvement in terms of decreased modal complexity by 5.5% for 3 modes out of 10, which were especially affected by periodic components.

Additionally, comparison of structural responses and estimated modal parameters before and after harmonics extraction is useful for in-depth analysis of the structures condition.

In Section 3.3 Modal Field Comparison Method was introduced. This method is very useful for pre-analysis of measured structural responses without the need to estimate modal parameters. This saves analysis time and allows to employ less skilled personnel for operating such a step in real life. As the result, the method can identify a measurement which shows modification of structural properties, whether it is a mass increase or stiffness change induced by damage.

Tests on the aluminium beam showed the following. The reference state value of the MFCM parameter is 1, whereas the healthy state threshold is at 1.9 units. A notable parameter change (MFCM value around 3.36 units) has been achieved for mass change of approximately 3.6 % of the total beam mass and some undefined stiffness change. It was observed that washer's weight on the beam increase in 2.5 times (from 9.8 g to 24 g) resulted in parameter value increase approximately 8 times (from 3.36 to 25-27 units).

The disadvantage of MFCM is that it does not take into account variability in external conditions, so extra load or temperature change will potentially sound a false alarm. However, this disadvantage is dealt with by introduction of modal passport.

Modal passport was introduced and formulated in this thesis. Modal passport is a framework for modal parameters assessment between multiple measurements of a structure with different operating conditions. It is both a database for storing existing measurement data (modal

parameters and external influence factors, like operational loads, temperature, etc.) and a set of tools realized in *Excel* or *Matlab*. The main damage assessment tool is Modal Parameter Variation and its integrated version MPVI. It uses straightforward arithmetical calculations to assess modal frequencies and mode shapes between different measurements. MPV allows to conveniently detect damage and make conclusions about damage type and localization.

MPV was successfully implemented for damage detection of a global defect on the mentioned wind turbine model foundation and a local defect on the structures side. The difference between the local and global defects is the number of modes having MPV value higher than the healthy threshold. For example, global defect resulted in MPV values of 3.4, 2.2, 2.8 and 2 % for modes 1 to 4 accordingly, which was above of 1.8 % healthy state reference level. At the same time, local defect resulted in MPV values of 1.1, 0.9, 3.3 and 1 % for modes 1 to 4 accordingly. This clearly shows that only the 3rd mode MPV signalizes changes in modal parameters. By observing this particular modes' shape, it was possible to draw conclusions on the location of the defect.

It was shown, that SHM can be done also using multi-patch OMA, which is an effective way to save costs. Another advantage of multi-patch OMA is the fact that the system receives more excitation energy due to longer measurement time, which stabilizes MPV parameter for reference state. This allows for higher damage detection precision in later stages. Tests on a wind turbine laboratory model showed that multi-patch OMA results in 1.5 – 2 times lower initial MPV parameter values compared to simultaneous OMA measurements. The main and serious disadvantage of multi-patch OMA is that it is quite time consuming, so further study was based on simultaneous OMA measurements.

The optimization of modal passport to include MFCM parameter was not done, as this was not set as a task of this thesis, and a more technically available approach of using modal parameters for damage identification was used to complete thesis tasks.

The framework of modal passport simplifies different research and industrial procedures related to modal analysis as illustrated on the results of composite blade testing in Section 4.3. It allows identification of vibration/deformation modes of individual structure using data independent from test or operation conditions. For instance, data measured in winter or summer, from fixed or rotating structure, maximally loaded or in idle mode could be used. However, tests under varying temperatures have not been performed in the scope of this thesis and is a topic for future studies.

In order to predict change of individual structure properties as a function of some operational factor, one does not need to study behaviour of this particular blade. It is enough to have only its modal parameters in static state and then use the generalized dependence of typical modal passport on above operational factor.

In terms of diagnostics (SHM) it is important to predict condition modification of a particular operating structure using just the modal parameters of the static test. Based on the dependencies of the typical passport a prediction can be made independently on operational

mode and without respective tests of that structure. It means that for an individual structure its modal properties can be simulated for any combination of typical operating factors. The simulated properties are characterized by both the predicted value and confidence intervals (MPVI). If some modal parameter of a particular structure exceeds the intervals, it indicates that its modal and mechanic properties exceed the typical ones.

The presented set of technological and methodological solutions is combined into a structural health monitoring system prototype for usage during varying operating conditions. The underlying technology would benefit from further research, particularly in application of modal passport for different structures and testing of temperature influence on modal parameters, which was not part of this thesis. There is a research project going on, which tests the proposed SHM system on a set of glass fibre composite cylinders, together with temperature tests, apart from everything else.

REFERENCES

- [1] M. Derriso, C. McCurry and C. Chubert Kabban, “2 - A novel approach for implementing structural health monitoring systems for aerospace structures,” in *Structural Health Monitoring (SHM) in Aerospace Structures*, Woodhead, 2016, pp. 33-56.
- [2] “Annual Analyses of the EU Air Transport Market 2016,” European Commission, 2016.
- [3] Y. Lin, L. Tu, H. Liu and W. Li, “Fault analysis of wind turbines in China,” *Renewable and Sustainable Energy Reviews*, vol. 55, pp. 482-490, 2016.
- [4] “Sāremā salā nolūzusi un apgāzusies 60 metru augsta vēja turbīna,” Apollo.lv, 16 February 2022. [Online]. Available: <https://www.apollo.lv/7455790/sarema-sala-noluzusi-un-apgazusies-60-metru-augsta-veja-turbina>. [Accessed 15 March 2022].
- [5] “This Day in the Aviation History - On April 1, 2011, Southwest Airlines Flight 812 suffered rapid depressurization due structural failure,” FL360aero, 1 April 2021. [Online]. Available: <https://fl360aero.com/detail/this-day-in-the-aviation-history-on-april-1-2011-southwest-airlines-flight-812-suffered-rapid-depressurization-due-structural-failure/155>. [Accessed 15 March 2022].
- [6] H. F. Zhou, H. Y. Dou, L. Z. Qin, Y. Chen, Y. Q. Ni and J. M. Ko, “A review of full-scale structural testing of wind turbine blades,” *Renewable and Sustainable Energy Reviews*, vol. 33, p. 177–187, 2014.
- [7] B. Chen, S. You, Y. Yu and Y. Zhou, “Acoustical damage detection of wind turbine blade using the improved incremental support vector data description,” *Renewable Energy*, vol. 156, pp. 548-557, 2020.
- [8] R. Yang, Y. He and H. Zhang, “Progress and trends in nondestructive testing and evaluation for wind turbine composite blade,” *Renewable and Sustainable Energy Reviews*, vol. 60, p. 1225–1250, 2016.
- [9] D. Balageas, C.-P. Fritzen and A. Güemes, *Structural Health Monitoring*, Hoboken, New Jersey: Wiley & Sons, 2006.
- [10] HBM, “Structural Health Monitoring | HBM,” [Online]. Available: https://www.hbm.com/en/5530/structural-health-monitoring/?product_type_no=Structural%20Health%20Monitoring. [Accessed 24 May 2022].
- [11] SGS, “Structural Health Monitoring | SGS,” [Online]. Available: <https://www.sgs.com/en/industries-and-environment/power/asset-integrity-management-services/non-destructive-testing-ndt/structural-health-monitoring>. [Accessed 24 May 2022].
- [12] C. P. Fritzen, “Vibration-Based Structural Health Monitoring – Concepts and Applications,” *Key Engineering Materials*, Vols. 293-294, pp. 3-20, 2005.
- [13] N. M. M. Maia and J. M. M. Silva, *Theoretical and Experimental Modal Analysis*, Wiley, 1997.
- [14] C. Ventura and R. Brincker, *Introduction to Operational Modal Analysis*, Wiley, 2015.
- [15] M. Döhler, P. Andersen and M. Mevel, “Data Merging for Multi-Setup Operational Modal Analysis with Data-Driven SSI,” in *Proceedings of the IMAC-XXVIII*, Jacksonville, Florida USA, 2010.

- [16] L. Zhang, T. Wang and Y. Tamura, "A frequency–spatial domain decomposition (FSDD) method for operational modal analysis," *Mechanical Systems and Signal Processing*, vol. 24, no. 5, pp. 1227-1239, 2009.
- [17] M. Döhler, E. Reynders, F. Magalhaes, M. Mevel, G. De Roeck and A. Cunha, "Pre- and Post-identification Merging for Multi-Setup OMA with Covariance-Driven SSI," in *Proceedings of the IMAC-XXVIII*, Jacksonville, Florida USA, 2010.
- [18] L. Zhang, M. Boeswald, D. Goge and H. Mai, "Application of Operational Modal Analysis for Wind-Tunnel Testing of an Aircraft Wing Model with Control-Surface," in *IMAC XXVI conference*, Orlando, Florida, 2008.
- [19] E. Neu, F. Janser, A. A. Khatibi, C. Braun and A. C. Orifici, "Operational Modal Analysis of a wing excited by transonic flow," *Aerospace Science and Technology*, vol. 49, pp. 73-79, 2016.
- [20] M. L. Wymore, J. E. Van Dam, H. Ceylan and D. Qiao, "A survey of health monitoring systems for wind turbines," *Renewable and Sustainable Energy Reviews*, vol. 52, pp. 976-990, 2015.
- [21] A. Güemes, A. Fernandez-Lopez, A. R. Pozo and J. Sierra-Pérez, "Structural Health Monitoring for Advanced Composite Structures: A Review," *Journal of Composites Science*, vol. 4, no. 1, 2020.
- [22] H.-C. Lin, Y.-C. Ye, B.-J. Huang and J.-L. Su, "Bearing vibration detection and analysis using enhanced fast Fourier transform algorithm," *Advances in Mechanical Engineering*, vol. 8, no. 10, 2016.
- [23] D. Roach and S. Neidigk, "Does the Maturity of Structural Health Monitoring Technology Match User Readiness?," in *In Proceedings of the International Workshop on SHM*, Stanford, USA, 2011.
- [24] "LAN-XI Data acquisition system," Brüel & Kjær, [Online]. Available: <https://www.bksv.com/en/instruments/daq-data-acquisition/lan-xi-daq-system>. [Accessed 16 January 2022].
- [25] "Data Acquisition (DAQ)," National Instruments, [Online]. Available: <https://www.ni.com/en-us/shop/data-acquisition.html>. [Accessed 16 January 2022].
- [26] "ARTeMIS Modal - Structural Vibration Solutions," Structural Vibration Solutions, [Online]. Available: <https://svibs.com/>. [Accessed 16 January 2022].
- [27] D. Coronado and k. Fischer, "Condition monitoring of wind turbines: state of the art, user experience and recommendations," Fraunhofer Institute for Wind Energy and Energy System Technology IWES Northwest, Bremerhaven, 2015.
- [28] S. Chauhan, "Parameter estimation algorithms in operational modal analysis: a review," in *6th International Operational Modal Analysis Conference*, Gijon, Spain, 2015.
- [29] E. Bechhoefer and M. Kingsley, "A Review of Time Synchronous Average Algorithms," in *Proceedings of the Annual Conference of the PHM Society 2009, Vol. 1 No. 1*, 2009.
- [30] F. B. Zahid, Z. C. Ong and S. Y. Khoo, "A review of operational modal analysis techniques for in-service modal identification," *Journal of the Brazilian Society of Mechanical Sciences and Engineering*, vol. 42, no. 398, 2020.
- [31] R. Brinkcer and L. Zhang, "Frequency Domain Decomposition Revisited," in *Proceedings of the 3rd International Operational Modal Analysis conference - IOMAC*, 2009.

- [32] R. Brincker, L. Zhang and P. Andersen, “Modal identification from ambient responses using frequency domain decomposition,” in *IMAC 18 : Proceedings of the International Modal Analysis Conference (IMAC)*, San Antonio, Texas, USA, 2000.
- [33] S. Qin, J. Kang and Q. Wang, “Operational Modal Analysis Based on Subspace Algorithm with an Improved Stabilization Diagram Method,” *Shock and Vibration*, vol. 2016, pp. 1-10, 2016.
- [34] D. Mironovs, MSc thesis: Estimation of global modal parameters in multi-patch Operational Modal Analysis, Lyngby: Technical University of Denmark, 2016.
- [35] M. Goursat, M. Döhler, L. Mevel and P. Andersen, “Crystal clear ssi for operational modal analysis of aerospace vehicles,” in *International Modal Analysis Conference*, Jacksonville, Florida, 2010.
- [36] P. Andersen, “Operational Modal Analysis,” Structural Vibration Solutions, [Online]. Available: <https://svibs.com/applications/operational-modal-analysis/>. [Accessed 31 May 2022].
- [37] D. Mironovs and S. Chauhan, “Modal Parameter Estimation in multi-patch Operational Modal Analysis: Perspectives and Approaches,” in *35th International Modal Analysis Conference*, Garden Grove, California, USA, 2017.
- [38] X. P. Qing, S. J. Beard, A. Kumar, T. K. Ooi and F. K. Chang, “Built-in Sensor Network for Structural Health Monitoring of Composite Structure,” *Journal of Intelligent Material Systems and Structures*, vol. 18, pp. 39-49, 2017.
- [39] Z. Su, X. Wang, Z. Chen, L. Ye and D. Wang, “A built-in active sensor network for health monitoring of composite structures,” *Smart Mater. Struct.*, vol. 15, p. 1939–1949, 2006.
- [40] Y. J. Yan and L. H. Yam, “Online detection of crack damage in composite plates using embedded piezoelectric actuators/sensors and wavelet analysis,” *Compos. Struct.*, vol. 58, pp. 29-38, 2002.
- [41] C. C. Bowland, Y. Wang and A. K. Naskar, “Development of nanoparticle embedded sizing for enhanced structural health monitoring of carbon fiber composites,” in *roc. SPIE 10169, Nondestructive Characterization and Monitoring of Advanced Materials, Aerospace, and Civil Infrastructure 2017, SPIE Smart Structures and Materials + Nondestructive Evaluation and Health Monitoring*, Portland, Oregon, USA, 2017.
- [42] S. Bhalla and C. K. Soh, “Structural Health Monitoring by Piezo-Impedance Transducers. I: Modeling,” *Journal of Aerospace Engineering*, vol. 17, no. 4, 2004.
- [43] J. H. Nienwenhui, J. J. Nuemann, D. W. Greve and I. J. Oppenheim, “Generation and detection of guided waves using PZT wafer transducers,” *IEEE Transactions on Ultrasonics, Ferroelectrics and Frequency Control*, vol. 52, no. 11, pp. 2103-2111, 2005.
- [44] H. Kawai, “The piezoelectricity of poly(vinylidene fluoride),” *Japanese Journal of Applied Physics*, vol. 8, no. 7, p. 975–976, 1969.
- [45] D. Liu, M. Luo, Z. Zhang and Y. Hu, “Operational modal analysis based dynamic parameters identification in milling of thin-walled workpiece,” *Mechanical Systems and Signal Processing*, Vols. 167, Part A, no. 108469, 2022.
- [46] T. Bregar, B. Starc, G. Čepon and M. Boltežar, “On the Use of PVDF Sensors for Experimental Modal Analysis,” in *Topics in Modal Analysis & Testing, Volume 8, Proceedings of the 38th IMAC, A Conference and Exposition on Structural Dynamics 2020*, Cham, Springer, 2020.

- [47] M. Luo, H. Huo, D. Axinte and D. S. Liu, “A wireless instrumented milling cutter system with embedded PVDF sensors,” *Mechanical Systems and Signal Processing*, vol. 110, p. 556–568, 2018.
- [48] Measurement Specialties, Inc., “Piezo Film Sensors Technical Manual,” Norristown, PA, 1999.
- [49] R. Wu, P. A. Selvadurai, C. Chen and et al, “Revisiting Piezoelectric Sensor Calibration Methods Using Elastodynamic Body Waves,” *J. Nondestruct. Eval.*, vol. 40, no. 68, 2021.
- [50] D. Li, S.-C. M. Ho, G. Song, L. Ren and et al., “A review of damage detection methods for wind turbine blades,” *Smart Mater. Struct.*, vol. 24, no. 033001, 2015.
- [51] S. Nain, J. S. Rathore and N. N. Sharma, “Comparison of Piezo-material based Energy Transduction Systems for Artificial Nanoswimmer,” in *IOP Conf. Ser.-Mat. Sci.*, 346, 012079, 2018.
- [52] Y.-J. Li, G.-C. Wang, H.-Y. Cui, S.-K. Cao and et al, “Dynamic characteristics and optimization research on PVDF piezo electric film force sensor for steel ball cold heading machine,” *ISA T.*, vol. 94, pp. 265-275, 2019.
- [53] M. Electronics, “Vibration Sensors DT2-028K W/RIVETS,” Measurement Specialties, [Online]. Available: <https://eu.mouser.com/ProductDetail/Measurement-Specialties/1-1003744-0?qs=sGAEpiMZZMs29kr3d%252BndI2Ss0dvAm%252B%252B8smsI%2Fyg21D0%3D>. [Accessed 28 February 2022].
- [54] Measurement Specialties, Inc., “SDT Shielded Piezo Sensors, Technical Data,” 2009.
- [55] E. L. Oliveira, N. M. M. Maia, A. G. Marto, R. G. A. da Silva and et al, “Modal characterization of composite flat plate models using piezoelectric transducers,” *Mech. Syst. Signal Pr.*, vol. 79, pp. 16-29, 2016.
- [56] A. K. Pandey, M. Biswas and M. M. Samman, “Damage detection from changes in curvature mode shapes,” *J. Sound Vib.*, vol. 145, p. 321–332, 1991.
- [57] A. Deraemaeker, “On the use of dynamic strains and curvatures for vibration based damage localization,” in *Proceedings of the 5th European Workshop on Structural Health Monitoring*, Sorrento, Italy, 2010.
- [58] Y. Gu, L. Long and P. Tan, “Surface strain distribution method for delamination detection using piezoelectric actuators and sensors,” in *Proceedings of 9th International Conference on Damage Assessment of Structures*, Oxford, UK, 2011.
- [59] Y. Xin, H. Sun, H. Tian, C. Guo and et al, “The use of polyvinylidene fluoride (PVDF) films as sensors for vibration measurement: A brief review,” *Ferroelectrics*, vol. 502, no. 1, pp. 28-42, 2016.
- [60] TE connectivity, “Piezoelectric Sensors,” TE connectivity, [Online]. Available: <https://www.te.com/usa-en/products/sensors/piezo-film-sensors.html?tab=pgp-story>. [Accessed 1 June 2022].
- [61] A. Safonovs, A. Mironov, P. Doronkin and V. Kuzmickis, “Sensitivity spread of piezo electric films used as sensors for machine and structural monitoring,” in *Engineering for Rural Development*, Jelgava, 2023.
- [62] M. Lin and F. K. Chang, “The manufacture of composite structures with a built-in network of piezoceramics,” *Composites Science and Technology*, vol. 62, p. 919–939, 2002.

- [63] A. Ghoshal, J. Ayers, M. Gurvich, M. Urban and N. Bordick, “Experimental investigations in embedded sensing of composite components in aerospace vehicles,” *Composites: Part B*, vol. 71, pp. 52-62, 2015.
- [64] M. B. Lemistre, “Electric and Electromagnetic Properties Sensing,” in *Encyclopedia of Structural Health Monitoring*, Wiley, 2009.
- [65] X. P. Qing, S. J. Beard, A. Kumar, T. K. Ooi and F. K. Chang, “Built-in Sensor Network for Structural Health Monitoring of Composite Structure,” *Journal of Intelligent Material Systems and Structures*, vol. 18, pp. 39-49, 2017.
- [66] M. Melnykowycz and A. J. Brunner, “The performance of integrated active fiber composites in carbon fiber laminates,” *Smart Mater. Struct.*, vol. 20, no. 7, p. 075007, 2011.
- [67] R. Paradies and B. Schlapfer, “Finite element modeling of piezoelectric elements with complex electrode configuration,” *Smart Mater. Struct.*, vol. 18, p. 025015, 2009.
- [68] P. D. Foote, “Integration of structural health monitoring sensors with aerospace,” *Composite materials and structures*, vol. 46, no. 2, pp. 197-203, 2015.
- [69] J. R. Zayas, D. P. Roach, M. A. Rumsey, W. R. Allan and W. R. Horsley, “Low-Cost Fiber Bragg Grating Interrogation System for in situ Assessment of Structures,” in *Sensors and Smart Structures Technologies for Civil, Mechanical, and Aerospace Systems*, San Diego, CA, USA, 2007.
- [70] R. De Oliveira, C. A. Ramos and A. T. Marques, “Health monitoring of composite structures by embedded FBG and interferometric Fabry–Perot sensors,” *Comput Struct*, vol. 86, no. 3, p. 340–346, 2008.
- [71] M. Majumder, T. K. Gangopadhyay, A. K. Chakraborty and et al, “Fibre Bragg gratings in structural health monitoring – present status and applications,” *Sensor Actuat A: Phys*, vol. 147, no. 1, p. 150–164, 2008.
- [72] M. Frövel, G. Carrión, J. M. Pintado, J. Cabezas and F. Cabrerizo, “Health and usage monitoring of Spanish National Institute for Aerospace Technology unmanned air vehicles,” *Structural Health Monitoring*, vol. 16, no. 4, p. 486–493, 2016.
- [73] J. Alvarez-Montoya, A. Carvajal-Castrillón and J. Sierra-Pérez, “In-flight and wireless damage detection in a UAV composite wing using fiber optic sensors and strain field pattern recognition,” *Mechanical Systems and Signal Processing*, vol. 136, p. 106526, 2020.
- [74] T. J. Arsenault, A. Achuthan, P. Marzocca, C. Grappasonni and G. Coppotelli, “Development of a FBG based distributed strain sensor system for wind turbine structural health monitoring,” *Smart Mater. Struct.*, vol. 22, p. 075027, 2013.
- [75] H. Cheng-Yu, Z. Yi-Fan, Z. Meng-Xi, L. L. M. Gordon and L. Li-Qiang, “Application of FBG sensors for geotechnical health monitoring, a review of sensor design, implementation methods and packaging techniques,” *Sensors and Actuators A*, vol. 244, p. 184–197, 2016.
- [76] M. Yeager, M. Todd, W. Gregory and C. Key, “Assessment of embedded fiber Bragg gratings for structural health monitoring of composites,” *Structural Health Monitoring*, vol. 16, no. 3, pp. 262-275, 2017.
- [77] L. C. Heaton, M. Kranz and J. Williams, “Embedded fiber optics for structural health monitoring of composite motor cases,” in *Nondestructive Evaluation and Health Monitoring of Aerospace Materials and Composites III, NDE for Health Monitoring and Diagnostics*, San Diego, CA, United States, 2004.

- [78] H. Herranen, J. Majak, P. Tsukrejev, K. Karjust and O. Märtens, “Design and Manufacturing of composite laminates with structural health monitoring capabilities,” in *Procedia CIRP*, vol. 72, pp. 647-652, 2018.
- [79] G. Luyckx, E. Voet, N. Lammens and J. Degrieck, “Strain Measurements of Composite Laminates with Embedded Fiber Bragg Gratings: Criticism and Opportunities for Research,” *Sensors*, vol. 11, no. 1, pp. 384-408, 2011.
- [80] B. A. Sjogren, “Static strength of CFRP laminates with embedded fiber-optic edge connectors,” *Compos. A Appl. Sci. Manufact.*, vol. 32, pp. 189-196, 2001.
- [81] A. K. Green, M. Zaidman, E. Shafir, M. Tur and S. Gali, “Infrastructure development for incorporating fiber-optic sensors in composite materials,” *Smart Mater. Struct.*, vol. 9, pp. 316-321, 2000.
- [82] A. J. van Wyk and C. V. Robertson, “A Systems Engineering approach to Structural Health Monitoring of Composites using Embedded Optical Fibre Bragg Sensors for Aeronautical applications,” in *Proc. SPIE 8066, Smart Sensors, Actuators, and MEMS V*, 2011.
- [83] M. Wang, N. Li, G. D. Wang, S. W. Lu, Q. D. Zhao and X. L. Liu, “High-sensitive flexural sensors for health monitoring of composite materials using embedded carbon nanotube (CNT) buckypaper,” *Composite Structures*, vol. 261, 2021.
- [84] A. Tayebi and M. M. Ul Hoque, “Design of experiments optimization of embedded MEMS sensors in composites for structural health monitoring,” in *Proc. SPIE 5057, Smart Structures and Materials 2003: Smart Systems and Nondestructive Evaluation for Civil Infrastructures, Smart Structures and Materials*, San Diego, California, USA, 2003.
- [85] G. C. Kahandawa, J. Epaarachchi, H. Wang, J. Canning and K. T. Lau, “Extraction and processing of real time strain of embedded FBG sensors using a fixed filter FBG circuit and an artificial neural network,” *Measurement*, vol. 46, pp. 4045-4051, 2013.
- [86] G. Pereira, C. Frias, H. Faria, O. Frazão and A. Marques, “Study of strain-transfer of FBG sensors embedded in unidirectional composites,” *Polymer Test.*, vol. 32, no. 6, p. 1006–1010, 2013.
- [87] A. Vieira, R. de Oliveira, O. Frazão, J. M. Baptista and A. T. Marques, “Effect of the recoating and the length on fiber Bragg grating sensors embedded in polymer composites,” *Materials & Design*, vol. 30, p. 1818–1821, 2009.
- [88] R. Brincker, P. Andersen and N. Møller, “An indicator for separation of structural and harmonic modes in output-only modal testing,” in *European COST F3 Conference on System Identification and Structural Health Monitoring*, Universidad Politecnica de Madrid, Spain, 2000.
- [89] J. M. Ha and et al, “Autocorrelation-based time synchronous averaging for condition monitoring of planetary gearboxes in wind turbines,” *Mechanical Systems and Signal Processing*, Vols. 70-71, pp. 161-175, 2016.
- [90] M. D. Coats, N. Sawalhi and R. B. Randall, “Extraction of tacho information from a vibration signal for improved synchronous averaging,” in *Proceedings of ACOUSTICS 2009*, Adelaide, Australia, 2009.
- [91] A. Deraemaeker, E. Reynders, G. De Roeck and J. Kullaa, “Vibration-based structural health monitoring using output-only measurements under changing environment,” *Mech. Syst. Signal Pr.*, vol. 22, pp. 34-56, 2008.

- [92] P. S. Rao and C. Ratnam, "Health monitoring of welded structures using statistical process control," *Mech. Syst. Signal Pr.*, vol. 27, pp. 683-695, 2012.
- [93] L. Colone, M. K. Hovgaard, L. Glavind and R. Brincker, "Mass detection, localization and estimation for wind turbine blades based on statistical pattern recognition," *Mech. Syst. Signal Pr.*, vol. 107, pp. 266-277, 2018.
- [94] M. Martinez-Luengo, A. Kolios and L. Wang, "Structural health monitoring of offshore wind turbines: A review through the Statistical Pattern Recognition Paradigm," *Renew. Sust. Energ. Rev.*, vol. 64, pp. 91-105, 2016.
- [95] D. Garcia and D. Tcherniak, "An experimental study on the data-driven structural health monitoring of large wind turbine blades using a single accelerometer and actuator," *Mech. Syst. Signal Pr.*, vol. 127, pp. 102-119, 2019.
- [96] E. Neu, F. Janser, A. A. Khatibi and A. C. Orifici, "Fully Automated Operational Modal Analysis using multi-stage clustering," *Mech. Syst. Signal Pr.*, vol. 84, pp. 308-323, 2017.
- [97] D. J. Ewins, "Model validation: Correlation for updating," *Sadhana*, vol. 25, pp. 221-234, 2000.
- [98] R. Janeliukstis, R. Riva, E. Di Lorenzo, Luczak M and et al, "Comparison of wind turbine blade models through correlation with experimental modal data," in *Proceedings of ISMA and USD, International Conference on Noise and Vibration Engineering and International Conference on uncertainty in Structural Dynamics*, Belgium, Leuven, 2020.
- [99] C. Devriendt, F. Presezniak, G. De Sitter, K. Vanbrabant and et al, "Structural health monitoring in changing operational conditions using transmissibility measurements," *Shock Vib.*, vol. 17, pp. 651-675, 2010.
- [100] Y. Zhou, R. Perera and E. Sevilano, "Damage identification from power spectrum density transmissibility," in *Proceeding of the 6th European Workshop on Structural Health Monitoring*, 2012.
- [101] Y. L. Zhou, N. M. M. Maia, R. P. C. Sampaio and M. Abdel Wahab, "Structural damage detection using transmissibility together with hierarchical clustering analysis and similarity measure," *Struct. Health Monit.*, vol. 16, no. 6, pp. 711-731, 2017.
- [102] S. Ručevskis, T. Rogala and A. Katunin, "Optimal Sensor Placement for Modal-Based Health Monitoring of a Composite Structure," *Sensors*, vol. 22, no. 10, 2022.
- [103] S. Timoshenko, "Part 1. Elementary Theory and Tasks," in *Strength of materials*, Leningrad, 1932, p. 336.
- [104] A. Priklonskiy, Investigation of the possibilities of holographic interferometry in determining the stress state of thin-walled structures. Dissertation for the degree of candidate of technical sciences., Riga, 1982.
- [105] V. Demenko, *Mechanics of Materials and Structures*, 2013.
- [106] N. Erdedi and A. Erdedi, *Strength of materials*, Konorus, 2013.
- [107] G. Fihntengoltz, *Course of differential and integral calculus (In 3 volumes)*, Fizmatlit, 2001.
- [108] A. Priklonskiy and V. Novickiy, "Analysis of the parameters of the stress-strain state at specific points on the surface of thin-walled structural elements using holographic interferometry methods," in *Vibration strength and reliability of aircraft engines. Abstracts at 5-th VNT conference*, Kuibyshev, 1981.

- [109] A. Mironov, A. Safonovs, D. Mironovs, P. Doronkin and V. Kuzmickis, “Health Monitoring of Serial Structures Applying Piezoelectric Film Sensors and Modal Passport,” *Sensors*, 2023.
- [110] D. Solovyev, S. Dadunashvili, A. Mironov, P. Doronkin and D. Mironovs, “Mathematical Modeling and Experimental Investigations of a Main Rotor Made from Layered Composite Materials,” *Mechanics of Composite Materials*, vol. 56, no. 1, pp. 103-110, 2020.
- [111] J. Petersen, A. Kube, S. Geier and P. Wierach, “Structure-Integrated Thin-Film Supercapacitor as a Sensor,” *Sensors*, vol. 22, no. 18, 2022.
- [112] A. Mironov, P. Doronkin, A. Priklonskiy and I. Kabashkin, “Structural Health Monitoring of rotating blades on helicopters,” *Aviation*, vol. 20, pp. 110-122, 2016.
- [113] N. Pfenning, *Elementary Statistics: Looking at the Big Picture*, Cengage Learning, 2010.
- [114] V. Badami and P. de Groot, “Displacement measuring interferometry,” in *Handbook of optical dimensional metrology*, CRC Press, 2013, p. 82.
- [115] A. Mironov, P. Doronkin and A. Priklonskiy, “Experimental technology of operational pipeline condition monitoring,” in *MATEC web of conferences 24 02005*, 2015.
- [116] R. Janeliukstis, S. Rucevskis, M. Wesolowski and A. Chate, “Experimental structural damage localization in beam structure using spatial continuous wavelet transform and mode shape curvature methods,” *Measurement: J. Int. Measure. Conf.*, vol. 102, pp. 253-270, 2017.
- [117] L. Zhang, R. Brincker and P. Andersen, “An Overview of Operational Modal Analysis: Major Development and Issues,” in *1st International Operational Modal Analysis Conference*, Copenhagen, 2005.
- [118] W.-H. Hu, *Operational modal analysis and continuous dynamic monitoring of footbridges, PhD thesis*, Porto: Faculty of Engineering, University of Porto, 2011.
- [119] A.-M. Yan, G. Kerschen, P. De Boe and J.-C. Golinval, “Structural damage diagnosis under varying environmental conditions—Part I: A linear analysis,” *Mechanical Systems and Signal Processing*, vol. 19, pp. 847-864, 2005.
- [120] C. B. Do, *The Multivariate Gaussian Distribution*, CS229 – Machine Learning. Stanford University., 2008.
- [121] M. Sokolova, N. Japkowicz and S. Szpakowicz, “Beyond accuracy, f-score and roc: a family of discriminant measures for performance evaluation,” in *Australasian Joint Conference on Artificial Intelligence*, Springer, 2006.
- [122] W. Cheng, Z. Zhang, S. Lee and Z. He, “Source Contribution Evaluation of Mechanical Vibration Signals via Enhanced Independent Component Analysis,” *The Journal of Manufacturing Science and Engineering*, vol. 134, no. 2, 2012.
- [123] A. Mironov, P. Doronkin, A. Priklonskiy and S. Yunusov, “Adaptive Technology Application for Vibration-Based Diagnostics of Roller Bearings on Industrial Plants,” *Transport and Telecommunication Journal*, vol. 15, no. 3, pp. 233-242, 2014.



Deniss Mironovs was born in 1990 in Riga. He received a Bachelor's degree in Electrical Engineering from Riga Technical University in 2012 and a Master's degree from the Danish Technical University in Acoustical Engineering in 2016. From 2016 to 2019, he was a vibration engineer and researcher at the Aviation Research Centre. Currently, he is a researcher at Riga Technical University and an acoustics consultant and board member of "Akukon-Būvakustika" Ltd. While studying in Denmark, he worked at Brüel & Kjær as a Labshop software tester. His scientific interests are related to acoustics, vibration, and modal analysis.